University of Zurich[UZH]

Constraining the Congo Basin Sulfur Cycle using Sulfur and Oxygen Isotopes

ESS 511 Master's Thesis

Author
Yiduo Zou
21-749-973

Supervised by
Prof. Dr. Jordon Hemingway (jordon.hemingway@erdw.ethz.ch)

Faculty representative
Prof. Dr. Jan Seibert

19.05.2024
Department of Geography, University of Zurich

Contents

List of Figures

List of Tables

Acknowledgements

This thesis project was made possible by the collaboration between the University of Zurich (UZH) and the Federal Institute of Technology Zurich (ETH Zurich). I am deeply thankful for this incredible opportunity to experience world-leading research in Earth Science, which has significantly broadened my academic knowledge.

I am deeply grateful for the extensive academic support I received during my thesis project under Prof. Jordan Hemingway and the Surface Earth Evolution team in ETH. Thank you, Prof. Jordan, for introducing me to the real academic world and supervise me whenever I struggled. Your guidance taught me how to think scientifically, this is a precious gift that will benefit me throughout my academic life. I also want to extend my thanks to all members of Jordan's team; you were incredibly friendly and supportive. I learned so much from each of you and am grateful for all advice.

Special thanks to Prof. Jan Seibert at UZH for being my faculty representative. I appreciate your help in university-related matters, especially when I was struggling with a foreign language. Your initial support was like sunshine in winter, providing much-needed encouragement.

I am profoundly grateful to my parents for their mental and financial support. Words cannot express how thankful I am and how much I love you. You have given everything to provide me with the chance to see the world, experience a colorful life, and explore the infinite possibilities of the future. I am always proud and feel lucky to have such wonderful parents, the best parents in the world!

And thanks to all my friends in Zurich and New Zealand, your company and care have dispelled the loneliness of living in a foreign country.

Thanks to everyone who has been part of my life. I truly appreciate being connected to each of you!

Abstract

The sulfur cycle is a key biogeochemical cycle in the Earth system that directly and indirectly controls the hydrosphere chemistry, Earth surface evolution and climate change. In terrestrial environments, sulfur is primarily transported by large river systems. Rock weathering contributes the majority of dissolved sulfate to river water, including through the dissolution of evaporites and the oxidation of pyrite. However, detailed research on large river systems, especially in tropical environments, is insufficient. This study uses the Congo River Basin as a case study to trace sulfur cycling processes by analysing the sulfur and oxygen isotopes in dissolved sulfate. $\delta^{34}S$ and $\delta^{18}O$ values from 32 tributaries narrowly distribute between 10 to 14 ‰and 8 to 12 ‰. An inversion model has been applied to solve multimixing equations, enabling the quantification of contributions from each sulfur source (carbonates, evaporites, silicates and atmosphere) for each tributary. The result indicates that the majority of dissolved sulfate originates from the oxidation of pyrite, with partial contributions from the dissolution of evaporites and sea water spray. Other factors such as land cover types, erosion intensity, ecosystem affection, and human activities may impact the sulfur cycle, but the correlation is not strong enough to clearly seen in the current results. Unlike other high sulfur containing rivers, the sulfur cycle in the Congo River, especially in Kasai tributaries, is characterized by low concentration of dissolved sulfate, which makes isotope results more susceptible to alteration during transportation processes. Further isotopic research and more solid samples are needed for better results. In conclusion, pyrite weathering is significant for the sulfur dynamics in the Congo Basin. Results from this research not only contribute to providing data that help understand the local sulfur cycle but also are valuable for meta-analysis to build global research and models in biogeochemical cycles and related fields.

Key Words: Sulfur cycle, Congo Basin, Kasai Basin, sulfur isotopes, dissolved sulfates, pyrite, Earth surface rock weathering.

1 Introduction

Sulfur (S) is one of the key elements in biogeochemical cycles, because sulfur is a fundamental building block of life (Sievert et al., 2007) and it is a key process that able to affect the redox condition of the Earth's surface (Zhang et al., 2020). As a common element on Earth (Torres et al., 2020), this element exists in various oxidized and reduced forms within the lithosphere, hydrosphere, atmosphere, and biosphere, contributing to the complex dynamics of sulfur cycle in the Earth system (Canfield and Raiswell, 1999). The biogeochemical cycling of sulfur is a complex and multifaceted process that plays a pivotal role in regulating Earth's climate, environmental health, and ecological systems (Ivanov and Freney, 1983). Transformations of sulfur and transitions between its various oxidation states and species drive a network of chemical reactions fundamental to atmospheric, terrestrial, and aquatic systems and also bioactivities (Jørgensen et al., 2019).

Even though sulfur itself, as one of the macro-nutrient elements, is already important enough to be deeply researched (Li et al., 2020), its intimate connection with surface weathering processes enables it to affect global climate by disturbing the carbon cycle (Ross et al., 2018). Therefore, the sulfur cycle closely relates to, mirrors, and controls Earth's surface conditions. Rock weathering is a highlighted part of the terrestrial sulfur cycle because when sulfur-bearing minerals undergo weathering, sulfuric acid is produced; then silicates and carbonates both weather differently under sulfuric acid compare to the carbonic acid exist environment (Ross et al., 2018)(Kemeny et al., 2021a). As a result, the sulfur cycle can affect global climate and other biogeochemical cycles (Burke et al., 2018) .

Investigating the geobiochemical cycles in large river systems helps in understanding weathering processes, matter cycles between continents, rivers, and oceans, and continental surface weathering processes with CO_2 consumption flux (Fan et al., 2014). Riverine sulfur is the major source of sulfate to the ocean, supplying approximately 4.7 Tmol/y, and sulfur to the ocean mainly from dissolution of sulfate minerals or oxidative weathering of sulfide minerals (Relph et al., 2021)(Burke et al., 2018). To identify the source of the sulfur and assist in chemical weathering fluxes, sulfur isotopes with oxygen isotopes are therefore used (Burke et al., 2018).

However, the modern global sulfur cycles are not fully understood in many aspects (Burke et al., 2018), tropical environment are important as the hot and and humid

climate generates different weathering processes and varies in weathering intensity, compare to other climate environment (Deng et al., 2022). This research fills part of the gap in sulfur cycle using the Congo Basin as a case study. The Congo Basin, characterized by its vast expanse of tropical rain forest and a sprawling river system, presents a unique case study to explore these biogeochemical dynamics (Fig.1). In this research, 32 river water samples were analysed and we try to adequately understand the sulfur cycle with reference to dissolved sulfate concentrations, sulfur and oxygen isotope values, lithology, and land cover.

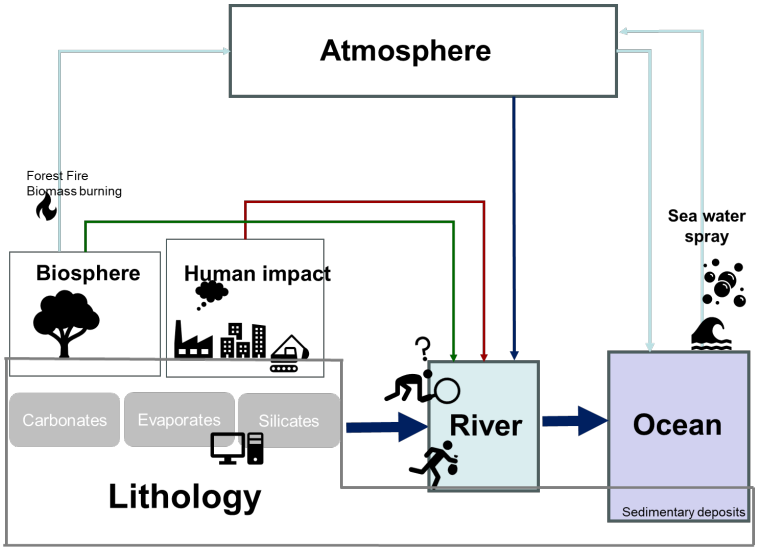

Figure 1: Overview of the main research aspects in the Congo Basin, illustrating the impacts of lithology weathering, ocean spray, and biological activities on the regional ecosystem.

1.1 Biogeochemical Sulfur Cycle in Earth System

Biogeochemical cycles are also referred to as the cycles of nature or nutrient cycles, as they relate organisms to abiotic features on Earth and involve compounds that provide nutritional support to living organisms (Madsen, 2011). As a key member in macro elements, sulfur exists almost everywhere in both inorganic materials and biomass (Li et al., 2020). Biochemically, sulfur supports essential life activities by constructing proteins and acting as oxidants or reductants in microbial respiration, which involves sulfur oxidation (converting sulfide and sulfur to sulfate) and sulfate reduction (electron acceptor sulfate converts to sulfur and sulfide) (Madsen, 2011). In geochemistry, sulfur cycles through mineral weathering (Burke et al., 2018) and is transported by natural transmission mediums such as water or air (Johnston, 2011).

As elements cycle through the Earth, they undergo a complex cyclical journey, and processes are all closely related; thus, both biochemical and geochemical processes are considered in sulfur biogeochemical cycles (Jacobson et al., 2000).

The sulfur cycle moves through various spheres, intricately linking various environmental systems. These processes characterized by transformations from one chemical form to another, as well as transformations between different sulfur species (Jacobson et al., 2000). Sulfur cycle attributes to the evolution of Earth's surface chemistry, atmospheric and ocean chemistry, and concomitant changes in the ecology of sulfur-utilizing organisms (Farquhar and Wing, 2003)(Farquhar et al., 2010). Here is a summarized and simplified description of sulfur fluxes (Fig.2, picture modified from (Schoonen, 2018)) and how it cycles though spheres presents: sulfur undergoes burial in lithology, weathering out and transportation in the atmosphere and hydrosphere, and uptake or decay by organisms (Schoonen, 2018). Sulfur is introduced into marine ecosystems through runoff from land, direct fallout from the atmosphere, and underwater geothermal vents. Ocean water is a large reservoir of dissolved sulfate, from which organisms take sulfate that is then buried in sedimentary minerals, mainly as pyrite FeS_2. Another pathway of ocean water transformation to a solid phase is the generation of evaporite rocks through evaporative processes. Over time, and with tectonic movements, deep sedimentary rocks are uplifted and undergo physical and chemical weathering. River systems play important roles in eroding and transporting dissolved and particulate materials, including sulfur, into the ocean. SO_2 and aerosols that contain sulfate are the main forms of sulfur present in the atmosphere, originating from volcanic activities, sea spray, fossil fuel and biomass burning, industrial emissions, and biogenic emissions.

1.2 Various Source of Sulfur to River Systems

Soluble sulfate is the main form of sulfur present in river water, mainly composed of continental weathering-derived sulfate and anthropogenic sulfate (Zhang et al., 2020). Natural sources of dissolved sulfate (SO_4^{2-}) in freshwater ecosystems encompass sulfur originating from mineral weathering, sea spray aerosols, volcanic activities, organics decay, and sulfides oxidation (Zak et al., 2021). The primary anthropogenic sources contributing to sulfate input in water bodies including acid mine drainage, fertilizer leaching from agricultural soils, drainage of wetlands, runoff from agricultural and industrial wastewater, and changes in sea levels (Zak et al., 2021). A detailed explanation is present as below.

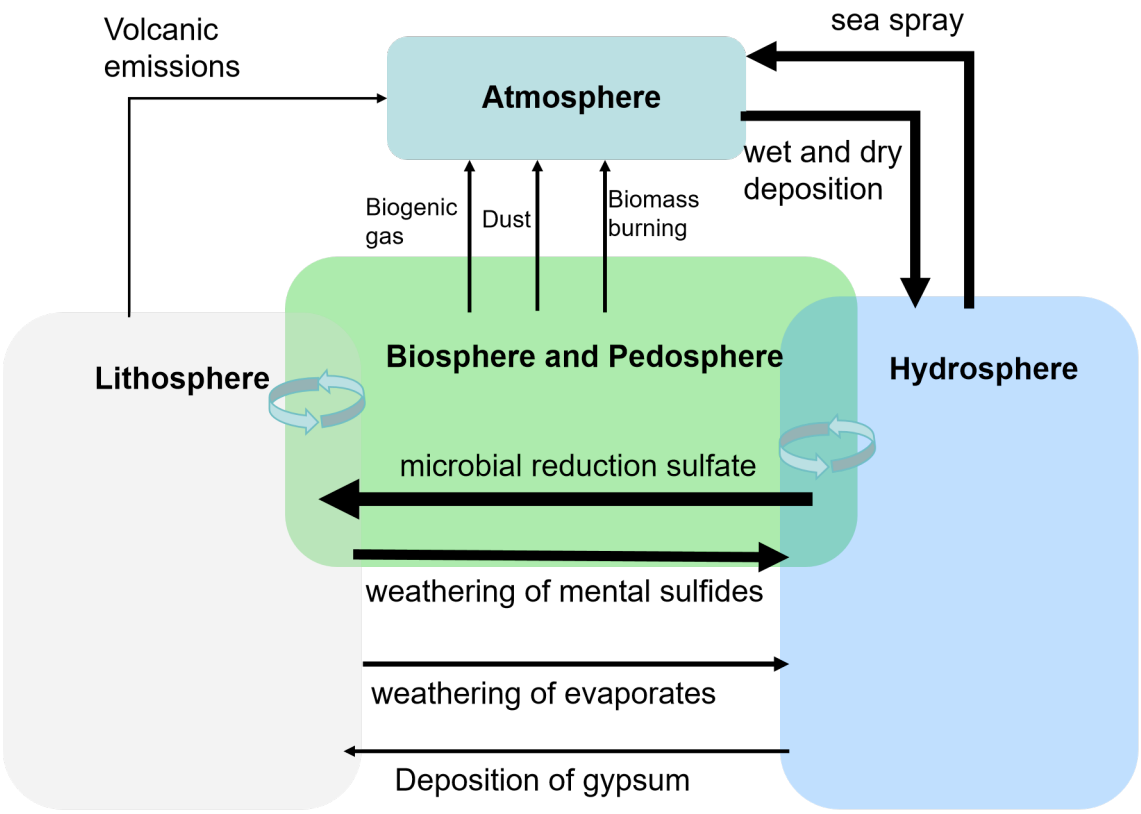

Figure 2: The S cycle in Earth system, with the flux intensity shown by the size of arrows.

1.2.1 Aerosol Deposition and Anthropogenic Impacts

Aerosols, including small particles and droplets in the atmosphere, are key carriers for sulfur transport and deposition across diverse environmental matrices (Zak et al., 2021). Sulfur sourced from the atmosphere globally influences environmental and climatic systems (Zak et al., 2021). Aerosol-mediated sulfur deposition has the capacity to redistribute sulfur from terrestrial and marine sources on a larger geological scale, and as a result, affecting the water and soil chemistry, ecosystem environments, nutrient availability, and also other elements cycles, including but not limited to carbon and nitrogen (Vile et al., 2003) (Gao et al., 2018). In terms of climate, sulfate is an effective radiative-cooling aerosols in the atmosphere (Huang et al., 2014). The sulfur-containing aerosols change the radiation balance by directly affecting solar radiation scattering and indirectly modifying cloud properties (Pei et al., 2021). Volcanic activities, sea spray, and biogenic emissions generate natural sulfur aerosols, while fossil fuel burning and industrial processes add anthropogenic sulfur sources in gaseous or aerosol forms (Huang et al., 2014). Many gaseous sulfur compounds undergo chemical transformations due to atmospheric influences,

generally being oxidized into sulfate (SO_4^{2-}) and forming sulfur-containing aerosols as the final product (Pei et al., 2021).

Anthropogenic sulfate sources includes agricultural sulfate, industrial sulfate, and domestic sulfate (Zhang et al., 2020). The total riverine sulfur flux is around 4.7 Tmol/y and 1.3 Tmol/y of the flux is contributed by human activities (Zhang et al., 2020). Human impacts on nature are increasingly significant with industrial development and population growth, leading to increased anthropogenic impacts on sulfur(Jacobson et al., 2000). The impact can be divided into two categories: one is adding extra sulfur sources through pollution emissions, such as biomass burning, biofuel combustion, pulp and paper industry pollution, over-fertilized soils, wastes, etc. (Lee and Brimblecombe, 2016); the other is by indirectly affecting other sulfur-related processes, such as disturbing erosion processes through mining or changing land use to agricultural areas (Pacheco et al., 2013).

1.2.2 Lithologic Sources

Rock weathering occurs when bedrock is exposed to the surface. This natural adjustment mechanism transforms solid bedrock into forms that are easily transported, such as original component particles, secondary minerals, or dissolved phases (Depetris et al., 2014). Weathering processes lead to the transformation of various sulfur species (Table 1) and contribute a variety of dissolved ions to river water, including sulfur. The source of dissolved sulfate in rivers is not solely the oxidative weathering of pyrite (FeS_2); it may also arise from multiple sources such as the dissolution of gypsum ($CaSO_4{\cdot}2H_2O$) and anhydrite ($CaSO_4$) (Relph et al., 2021). These weathering processes convert sulfur elements into dissolved sulfate form ($SO_4{}^{2-}$). Both minerals weathering provides the dissolved sulfate in river water, with the flux of riverine sulfate 1.3 ± 0.2 Tmol S/y from pyrite and 1.5 ± 0.2 Tmol S/y form sedimentary sulfate minerals (Burke et al., 2018).

Sulfur Species	Chemical Formula	Oxidation state	Common Forms
Sulfate	SO_4^{2-}	+6	gypsum, epsomite
Sulfide	S^{2-}	-2	pyrite, galena
Sulfuric Acid	H_2SO_4	+6	dissolved sulfate

Table 1: Common sulfur species and related minerals.

Pyrite, commonly found in sulfide deposits, undergoes oxidation that can indirectly influence the carbon cycle by producing sulfuric acid (H_2SO_4) (Relph et al.,

2021). The overall reaction is:

$$4\,FeS_2 + 15\,O_2 + 10\,H_2O \longrightarrow 4\,Fe(OH)_3 + 8\,H_2SO_4 \tag{1}$$

Weathering of pyrite involves a complex series of step-by-step chemical reaction(Byrne et al., 2012):

$$2\,FeS_2(s) + 2\,H_2O + 7\,O_2 \longrightarrow 2\,Fe^{2+} + 4\,{SO_4}^{2-} + 4\,H^+ \tag{2}$$

$$4\,Fe^{2+} + O_2 + 4\,H^+ \longrightarrow 4\,Fe^{3+} + 2\,H_2O \tag{3}$$

$$2\,FeS_2(s) + 14\,Fe^{3+} + 8\,H_2O \longrightarrow 15\,Fe^{2+} + 2\,{SO_4}^{2-} + 16\,H^+ \tag{4}$$

$$Fe^{3+} + 3\,H_2O \longrightarrow Fe(OH)_3 + 3\,H^+ \tag{5}$$

This chemical weathering of sulfide minerals contrasts with sulfate minerals which produce dissolved sulfate through dissolution processes. Evaporites are sedimentary mineral deposits formed through crystallization and concentration processes driven by the evaporation of sea water from a solution. The evaporite source is typified by sulfates (gypsum, $CaSO_4 \cdot 2\,H_2O$), and chlorides (halite, NaCl)(Charlson et al., 2000). Evaporite weathering involves the processes of physical dehydration and ionization. Evaporites weather rapidly and completely, contributing various cations (including Na^+, Mg^{2+}, Ca^{2+}, K^+) and anions (halides, sulfates) to rivers, without involving carbonates. In terms of sulfur, the more weathering of gypsum occurs, the more dissolved sulfate will be produced.

- Gypsum weathering:

$$CaSO_4 \cdot 2\,H_2O \longrightarrow Ca^{2+} + {SO_4}^{2-} + 2\,H_2O \tag{6}$$

- Halite weathering:

$$NaCl \longrightarrow Na^+ + Cl^- \tag{7}$$

1.3 Sulfur Cycle relates to Carbon Cycle

Chemical weathering is one of the most important factors affecting the global climate on a geological scale because it involves several reactions that consume or release carbon dioxide (CO_2) over geologic timescales (Burke et al., 2018). Silicate weathering processes temporarily store carbon dioxide in weathering products or permanently in lithified marine sediments (Goudie and Viles, 2012). This process not only leads to the physical breakdown of rocks but also plays a crucial role in the global carbon cycle by transporting carbon from the atmosphere to the lithosphere and the oceans. Carbonates, silicates, and evaporites are the three most influential lithology types on Earth's surface (Kemeny and Torres, 2021), but these rocks undergo distinct weathering processes, each contributing uniquely to carbon cycling and the chemical composition of river waters (Fan et al., 2014).

Silicate and carbonate rocks not only undergo different chemical weathering processes, but the same type of rock can also weather differently under carbonic acid or sulfuric acid conditions, which affects the net balance of atmospheric CO_2(Torres et al., 2016). The primary natural source of sulfuric acid is the weathering of sulfur-bearing minerals, as mentioned earlier. Weathering of silicate rocks has been the focus of extensive study because it is thought to regulate Earth's climate via the silicate weathering feedback mechanism. However, recent research has highlighted the importance of alternative pathways that release carbon dioxide and thus counteract the silicate weathering feedback; among these, pyrite weathering is particularly noteworthy.

1.3.1 Carbonate Weathering

Carbonate weathering by carbonic acid:

$$\mathrm{CaCO_3 + CO_2 + H_2O \longrightarrow Ca^{2+} + 2\,HCO_3^-} \tag{8}$$

When all these dissolved materials are carried into the ocean, a portion of the bicarbonate (HCO_3^-) is converted back to carbon dioxide (CO_2) and water (H_2O) by the following reaction:

$$\mathrm{HCO_3^- + H^+ - \uparrow + H_2O} \tag{9}$$

This equation simplifies the release of carbon dioxide from bicarbonate into the

atmosphere, thereby completing the carbon cycle within geochemical processes. Typically, when 1 mole of carbonate undergoes weathering, it results in the formation of 2 moles of bicarbonate. These bicarbonates are transported into the aquatic system, where approximately half (1 mole) can be released back into the atmosphere as CO_2, and the remaining half is sequestered in ocean sediments. Considering the entire life-cycle of these processes, they are effectively CO_2 neutral over geological timescales.

However, if carbonate weathers by sulfuric acid:

$$CaCO_3 + H_2SO_4 \longrightarrow Ca^{2+} + {SO_4}^{2-} + CO_2 + H_2O \tag{10}$$

The CO_2 is directly released into the atmosphere. This means if the same 1 mole of carbonate is weathered by sulfuric acid (instead of carbonic acid), the total atmospheric CO_2 will increase by 1 mol. Consequently, greenhouse gases accumulate, leading to climate changes compared to the situation where weathering occurs with carbonic acid.

1.3.2 Silicate Weathering

Chemical weathering of silicate rocks is a crucial process for removing CO_2 from the atmosphere and converting it into soluble bicarbonates in the ocean, thereby influencing long-term carbon storage (West et al., 2005; Penman et al., 2020). The main mechanism through which silicate rocks affect the carbon cycle is illustrated in the following equations, which represent the overall reaction for a generalized calcium silicate (Goudie and Viles, 2012).

Silicate weathering by carbonic acid:

$$CaSiO_3 + 2\,CO_2 + H_2O \longrightarrow Ca^{2+} + 2\,{HCO_3}^{-} + SiO_2 \tag{11}$$

Silicate weathering by sulfuric acid:

$$CaSiO_3 + H_2SO_4 \longrightarrow Ca^{2+} + {SO_4}^{2-} + SiO_2 + H_2O \tag{12}$$

Comparing these two reactions, the ability of silicate weathering to lock in CO_2 becomes apparent. For every 1 mole of silicate weathered, 2 moles of CO_2 is

captured. After the entire process in the ocean, only 1 mole is expected to return to the atmosphere, therefore, 1 mole of carbon is effectively buried in the ocean. However, sulfur-related weathering does not contribute to the absorption of CO_2.

To sum up the relationship between weathering processes and the carbon cycle, simply but importantly, the involvement of sulfuric acid counteracts the ability of surface rocks to sequester CO_2 (Fig.3,(Colbourn et al., 2015)). the weathering process of silicate rocks not only captures CO_2 but also results in the formation of bicarbonate ions, which are transported to the ocean and can precipitate as carbonate minerals. Pyrite oxidation is the CO_2 source, while the evaporite dissolution does not directly affect gaseous carbon budget. It is therefore important to be able to distinguish and separate how much sulfate in a river is coming from each source. Isotope analyse is used to answer this question (Seal, 2006).

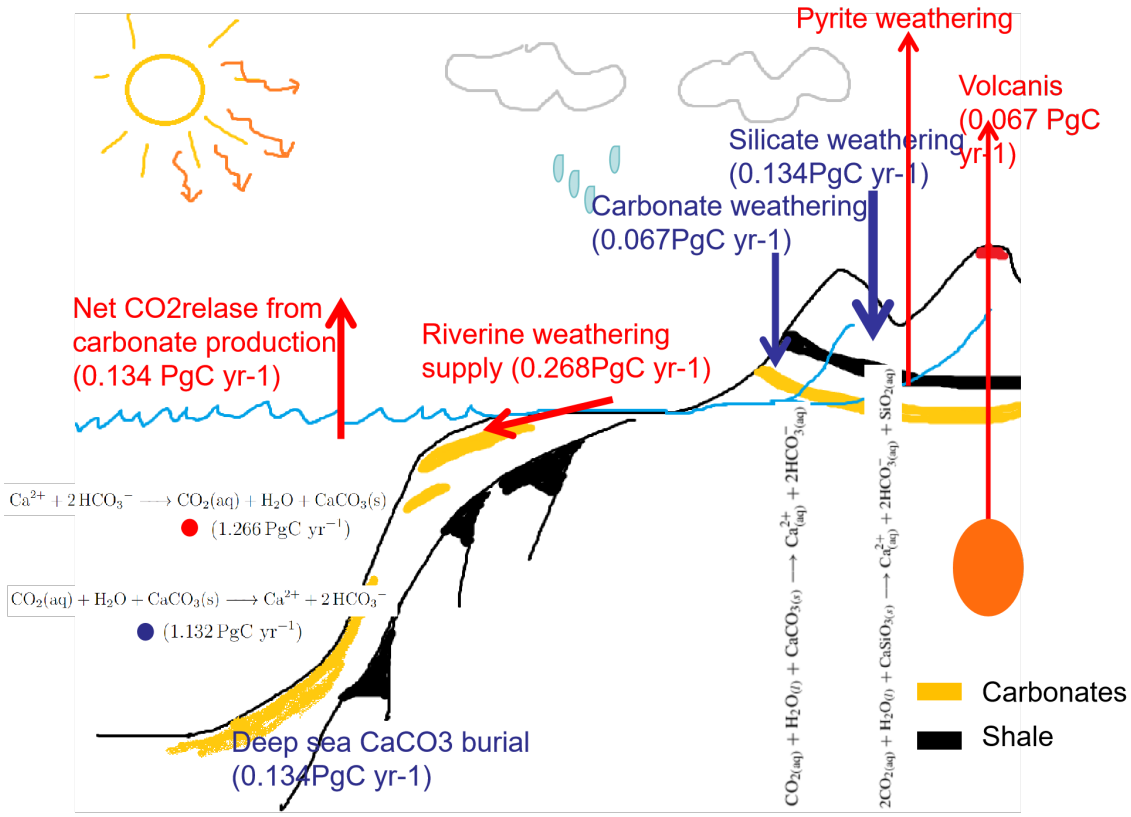

Figure 3: Schematic of different weathering fluxes and their impact on CO2 fluxes. Blue arrows present co_2 sink,while red arrows present co_2 gas sources.

1.4 Applications of Stable Isotopes in Sulfur cycles Research

Isotope knowledge is applied to track elements source and traveling processes (Jacobson et al., 2000). Each source and transport process has its specific isotope ratio and unique differentiation method. Therefore, as the elements travel, they run out from their original source with the same value of the source and fixed by biomass or altered by surrounding environment.

1.4.1 Sulfur Isotopes and oxygen isotopes

Isotopes of an element are defined as individual forms of the element that characterized by the number of neutrons they contain(Jacobson et al., 2000). Naturally, sulfur has 4 forms of stable isotopes that is geochemically important, they are ^{32}S, ^{33}S, ^{34}S, and ^{36}S (Jacobson et al., 2000). Among them, the light ^{32}S and heavy ^{34}S are the most abundant, comprising 99.22% of sulfur on Earth, with ^{32}S occupying the vast majority (95.02%) of the total sulfur on Earth(Jacobson et al., 2000). The ratio of $^{34}S/^{32}S$ is the most common method of studying sulfur isotopes, and difference sulfur reservoirs has different $\delta^{34}S$ values (Fig.4), which helps in tracking the sulfur source in the Earth system. $\delta^{34}S$ will be introduced in the following section.

Oxygen has 3 isotopes with different enrichment on the Earth, ^{16}O (99.8%), ^{17}O (0.038%), and ^{18}O(0.205%). It is one of the most common isotopes used in isotopes and nature studies, hydrology and climatology, as well as in reconstructing the paleoclimate (Grossman and Joachimski, 2020). Tracing water sources or pollutions, studying evaporation and condensation processes, mixing of different hydrological systems, and estimating groundwater recharge rates can all be achieved by analyzing distinct isotopic ratios of oxygen isotopes (Bao et al., 2016)(Jacobson et al., 2000).

1.4.2 Different Fractionation and Isotope Characteristics

Isotope fractionation forms the foundation of isotope studies, and the distinct isotopic signatures of natural or anthropogenic sources can serve as unique "fingerprints" to identify the origins and previous transformations (Hermes et al., 2022). Fractionation is defined as the partial separation of isotopes; once isotopes are unevenly distributed, the ratio of lighter to heavier isotopes becomes a unique identifier for specific materials or processes (Galimov, 2012).

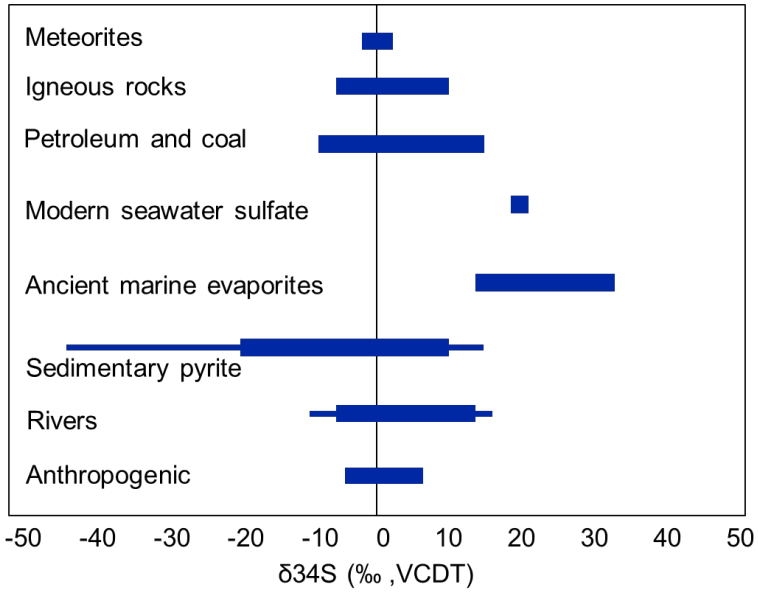

Figure 4: $\delta^{34}S$ of various sulfur sources (Seal, 2006)(Relph et al., 2021).

The fundamental principle behind the use of δ is the fractionation of sulfur isotopes that occurs during chemical reactions. The isotopic delta notation value for sulfur ($\delta^{34}S$) is calculated using the following formula:

$$\delta^{34}S = \left(\frac{\left(\frac{^{34}\mathrm{S}}{^{32}\mathrm{S}}\right)_{\text{sample}}}{\left(\frac{^{34}\mathrm{S}}{^{32}\mathrm{S}}\right)_{\text{standard}}} - 1 \right) \times 1000 \tag{13}$$

- $\left(\frac{^{34}\mathrm{S}}{^{32}\mathrm{S}}\right)_{\text{sample}}$ is the isotopic ratio of the sample.
- $\left(\frac{^{34}\mathrm{S}}{^{32}\mathrm{S}}\right)_{\text{standard}}$ is the isotopic ratio of the standard reference material.

This notation is used to express isotopic deviations in terms of enrichment or depletion relative to the standard. A positive $\delta^{34}S$ value indicates an enrichment of the heavier isotope (^{34}S), suggesting a higher concentration of this isotope compared to the standard. Conversely, a negative $\delta^{34}S$ value suggests a predominance of the lighter isotope (^{32}S) in the sample, indicating a depletion of the heavier isotope (^{34}S). The magnitude of the δ value quantifies the degree of isotopic deviation, which is crucial for understanding sulfur cycling and source identification in geochemical studies.

$\delta^{18}O$ is similar, it is a measure of the ratio of the stable isotopes ^{18}O to ^{16}O in

a sample compared to a standard. This isotopic ratio is expressed in per mille (‰) and is calculated using the following formula:

$$\delta^{18}O = \left(\frac{\left(\frac{^{18}\mathrm{O}}{^{16}\mathrm{O}}\right)_{\text{sample}}}{\left(\frac{^{18}\mathrm{O}}{^{16}\mathrm{O}}\right)_{\text{standard}}} - 1 \right) \times 1000 \tag{14}$$

- $\left(\frac{^{18}\mathrm{O}}{^{16}\mathrm{O}}\right)_{\text{sample}}$ is the isotopic ratio of the sample.
- $\left(\frac{^{18}\mathrm{O}}{^{16}\mathrm{O}}\right)_{\text{standard}}$ is the isotopic ratio of the standard reference material.

Fractionation factor (α or ϵ) is also introduced to quantify fractionation processes (Young et al., 2002), which is a measure of the preferential partitioning of isotopes between two substances or phases and is defined by the ratio of the concentrations of two isotopes in these phases (Young et al., 2002).

Fractionation factor α describes equilibrium fractionation processes:

$$\alpha = \left(\frac{R_A}{R_B} \right) \times 1000 \tag{15}$$

where R_A and R_B are the ratios of the heavy to light isotopes ($\frac{^{34}S}{^{32}S}$ or $\frac{^{18}O}{^{16}O}$) in substances A and B.

Epsilon (ϵ) is usually for kinetic processes, as the simplified and expressed form:

$$\epsilon \approx 1000 \times \left(\frac{R_B}{R_A} - 1 \right) \tag{16}$$

where ϵ and (ϵ) are expressed in parts per thousand or per mil (‰).

Isotope fractionation occurs in two scenarios: one is under thermodynamic equilibrium between two or more substances (Equilibrium Fractionation), and the other is in a dynamic environment such as during chemical reactions or physical processes (Kinetic Fractionation) that influence isotope distribution.

Equilibrium fractionation is used as isotopic paleothermometers or climate proxies. This type of fractionation is primarily influenced by changes in vibrational energy, notably zero-point energy, which occurs when a heavier isotope replaces a lighter

one in a molecule. A more massive isotope requires higher energy to move, resulting in lower vibrational frequencies and thus reducing the molecule's zero-point energy (Young et al., 2002). Light elements such as hydrogen, carbon, nitrogen, oxygen, and sulfur are particularly sensitive to these vibrational energies and experience more significant fractionation compared to elements with a higher atomic number. because they require less energy to utilize.

Kinetic fractionation, on the other hand, is direction-dependent away from isotopic equilibrium (Young et al., 2002). Organisms preferentially use lighter isotopic species (^{32}S and ^{16}O). The pathway and extent of microbial activity are then recorded. Sedimentary pyrite formation results from organic matter degradation by sulfate-reducing bacteria (Schippers and Jørgensen, 2002).

Pyrite is depleted in heavy isotopes and relative to sulfate due to microbial sulfate reduction, which fractionates against heavy isotopes. Microbial fractionation shapes pyrite's isotopic character: low (or even negative) ^{34}S and low $\delta^{18}O$ (Price and Shieh, 1979). Pyrite formation processes collect lighter isotopic species (^{32}S and ^{16}O), left heavy isotopes concentrated environment that evaporites form from. Evaporites have isotope compositions associated with the ancient oceans. Heavier isotopes are left behind, resulting in evaporites that consistently exhibit high $\delta^{34}S$ and $\delta^{18}O$. Therefore, using both sulfur and oxygen isotopes can help in understanding sources as these processes enhance each other to the different values though fractionation processes and these sources plot in separate regions of $\delta^{34}S$ and $\delta^{18}O$ (Fig.5)(Calmels et al., 2007)(Li and Ji, 2016).

1.4.3 Overprinting Processes

Secondary overprinting (such as sulfate reduction) and additional sources (for example atmospheric deposition) may complicate the interpretation of results based on oxygen and sulfur isotope ratios. Overprinting processes can obscure the original isotopic information from the source. Sulfate reduction is a major metabolic process that occurs in anoxic environments (Schippers and Jørgensen, 2002). Although it is particularly significant and intense in marine sediments, it can also occur in terrestrial settings. In these processes, sulfate serves as a key electron acceptor for respiration (Wing and Halevy, 2014).

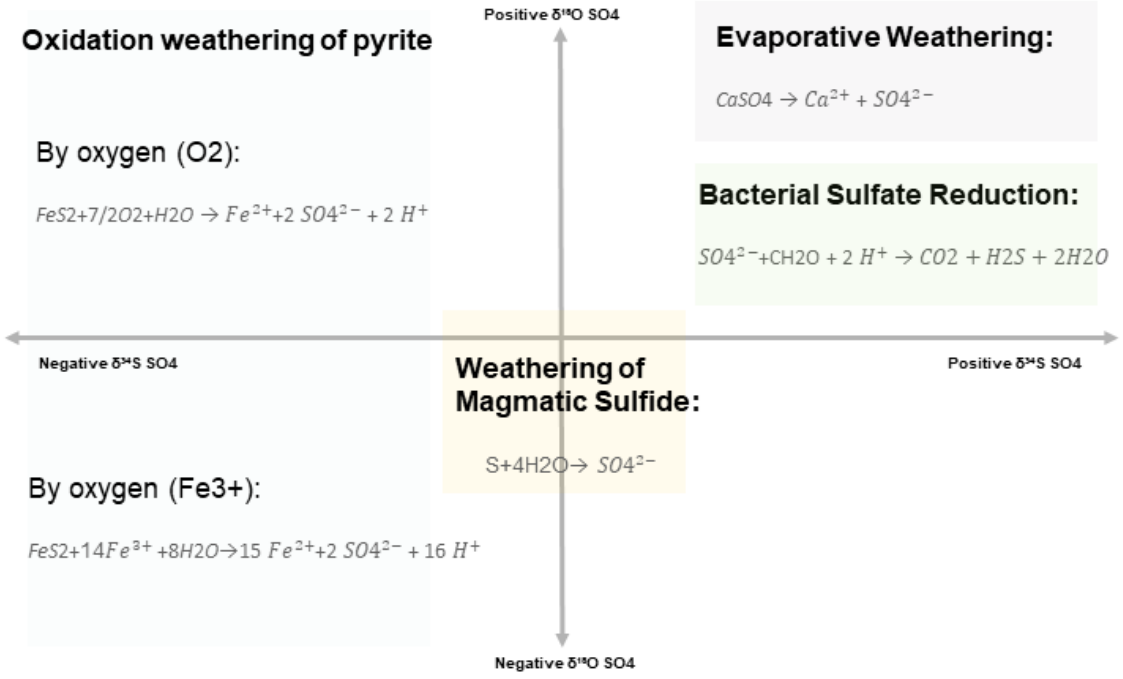

Figure 5: Sulfur-oxygen isotopes values present mineral weathering sources of riverine sulfate (Turchyn et al., 2013).

The general reaction formula for bacterial sulfate reduction is:

$$\mathrm{SO_4}^{2-} + 2\,\mathrm{CH_2O} \longrightarrow \mathrm{H_2S} + 2\,\mathrm{HCO_3}^{-} \tag{17}$$

Here, CH_2O represents organic matter (e.g., simple carbohydrates) used as an electron donor by the bacteria. This process reduces sulfate to hydrogen sulfide (H2S), which is significant in biogeochemical cycles.

Additionally, isotope ratios can vary due to processes occurring during transport, such as the addition of sources (e.g., from atmosphere) into the system and mixing. Isotope compositions within a compound can also be altered during transport by chemical reactions, such as oxidation by environmental oxygen (Hemingway et al., 2020). This is also a reason why the measured oxygen isotopes $\delta^{18}O$ in dissolved sulfate are adjusted by subtracting the environmental water $\delta^{18}O$ in this research .

2 Research Question

2.1 Motivation and Current Research Gap

Mechanisms of biogeochemical cycles, including the sulfur cycle, whether natural or influenced by human activities, are complex (Jacobson et al., 2000). Although the understanding of S-cycling in both geology and microorganisms has improved gradually (Yu et al., 2023), there are still important aspects that need to be further explored (Jørgensen, 2021). Research on these multifaceted biogeochemical processes in the Earth system is essential because these cycles play a pivotal role in regulating climate of Earth, surface environment, ecological systems and Earth paleoenviroment rebuilt, these knowledge are crucial for interpreting past exchanges, current states, and predicting the future of the Earth system with or without human interaction (Jacobson et al., 2000). The biogeochemical cycling of sulfur in terrestrial ecosystems is vital for regulating environmental processes, from influencing river chemistry to global climate patterns (closely related to the carbon cycle) (Torres et al., 2016). The modern riverine sulfur isotopic composition also provides information that helps estimate chemical weathering fluxes (Burke et al., 2018), which is useful for most processes on Earth's surface, not only involving sulfur (Burke et al., 2018).

However, clarifying and quantifying the source of sulfur in river water is challenging. Because in large mixed lithology basins, many factors contribute to affecting the cycle. Parts of the large river system have been researched, especially rivers in Europe, USA and Asia (Zak et al., 2021), but to fully understand the general mechanisms and build the geochemical database still requires more data all over the world; the more data we have, the better interpretations we can make (Martin et al., 2022; Klöcking, 2023). Even though the sulfur cycle is important to consider, it has not received as much academic attention as the carbon cycle. Worldwide, research on sulfate did not gain prominence until 2000, and the volume of published papers is still relatively low (Zak et al., 2021).

Among the limited research on the sulfur cycle, studies about tropical environments are even less. Chemical weathering, a slow but continuous process, occurs when water or an acid reacts with the minerals in the original rock, transforming them into secondary minerals (Goldich, 1938). Intensity of weathering accelerates in warm, humid climates, such as the humid tropics environments (Dinis et al., 2020). The

data from high temperatures, humid conditions, and lush vegetation can contribute to a better understanding chemical weathering. This high weathering rate makes tropical environments important on a global scale, as they occupy about a quarter of the Earth's land surface and provide large amounts of dissolved silica due to their large land area and high weathering rates(Turner et al., 2010). Therefore, studying biogeochemical cycles in tropical environments is important.

Earth science research within the Congo Basin offers a valuable opportunity for scientific exploration, given that the Congo represents one of the most under-explored major river basins globally (Alsdorf et al., 2016). With the second-largest tropical forest in the world, biogeochemical studies of the Congo Basin is insufficient, resulting in a gap in foundational data essential for informing global Earth system models (Barthel et al., 2022). The Kasai Basin, one of the most water-rich sub-basins of the Congo River Basin (Mushi et al., 2019), presents a unique opportunity to explore the intricacies of the sulfur cycle under diverse environmental conditions. Currently, there is no sulfur isotope research related to the Kasai Basin, nor such large numbers of systematically collected samples. This research is poised to significantly enhance our understanding of sulfur cycling in tropical river systems and to dissect and understand the mechanisms controlling the sulfur cycle within this basin. And further contributes to the local carbon flux research and global biogeochemical modeling.

2.2 Main Research Questions

The main research question of this master's project is to understand the mechanisms of the sulfur cycle using water samples from the Congo Basin. This includes determining the sources of sulfur and the operation of overprinting processes. The overarching question guides the investigation towards a comprehensive understanding of sulfur dynamics within the basin, incorporating both lithology and biology influences. 32 tributaries in Congo Basin were sampled, and both river chemistry and dissolved sulfate were analysed to answer the research question with two sub-questions.

Specifically, the main research question of this master project is:

> **What are key mechanisms of the sulfur cycle as analyzed through dissolved sulfate in water samples from the Congo Basin?**

Sub-question 1:

What are the predominant sources of sulfur in the Congo Basin?

This inquiry aims to identify and quantify the various sources contributing to the sulfur inventory in water systems of the Congo Basin.

Sub-question 2:

How do overprinting processes operate to modify the original sulfur signatures in the basin?

Focusing on the post-depositional alterations, this question investigates the secondary processes that modify the sulfur isotopic and concentration signatures from their original state. This includes exploring the roles of microbial reduction activities, oxidation reactions, interaction with organic matter, and the impact of hydrological pathways that may either dilute or concentrate sulfate ions, thereby altering the isotopic composition and revealing insights into the geochemical and biogeochemical cycling of sulfur within the Congo Basin.

3 Study Site

The main studying site of this research is the Congo River Basin (Fig.6). The majority of river water samples analyzed in this research were collected in its sub-basin, the Kasai River Basin, the largest sub-basin in the southwestern part of the Congo River Basin (Tshimanga et al., 2022).

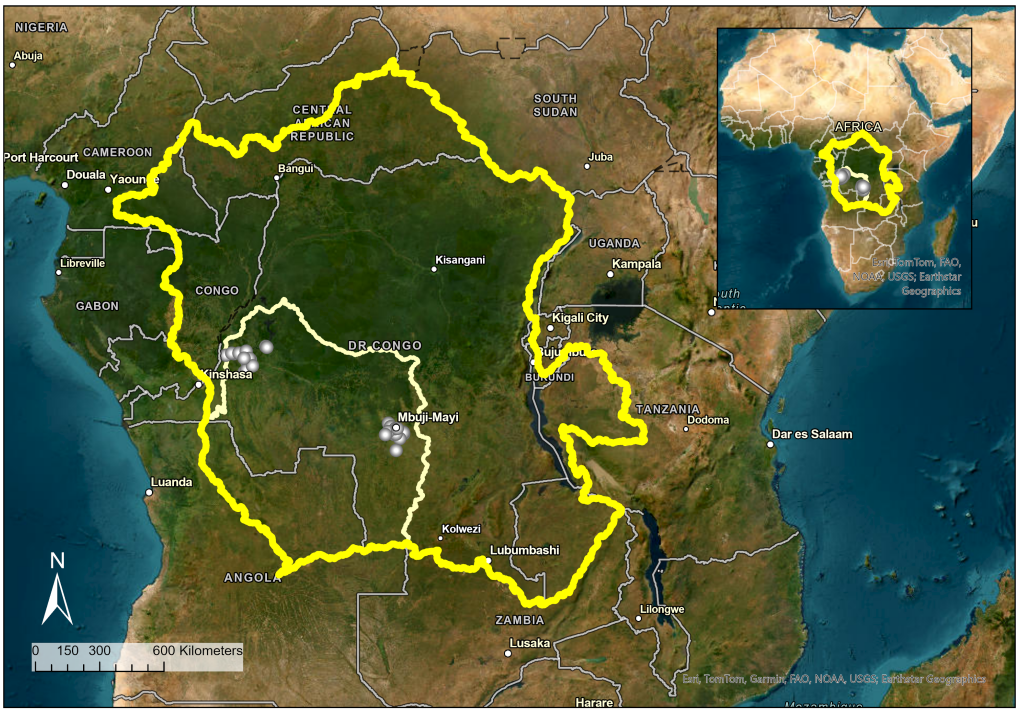

Figure 6: Study site and Sampling points location map.
The deep yellow line is the boundary of the Congo River Basin and the light yellow line lines the Kasai River Basin. Points present sampling locations.

3.1 Congo Basin

The Congo River Basin is the largest river basin in Africa and the second-largest in the world, it outlets enormous freshwater to the oceans with average discharge of 41000$m_{3/s}$ (Tshimanga et al., 2022). As one of the most prominent and significant tropical river basins, the Congo Basin holds substantial research value for understanding biogeochemical cycles in tropical environments (Bauters, 2018).

The Congo Basin is located in Central Africa, situated between latitudes 9°N and

14°S and longitudes 11°E and 31°E (Mushi et al., 2019), covering an area of around 3.7 million square kilometers (Alsdorf et al., 2016). It is bounded by elevated terrains to the north and south. Its eastern boundary is defined by the high peaks of the Albertine Rift, and the Angola Plateau to the south affects the drainage of the Kasai and other southern tributaries of the Congo River (Tshimanga et al., 2022). The basin extends from the Upper Congo's source in the eastern highlands, through the Kasai region and the Oubangi territories, and westward to the lower Congo, where the river ultimately flows into the Atlantic Ocean (Harrison et al., 2016).

Archaean and Proterozoic metamorphic basement rocks are distributed in the northern and eastern parts of the Basin, whereas the southwestern parts are composed of Mesozoic and Cenozoic sedimentary rocks (Bayon et al., 2019). The basin predominantly rests on the Precambrian Congo Craton, part of the ancient core of the African continent (Geological Atlas of Africa, 2008). This craton comprises extremely old rock formations, some dating back approximately 2 to 3 billion years. Surrounding and, in some areas, overlaying the craton are sedimentary basins filled with deposits from the adjacent highlands over millions of years. The Congo Basin is characterized as a composite and complex basin (Geological Atlas of Africa, 2008). These sediments, which include sandstone, shales, and conglomerates, have been deposited by the rivers traversing the basin. The central area of the Congo Basin, known as the Cuvette Centrale, is a vast depression filled with these sedimentary deposits, crucial to the basin's hydrology. The geological history of the Congo Basin features periods of tectonic stability interspersed with episodes of uplift and volcanic activity, particularly along its eastern margins influenced by the Great Rift Valley of East Africa. This tectonic activity has shaped the physical landscape and contributed to the formation of rich mineral resources, including diamonds, copper, and cobalt, which hold significant economic importance for the region (Milesi et al., 2006).

The climate of the Congo Basin is characterized by a humid tropical climate with a consistent Atlantic monsoon influence. The interannual average temperature is 26.1°C, with daytime averages reaching 37 to over 40 degrees (Sonwa et al., 2020). Positioned in a year-round humid equatorial region, the basin experiences annual rainfall exceeding 1000 mm, sometimes surpassing 2000 mm (Dinis et al., 2020). Evapotranspiration rates within the basin vary from as low as 800 mm annually in the southern Lualaba Basin to as high as 1200 mm in the eastern Oubangi

Basin, with evapotranspiration typically accounting for 75 to 85% of the total annual precipitation across the region (Creese et al., 2019).vegetation cover of the Congo Basin is characterised by large area of rain forest, which contains dense moist forest, submonatene forest, rural complex and young secondary forest, with a large area of wet lands. The South area dominated by grassland, also called savanna land, is covered by shrub, grass, swamp, woodland and sparse vegetation (Verhegghen et al., 2012).

3.2 Kasai River Basin

The Congo River provides around one-third of freshwater resources in Africa(Harrison et al., 2016), most water sources (65% of the Congo Basin) are stored in southern-most sub-basins Kasai (220-228 km_3) and Ubangi (109-169 km_3) (storage capacity) (Tourian et al., 2023). The length of Kasai River is approximately 2,153 kilometers, and its drainage basin covers over 890100 square kilometers, which is the largest sub-basin (km_2) among sub-basins of the Congo Basin (Lomami, Lower Congo, Middle Congo, Ruki, Sangha, Oubangui) (Alsdorf et al., 2016). The Kasai River Basin serves as an excellent research point due to its diverse geological formations, ecosystems, landscapes, and minimal human impact.

The ecosystem of the Kasai Basin is notably diverse, dominated by both rainforest and grassland (Savanna). Land is covered by dense forest flooded dense forest, open forest woodland, shrubs, grassland, cropland and cities and bare soil(Bayon et al., 2019). The rainforest, including wetlands, is primarily located in the lowland areas of the northern part of the basin. In contrast, the Savanna covers the southern part of the basin. Human activities modified lands (cities and croplands) mostly distributed around the Kasai river channel (Tshimanga et al., 2022).

The Kasai basin varies in elevation and slope from north to south. Ranges are mainly distributed in the southern part of the basin, and the northern is low in elevation and very flat. The primary control of solute chemistry is attributed to lithology (Gaillardet et al., 1999), and conversely, dissolved ion concentrations provide insights into the types of minerals that were weathered and dissolved into the river system. The basement of the study area includes the Congo Craton with Kasai Craton, overlaid by Cretaceous sediments (Roberts et al., 2015), which predominantly consist of continental clastic sediments (Schluter, 2006) and consist by thick Paleozoic marine formations and overlying Mesozoic-Cenozoic lacustrine

rocks(Alsdorf et al., 2016).

Sedimentary coverage in the Kasai portion of the Congo Basin is categorized into several distinct depositional sequences (Roberts et al., 2015):
The Permo-Carboniferous period features glacio-lacustrine deposits.The Jurassic era is characterized by arid to semi-arid laminated shales, siltstones, aeolian sandstones, ephemeral lake and sand dune sequences, interspersed with loess deposits, and occasional fluvial channels, associated with the Lualaba-Lubilash and Stanleyville Groups. The Lower Cretaceous consists of fluvial sandstone deposits rich in heavy minerals and sometimes basal conglomerates, linked to the Loia Group and the Calonda Formation.The Upper Cretaceous includes alluvial fan conglomerates that transition into laminated shales and siltstones or well-sorted and rounded, fine-grained sandstones typical of a semi-arid to arid environment with ephemeral lakes and small aeolian dunes, correlated with the Kwango Group. Paleogene is noted for its fluvial, aeolian, and lacustrine sediments, associated with parts of the Kalahari Group.

4 Methodology

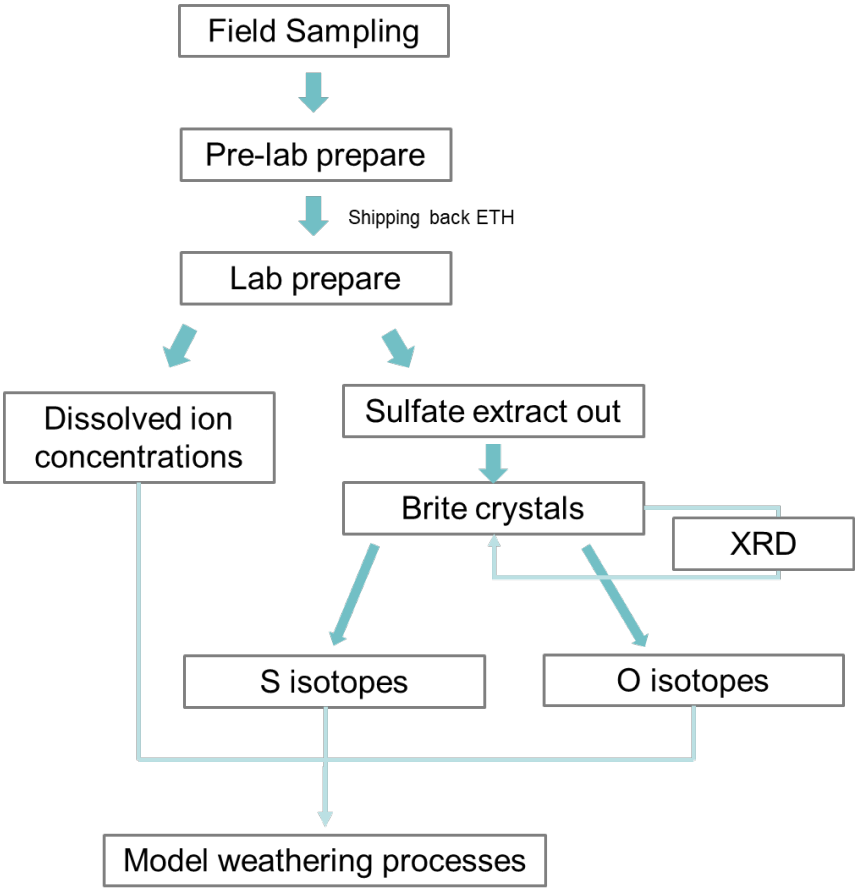

Figure 7: Flowchart of the experimental and analyse processes of this research

4.1 Field Sampling

River water samples from the Congo mainstream near Kinshasa and Kasaï River with its main tributaries, were systematically collected between 2022 to 2023. Each sampling location (Fig.6) is carefully designed to provide the best coverage of the study area and to represent the different environments within the study area, helping analyze the environmental impact. Collection efforts prioritized capturing the peak hydrological dynamics, offering a comprehensive understanding of the river system's biogeochemical behavior. Even though sampling points seem closely related in geography, the watersheds area they cover varies much, therefore they can generate much information about the S cycles.

River Name	River Lable	River Name	River Lable
Congo	R1	Lukala	R17
Kasai	R2	Kakangala	R18
Monkaba	R3		R19
Mbola	R4	Lubilanji	R20
Fimi	R5	Nkatshia	R21
Lobuia	R6	Mudiva	R22
Lukenyi	R7	Muswaya	R23
Leboma	R8	Bufa	R24
Kwilu	R9	Monzo	R25
Kwango	R10	Senga	R26
Kasai	R11		R27
	R12		R28
Lewana	R13	Lwilu upstream	R29
Bongono	R14		R30
Biemi	R15	Lubi	R31
Mbuma	R16	Mbuji Mayi	R32

Table 2: The river name and paired label in this study

Aqueous samples are meticulously and efficiently collected ensuring samples unpolluted and minimal atmospheric exposure. In each sampling point, river water was primarily sampled from the surface at the center of the channel, then stored in an acid-cleaned plastic bottle. Due to the low concentration of dissolved sulfate in studied rivers, more than 100 L of river water was collected to ensure there will be enough barite for later isotope analyses. After collection, all the river samples were kept in cool and dark environment and transported to the local lab as soon as possible.

All river samples were given a unique code for better identification. The main Congo river is marked as R1, and its main tributary, Kasai River sample is labeled as R2. Other 30 river samples are labeled from R3 to R32. As shown in 6, the distribution of sampling points concentrate roughly in two areas: a group (R3-R16) that covers by rain forest in the northern parts of the Kasai Basin, another group (R17-R32) that is dominated by savanna and located in the central of Kasai Basin. In addition to river water, two rainwater samples (P1 and P2) were also collected.

4.2 Laboratory Operations

4.2.1 Laboratory pre-processing in Congo

When arrived the local lab, river samples were filtered within 24h to minimise oxidation, evaporation, and dissolution of suspensions. Raw river water was salvaged and passed through a pre-cleaned 0.2 um polyethersulfone (PES) filter that pre-wetted by corresponding river water to remove any suspended material (such as sediment particles, live or dead particulate organic matter) (Lloyd et al.,2022). pH, dissolved oxygen, conductivity, and temperature were measured in-situ using a YSI multimeter, and alkalinity was determined in the field on $\tilde{1}$00 mL of filtered water using the Gran titration method. Then the filtered water samples were stored unacidified in pre-cleaned (rinsed 3 times with filtered river water) 125 mL HDPE bottles for several purposes: 1) For dissolved carbon and ion concentrations analyses, around 5L filtered river water of each samples was sealed and stored in fridges as soon as the aliquoting finish, prepared to been shipped back to Zurich. 2) More than 10L of the filtered water were loaded on the pre-conditioned columns (ion exchange resin, which contained 5ml Dowex 1X8-200, 100-200, anion exchange resin) to reserve and concentrate the dissolved sulfate ($SO_4{}^{2-}$) for subsequent isotopes analyses.

Around 15-20 L of filtered water was additionally passed through an anion exchange resin cartridge containing 3g of Dowex 1X-8 anion exchange resin (chloride form; pre-cleaned with 3 times column volumes of 8M nitric acid, 3 times column volumes of 3M HCl, 3 times column volumes of MilliQ water, to avoid pre-sampling pollution). Once finished collection of sulfate in each river water sample by exchange resins, resins were all well sealed by plastic film, carefully labeled, and stored in the fridges at 4 degrees. The reason refrigerated samples is reducing the temperature restrain the microbial activity within the sample to limits the damage and pollution from bioactivities. All these samples were shipped back to the ETH lab when the last sample is done.

4.2.2 Laboratory analysis in ETH

Before starting laboratory analysis, resin columns were kept sealed and refrigerated. In the controlled clean lab environment, sulfate ions are meticulously eluted out from the Dowex resin column by performing the standard rinse operation three times, using 60 mL of 0.8 M distilled hydrochloric acid (HCl) (*Dowex Ion Exchange Lab Guide*).

Once all the dissolved sulfate is washed out from the resin columns, the extracted sulfate solution was then mixed with barium chloride ($BaCl_2$) to initiate the precipitation of barite ($BaSO_4$).After standing overnight, the solutions were acidified to pH 3 with 6 M HCl in order to remove BaCO3 (Back dissolved phase and leave $BaSO_4$) and other extraneous anions, such as nitrate.

Further purification of the sample is necessary because the co-precipitation of organics and/or nitrate in the sample could interfere with subsequent oxygen isotope analyses. Therefore, barite is dissolved in 10 mL of 0.05M Ethylenediaminetetraacetic acid (EDTA) (Chen et al., 2008). A controlled re-precipitation is conducted by cautiously adjusting the pH to the 3–4 range by adding more $BaCl_2$. After standing for more than 24h, crystals were cleaned by ultrapure water 3 times with centrifuge (15000rpm/min). Clean barite crystals were finally dried 30h at 60°C in clean laboratory oven to prepare for isotopic ratio analysis.

4.3 Analytical Techniques

4.3.1 XRD Analyses

Confirmation of the prepared crystals from the is pure barite is the essential prerequisite analyse for accurate isotopes analysis result. The crystalline phases and their spatial distribution can be identified by X Ray Diffraction (XRD) techniques (Poonoosamy et al. 2016). Therefore, the XRD analyses is applied on all lab-born barite from Congo River samples, in order to ensure crystals for isotopes analyse are pure barite. The diffractometer in ETH lab was a microprocessor-controlled PANalytical X'Pert PRO MRD, Cu-K radiation and a scan recording in the 2θ angle range between 5 and 50 degrees.

Barite crystal powder were smashed in the fine grain powder with cleaned Agate Mortar and Pestle for precise XRD scanning. After grinding , XRD sample preparation end up by carefully applying the powder on to the alcohol-cleaned special tray.To clear the crystalline phases and their spatial distribution, selected areas of the sample tray were scanned with an intense micro focused X-ray beam at a photon energy of 17.04 keV. a single element Si drift diode (SDD) detector collected the fluorescence signal reflected from the sample crystals. Once all the signals were collected, the measurement data were performed at the microXAS beamline using

the XRDUA software for data analysis.

Standard mineral files of the Crystallographic Open Database (COD, 2017 version) with diffraction diagrams were compared with the result of the Congo river samples, to identify if it is pure barite.

4.3.2 Sulfur and Oxygen Isotopes Analysis

Coupled sulfur and oxygen isotopes values (δ^{34}S and δ^{18}O) were identified though isotopes analyse, to estimate sulfur-containing minerals weathering fluxes in individual river catchments (Burke et al., 2018).

After the XRD analyse confirmed that all barite are clean, the isotopes analyses followed up. The pivotal isotopic ratios (δ^{34}S and δ^{18}O) in dissolved sulfate are assessed utilizing gas source isotope ratio mass spectrometers (GS-IRMS) located in the earth surface Laboratory at ETH.

The isotopic compositions of δ^{34}S were determined by the following steps (Bernasconi et al., 2017): First wrapped 200–300 µg of powdered and homogenized sample in tin capsules with an equivalent amount of V2O5. Then converted them to SO_2 in a ThermoFisher Flash-EA 1112 coupled with a ConfloIV interface to a ThermoFisher Delta V isotope ratio mass spectrometer (IRMS). The method was calibrated with the reference materials NBS 127 (δ^{34}S = +21.1‰) and IAEA-SO-5 (δ^{34}S = +0.49‰) and IAEA-SO-6 (δ^{34}S = 34.05‰) distributed by the International Atomic Energy Agency. The unit of all the δ^{34}S data in this study is ‰VCDT, which is short written in ‰in the following parts.

The measurement of δ^{18}O is similar to the δ^{34}S lab operation processes (Brand et al., 2009): Wrapped 200–300 µg of powdered and homogenized sample in silver capsules with an equivalent amount of graphite. Then converted them to co_2 on a Thermo FlashSmart OH EA (graphite furnace operated at 1450 degrees, helium as carrier gas), and measured on a Thermo Delta V plus IRMS. Calibrated with the same international standards as for δ^{34}S . The unit of all the δ^{18}O data in this study is ‰VSMOW (Vienna Standard Mean Ocean Water; the precisions were 20.9 ± 0.5 and 0.0 ± 0.1 ‰ for δ^{34}S and δ^{18}O, respectively (Brand et al., 2009)).

It is important to be noticed that the oxygen isotopes used for interpretation in this

Ions	Ranges(ppm)
Na	2.5-10
K	1-4
Mg	1.65-6.6
Ca	1.65-6.6
Cl	0.5-5
SO4	0.3-3

Table 3: Standers used in the IC measuring operation

study is $\Delta d^{18}O$, which is the difference between measured δ^{18}O in dissloved sulfate and environmental water δ^{18}O. This is applied to avoid the effect of oxidation of the water (Hemingway et al., 2020) in analysing processes.

Prior to analysis, the IRMS is calibrated using international standards with known δ^{34}S and δ^{18}O values to ensure accurate isotopic measurement. Quality control includes the analysis of laboratory standards, blanks, and duplicates. The standards are selected to cover the range of isotopic compositions expected in the samples. Blanks assess the background levels of contaminants, and duplicates check for the precision and reproducibility of the analysis. Repeated measurements is employed to minimise the random errors in data. Samples were measured in duplicate (for δ^{34}S) or triplicate (for δ^{18}O), and results are the average of all replicates. Standards samples were periodically interspersed (between every 10 samples) in the analysing sequence in order to minimise the measurement error or shift through measuring processes.

4.4 Dissolved ions analysis

The dissolved ion concentration results reveal a distinct ionic profile for each sampled stream, reflecting the intricate interplay between geological substrates, hydrological processes, and ecological interactions within the watershed (Depetris, 2019).

Dissolved ion concentrations were measured by an ion chromatograph (Dionex Aquion with Dionex AS-DX) at the ETH lab. Standards for ion analyses were prepared and diluted to the proper concentration to cover the entire range of real samples with an appropriate gradient (Table3). Anion concentrations were measured using a Dionex AERS500 with 20 mmol methanesulfonic acid; cations were analyzed using a Dionex CSRS600 4 mm with 9 mmol sodium carbonate.

4.5 Modeling weathering processes in MATLAB

In order to distinguish contributions from various end-members, a mixing model with Monte Carlo uncertainty propagation, originally built up by Kemeny and Torres (2021), is modified and applied in this research dataset. The data of dissolved chemistry (Mixing elements and Isotopes) of rivers and a set of MATLAB scripts (MEANDIR) able to provide a reasonable dissolved river chemistry, and further understanding in the chemical weathering of the studying area(Kemeny et al., 2021a).

The MEANDIR inversion model was applied to partition measured solutes between different sources. This set of MATLAB scripts enables a highly customizable inversion of riverine dissolved elements with Monte Carlo propagation of uncertainties (Kemeny et al., 2021a). Before performing the inversion, the range of possible end-members were defined, as shown in Table 4, which includes carbonate, silicate, evaporites, and ocean water. Carbonate rock is mainly composed by carbonate minerals ($CaCO_3$) and dolomite ($CaMg(CO_3)_2$). The evaporate end-member reflects the stoichiometric combination of gypsum ($CaSO_4 \cdot 2\,H_2O$), halite (NaCl), and secondary contributions such as epsomite and sylvite. The ocean water composition is based on the generally agreed academic data of modern ocean water.

32 samples with all the data required for the requested inversion were put in to the model, with solving simulation with mldivide optimize imported river data. The model runs 100000 simulations with data source with variables Ca, Mg, Na, Cl, $SO_{42}{}^{-}$, Alkalinty, δ^{34}. Instead of absolute concentrations, normalized molar ratios input into the model, with or without the alkalinity and the S isotopes data. Elements ratio permit the comparison between rivers draining areas of high runoff (main Congo channel and Kasai river) and rivers draining arid areas (mainly in the Savanna area).

The simulation results that present finally were picked, once a simulation is decided as 'successful'. The selection process prioritizes simulations that closely match observations by retaining only those with the lowest misfit. It employs two key strategies: isolating the best fitting simulations for individual samples or the entire set, and a "sample matching" criterion that accepts simulations based on their ability to replicate observed data within a specified precision. For isotopic data, MEANDIR ensures accuracy by comparing the absolute difference between observed and modeled values against user-defined limits, thus ensuring simulations are both

Elements	Carbonates	Silicates	Evaporate	Ocean water
Ca min	0.5	0.039	0.0	0.09
Ca max	1.0	0.6	1.0	0.11
Mg min	0.00	0.0	0.0	0.048
Mg max	0.5	0.5	0.0	0.058
Na min	0.0	0.209	0.0	0.422
Na max	0.0	0.670	1.0	0.516
Cl min	0.0	0.0	0	0.491
Cl max	0.0	0.0	1.0	0.601
SO4 min	0.0	0.03	0	0.025
SO4 max	0.0	2.0	1.0	0.031
$\delta^{34}S$ min	10	-30	10	20.70
$\delta^{34}S$ max	30	10	35	21.30

Table 4: The ranges of each input end members for the model

precise and and representative of observed conditions.

To achieve the best fit in result, 4 scenarios of simulations were applied in the model, which are 1): contains all the data that listed in Table. 2): contains all the data expect the alkalinity. 3): contains all the data expect the isotope values. 4): contains all the data expect neither alkalinity nor isotope values.

4.6 GIS visualization and Data Analyses

The Congo River Basin has an incredibly large and complex river system with complex correlations between individual rivers. The spatial distribution of boundaries, altitudes, slopes, and areas of the catchments or sub-watersheds was processed and overlaid in ArcGIS 9.0 software.

Catchment areas of each sampled river were defined using the 'watershed tool package' in the specialized analysis tools of ArcGIS Pro software. The watershed area can be calculated by inputting the coordinates of each sampling point. This hydrological analysis integrated digital elevation models (DEMs) to determine the flow direction and accumulation, thus defining the contributing area of each river segment within the system (Miller et al., 2007). By overlaying the flow network derived from elevation data, the tool computed the catchment boundarie. Watershed boundaries for each river were extracted, demarcating the spatial extent from which surface runoff flows into a common outlet, characterizing the river's hydrological influence. The analysis was refined by incorporating river networks and their as-

sociated coordinates, ensuring accuracy in the watershed delineation process. This approach facilitated the analysis and visualization of the interplay between these variables and their impact on watershed characteristics.

The digital elevation model (DEM) data for the study area is downloaded as open-source from the USGS (Verdin, 2017). Other related data, were downloaded from the ArcGIS online database.

5 Results

5.1 Watershed Area

By inputting the geographical coordinates of each sampling location, the watershed areas which are presented on the map (Fig.8). Additionally, hierarchical structures based on their geographic distributions is shown in (Fig.6). Even though the sampling points seem closely related geographically, watershed of each tributary varies, which can provide information about the sulfur cycles in different environments, on both individual and systemic scales.

The R1 and R2 river samples are from the main channels of the Congo River and Kasai River. All tributaries sampled in this study is covered in R2 watershed. Among the 32 sampled rivers, tributaries collect water from different parts of the basin and can be roughly categorized into two groups: I) those sampled in the north part of the Kasai basin (Fig.8b), near the capital city Kinshasa; II) those samples group locates in the east part of the Kasai Basin (Fig.8c).

Thirteen of the sampled tributaries (R3, R4, R5, R6, R7, R8, R9, R10, R12, R13, R14, R15, R16) mainly covered the north rain forest dense area and open forest-Savanna-mix area (mentioned as rain forest group in following parts). Meanwhile, the other 16 samples (R17, R18, R19, R20, R21, R22, R23, R24, R25, R26, R27, R28, R29, R30, R31, R32) covered a relative smaller area in the southeast area of the Kasai Basin that is dominated by savanna (referred to as savanna group in following parts). The R11 sampling point is special because it is sampling point located in the rainforest area, but its watershed area covers all Savanna samples watershed areas.

Watershed areas of sampled tributaries vary not only in geographic location but also in the size of the catchment area (Table.5). The Congo River Basin (R1) has a catchment area of 3,609,877 square kilometers. The second largest is the Kasai River catchment area at 889,326 square kilometers, roughly a quarter of the Congo River Basin. The third largest catchment area is R11 (475,000 square kilometers), which covers all the watershed areas of samples R17 to R32 (savanna group) and a large area of the rainforest. The sizes of other tributary river catchments range from 174,983 square kilometers R10 to 14 square kilometers R30. Watershed areas of savanna group are relatively smaller compared to the rainforest group, with the largest in this region being R20, which covers 42,375 square kilometers.

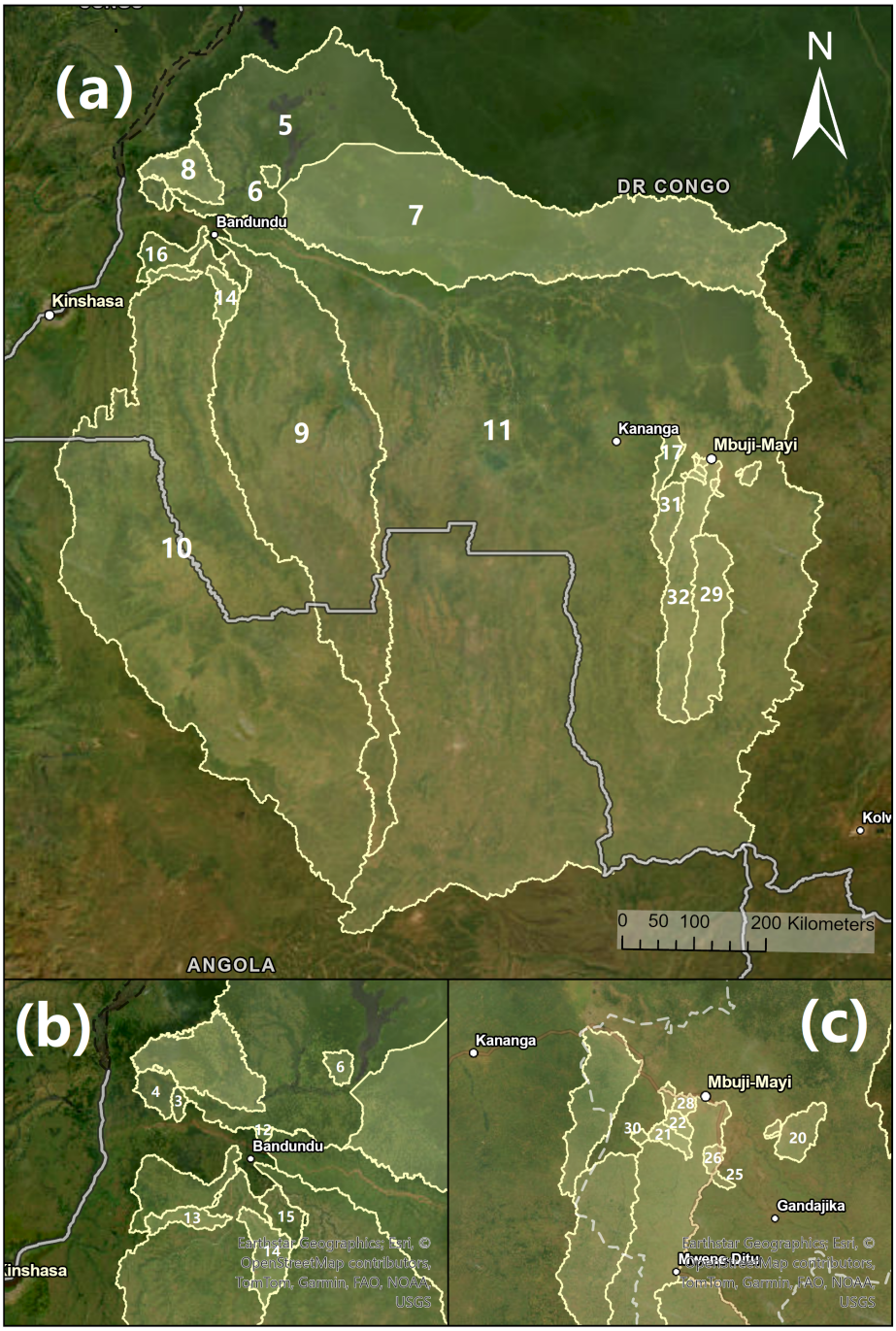

Figure 8: Distributions of catchment area of each sampled tributaries
Because the catchment area varies much, tributaries that have smaller catchment area are detailed present in smaller scale (b) is rainforest group and c) is Savanna area.

River number	Catchment Area (km2)	River number	Catchment Area (km2)
R1	3609877.5	R17	1929.9
R2	889326.4	R18	68.3
R3	300.5	R19	32.4
R4	1049.4	R20	42374.6
R5	135417.3	R21	215.8
R6	537.5	R22	155.26
R7	69184.3	R23	52.0
R8	4752.1	R24	14.6
R9	94313.0	R25	61.3
R10	174983.0	R26	137.8
R11	474905.6	R27	26.6
R12	156.9	R28	113.7
R13	953.3	R29	10801.5
R14	2105.9	R30	14.1
R15	1201.8	R31	3033.7
R16	3317.8	R32	13660.2

Table 5: Catchment area of each sampled rivers

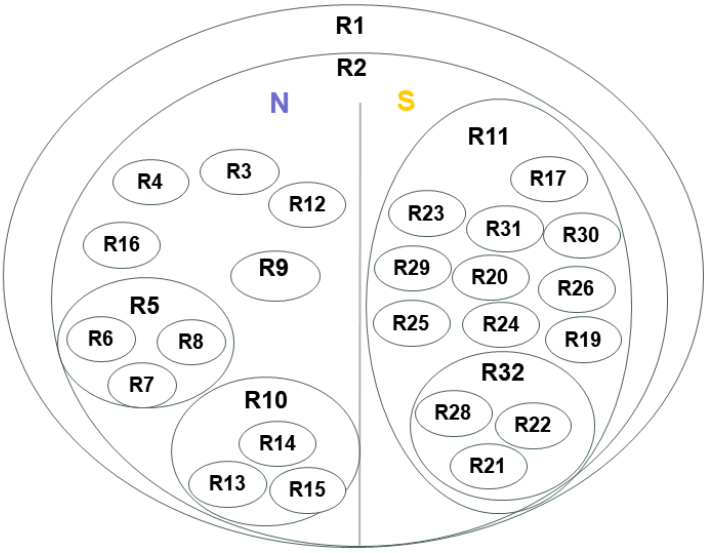

Figure 9: The spatial relationship between catchment areas

5.2 Hydrochemistry of river waters

The average water temperature is 25 degrees, ranging from 28.2 to 22.9 degrees. River water pH values are between 4.0 and 8.3, with a mean value of 6.6; and the river water alkalinity ranges from -72 to 2924 uM. The rain forest area waters are slightly alkaline (average pH 5.6, alkalinity 66.5 uM), whereas the savanna area river samples are more acidic (average pH 7.3, alkalinity 577.6uM). Some samples shows negative alkalinity including R5, R6, R14, R15, while some sample (R20,R22,R27) shows extremely high alkalinity up to 2923.6uM (R20). Dissolved organic carbon in water samples is low, mostly around 1-4 mg/L, expect some rich up to 28 mg/L.

5.2.1 Cations contractions

The cations concentration of each tributaries is presented in (Fig.10). Congo River and Kasai River have similar Ca concentrations, 75.6 μM and 63.1 μM respectively. Calcium ion concentrations (Ca^2+)of tributaries range from 6.5 μM (R28) to 1000 μM (R19) across the Kasai Basin. Calcium ions constitute 41% of the total dissolved ions on average, varies from 15% to 61% between tributaries. In the R3-R16 rainforest area, calcium ions represent an average proportion of 43%, while in the Savanna area, it is 39%. The average concentration of Ca is 38 μM, while the Savanna area has an average Ca concentration of 138 μM. The rainforest area samples are less variable compared to those from the Savanna area, which range from 8.2 μM to 78.9 μM. The highest Ca concentration is in R19, over 1000 μM, followed by R21 (376 μM). Although a 1000 μM concentration of Ca is not extremely high worldwide, the average river Ca concentration is around 93 μM and the long-term median calcium concentrations of central Africa are lower than 150 μM (Tipper et al., 2010)(Weyhenmeyer et al., 2019), making this high Ca concentration an outlier. Excluding R19, the average Ca concentration of the Savanna is 97 μM, which is still two times higher than the rainforest area.

Magnesium (Mg^2+) presents a similar distribution as calcium. The highest concentration is also in R19 (more than 536 μM), followed by R26 (178 μM) and R21 (161 μM). The Congo River's Mg concentration is 83 μM, higher than all samples in the rainforest area. The Kasai River's Mg concentration is 40 μM. The average Mg concentration in the rainforest area is 22.75 μM, and in the savanna, it is 89.64 μM, more than three times higher than that of the rainforest area.

Sodium (Na^+) concentrations extend from the lowest recorded value of 11 μM in sample R9 to a peak concentration of 362 μM in sample R21. The precipitation samples (P1 and P2) show relatively low Na concentrations compared to river samples. The sodium distribution in R2-R18 is relatively lower than in R19-32. Sodium concentrations varied significantly among the tributaries, suggesting variable influences of weathering processes of plagioclase and alkali feldspar minerals.

Potassium (K^+) levels display a similar variation, with the minimum at 10 μM in sample R6 and the maximum at 270 μM in sample R12. K concentrations of some samples (R1-R11) from the northern area are lower compared to those from the southern area. Potassium ion concentration levels were comparatively lower compare to the other cations, indicating its lesser mobility and potential retention within the biotic components of the ecosystem or adsorption onto clay minerals.

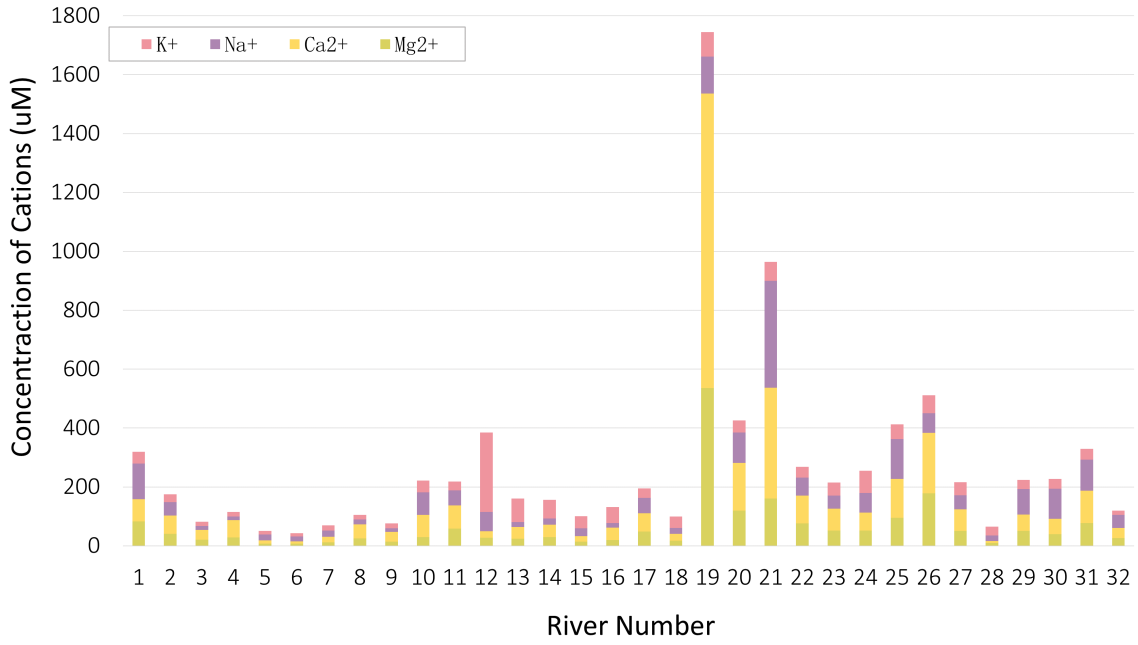

Figure 10: Concentrations of total cations in river waters

5.2.2 Anions concentrations

Chloride (Cl^-) and sulfate (SO_4^{2-}) in water samples is shown in (Fig.11). The total chloride and sulfate concentrations are notably high in rivers R12, R13, R14. Generally, the Savanna area features lower concentrations compared to the rainforest area.

Chloride (Cl^-) displays a variability ranging from a minimum of 6 µM in R27 to a maximum of 156 µM in R12. The Congo Basin water sample is average 32.3µM in chloride concentration. Congo river's chloride concentration in 76.2µM, the Kasai river is half in concentration (36.8µM). The average chloride concentration in rain forest area is 48.8µM, with several top high chloride concentration samples (R12-R16). The average chloride concentration in Savanna area is 14µM.

Sulfate (SO_4^{2-}) concentrations vary from 2.9 µM in R29 to 105 µM in R14 across the dataset. Sulfate concentrations consistently show a high peak in rivers R13 to R16, while concentrations in other rivers range from 2 to 30 µM, only one-fifth of the highest observed value. Meanwhile, concentrations in R18, R20, R22, R25, and R29 to R32 are all below 10 µM.

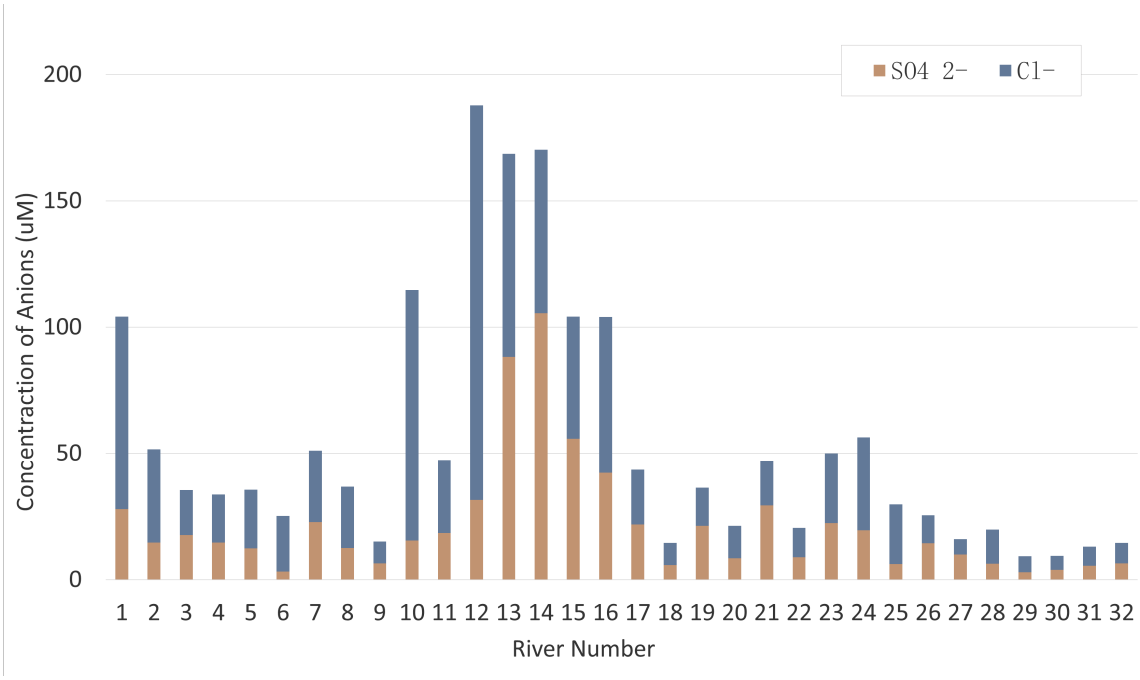

Figure 11: Concentrations of total anions ($Cl^-$and SO_4^{2-}) in river waters

5.3 XRD and Isotopes analyses results

5.3.1 XRD Result

X-ray diffraction (XRD) analysis result (Fig.12) shows all barite extracted from the ion exchange column are pure $BaSO_4$ crystals which is safe to use for the isotopes analysis.

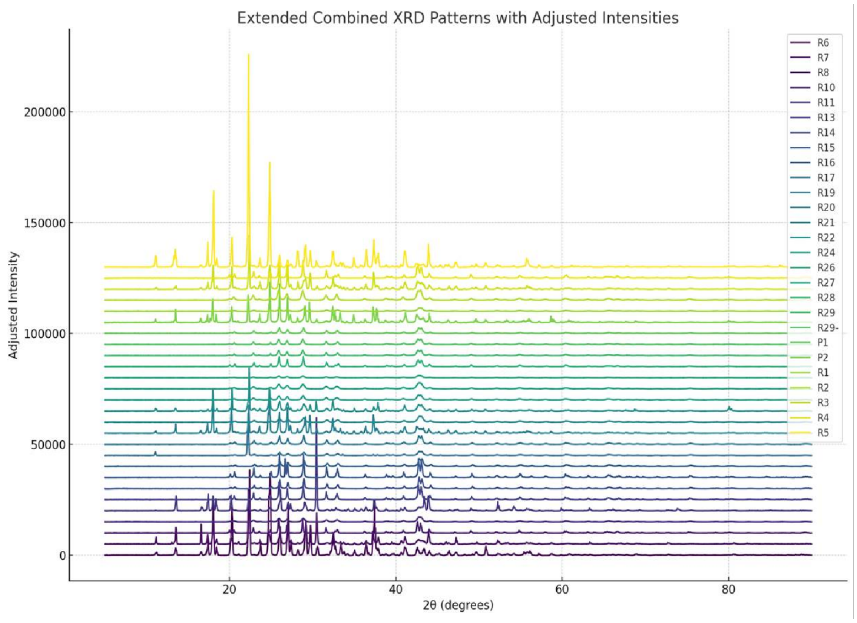

Figure 12: The XRD result of $BaSO_4$ samples

5.3.2 Sulfur and oxygen Isotopes Results

The $\delta^{34}S$ values of rivers in the Congo Basin mostly fall within the range between 10-14 per mil (‰VCDT) (Fig.13), indicating a relatively narrow range of isotopic variation for sulfur within these samples. On a smaller scale, $\delta^{34}S$ values vary among different river systems. The main Congo River has $\delta^{34}S$ value of 11.8‰, which is very close to the average of all sampled rivers (11.67‰). The Kasai River's $\delta^{34}S$ value is higher than that of the Congo, reaching 12.6‰. Some tributaries (R4,R5,R7,R13,R14,R22, and R32) are around 10‰, while R17 to R20, and R26 have higher $\delta^{34}S$ values that reach over 14‰, even up to 16‰(R26). In the rainforest area, only R10 has a $\delta^{34}S$ value higher than that of the Kasai River, and the second highest river is R15. The rest of the rivers in the rainforest area have $\delta^{34}S$ values lower than their main river. In contrast, the $\delta^{34}S$ values in the savanna area show

greater dispersion. The $\delta^{34}S$ values of rivers could indicate a complex interplay of sulfur sources and processes that vary in different environments.

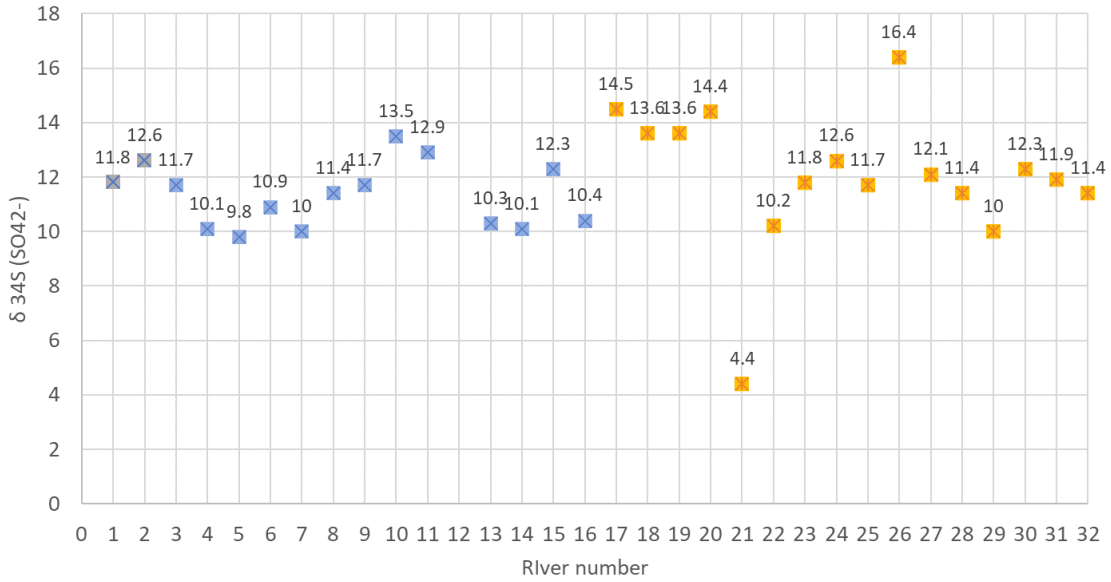

Figure 13: Sulfur isotopes values

The $\delta^{18}O$ value is the isotope composition of sulfate or of water. The difference between sulfate and water, $\Delta\delta^{18}O$ is present in (Fig.14), which is the oxygen isotopes value used in later analyses in this study. Calculated as the difference between sulfate and water, values are concentrated within a range of +8‰ to +12‰ VSMOW across the majority of samples. Δ $\delta^{18}O$ values range from as low as 4.44‰ in River 21 to as high as 13.66‰ in R19. $\Delta\delta^{18}O$ of some samples are relatively slightly higher, above 11‰ (R10, R14, R15 in the rainforest, and the R19, R23, R24, R25 in the Savanna), the lower values are around 9‰ (R4-R9, R16 in the rainforest, and R22, R25, R29 in the Savanna). Such variations suggest a diverse set of processes affecting the oxygen isotopic composition in these riverine sulfates. The Congo River has the $\Delta\delta^{18}O$value of 8.77‰, while the Kasai River is higher (10.88‰). Tributaries R4-R9 in the rainforest area are lower than the Kasai, while R10-R15 are all similar to or higher than the Kasai.

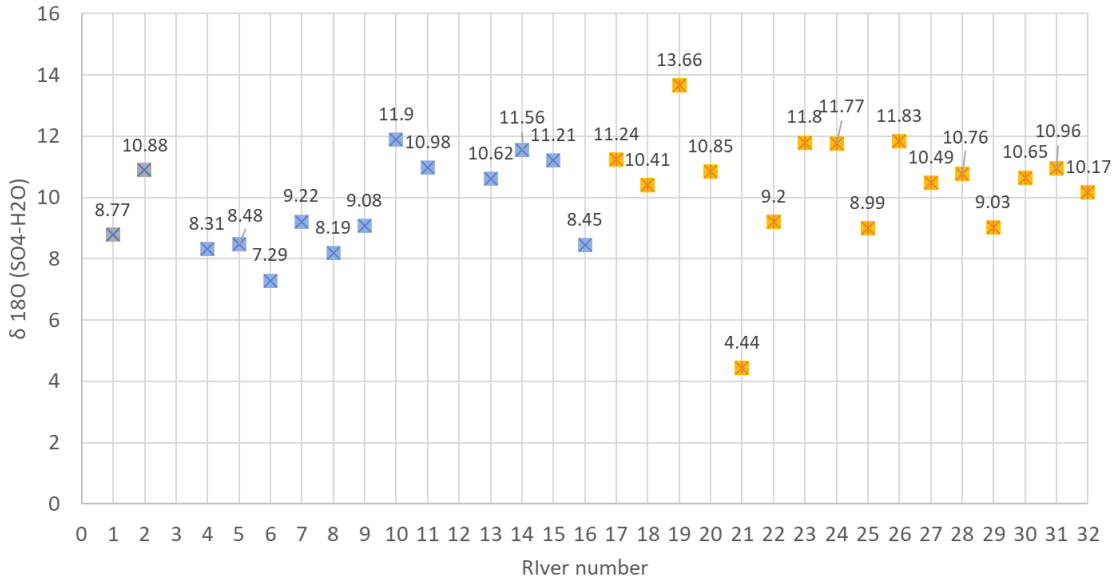

Figure 14: Oxygen isotope distribution

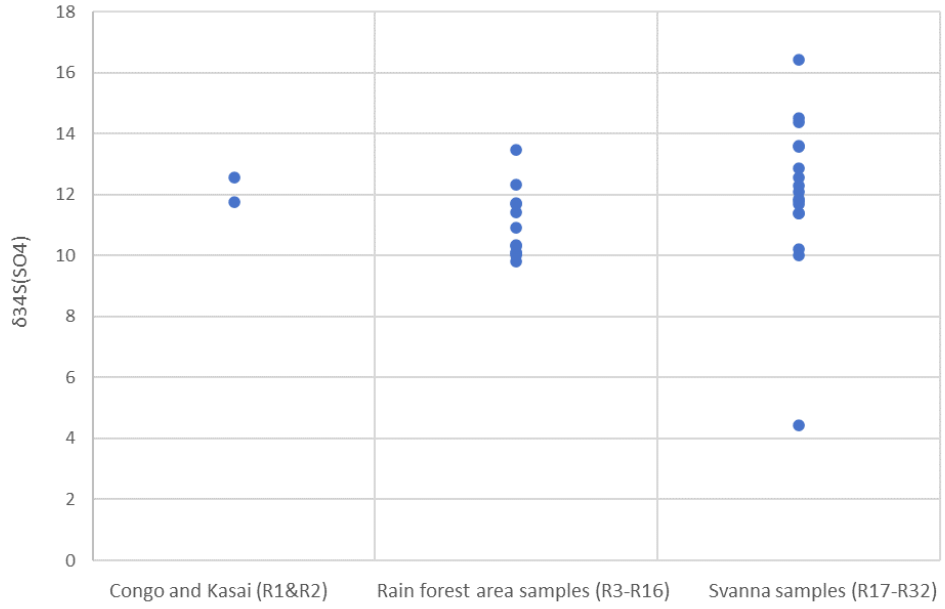

Figure 15: Rain forest group is slightly differ from the Savanna group samples in $\delta^{34}S$ distribution

5.4 Rain Forest versus Grassland Area

When comparing sulfur isotopes values between the two areas, we can see that the Savanna area has more diversity in isotopes values. Both the Congo River and Kasai River have $\delta^{34}S$ around 12‰, and tributaries concentrates around this number. But the rain forest area slightly lower $\delta^{34}S$ compare to the grassland.

6 Discussions

6.0.1 Weathering Fraction Compositions

The majority of the riverine sulfur dissolved load integrates contributions from three lithologies through weathering processes: silicate, carbonate, and evaporite rocks (Burke et al., 2018). Therefore, the model is established to quantify carbonates, silicates, and evaporites in the study area, with additional atmospheric contributions affecting riverine sulfate. The inverse modeling results, based on mixing weathering processes, refine compositions of each end-member and concentration to the river sulfate by calculating the best fit to the river samples. Comparing all sections of the modeling results, the scenario using ion concentrations and sulfur isotopes without the alkalinity data fits the observed facts best. Alkalinity data often confuse the model due to the presence of heavy organic materials in the river water. This is the reason why some sample (R5, R6, R14, R15) shows negative alkalinity. The significantly altered alkalinity is not accurate for modeling the lithology weathering processes. So the model result does not match well with the measured data.

According to the chemical composition and MATLAB model results (Fig.16), the interpretation that best aligns with the facts is that carbonate and silicate rocks dominate the weathering processes in the Kasai Basin, contributing over 0.8 of the total dissolved ions. Evaporite erosion processes is less important, even not exist in some tributaries (mainly in Savanna group). Averagely speaking, the dissolved ions in Congo River mainly from carbonates weathering (approximately 60%), with less than 20% from silicate weathering, and less than 10% from evaporite contributions to the dissolved ions in the river water. The influence of ocean water spray is relatively high in the main Congo channel (reaching 30% of the total sources, when compared to other tributaries. In contrast, the Kasai River collects less sea water spray (less than 10%).

The results suggest that carbonate weathering plays an important role in the local weathering process, contributing more than half of the total weathering processes in the majority of tributaries. But tributaries display high variability in carbonate and silicate weathering, especially in the rainforest area. Some tributaries (R2-R4, R8,R9) in the rainforest area are high in carbonate weathering (greater than 0.7). Other tributaries such as R5-7 and R13-16 are not dominated by carbonates. R13-16 are dominated by silicate weathering, without ocean water influence.

Especially in R15, the carbonate weathering is less than 2%. R3-10 are all low in silicates, contributing less than 0.3 to the total, while R13-15 present higher silicate weathering, exceeding half, higher than the carbonates contributions. R5 and R6 are significantly affected by ocean water spray. R7 has an evenly distributed weathering process of carbonates, silicates, and evaporites, with a slight ocean water contribution.Contributions from evaporite dissolving processes are all lower than 0.3 in the rainforest area. In the Savannah area, river samples show a large effect from carbonate weathering, followed by silicates and some ocean water spray effects. Evaporite weathering is only interpreted in R23, R24, and R28 in the Savannah area, indicating that this area does not have much available evaporite minerals.

However, the analysis mentioned above is based on the mean value of the result. The model displays uncertainty regarding each end member, as shown in (Fig.17). Most river samples fit the model well (0.9 of simulations provide a good fit), while a few river samples such as R21, R29, and R30 in the Savannah area do not fit well due to factors other than rock weathering influencing the river chemistry in the catchment area.

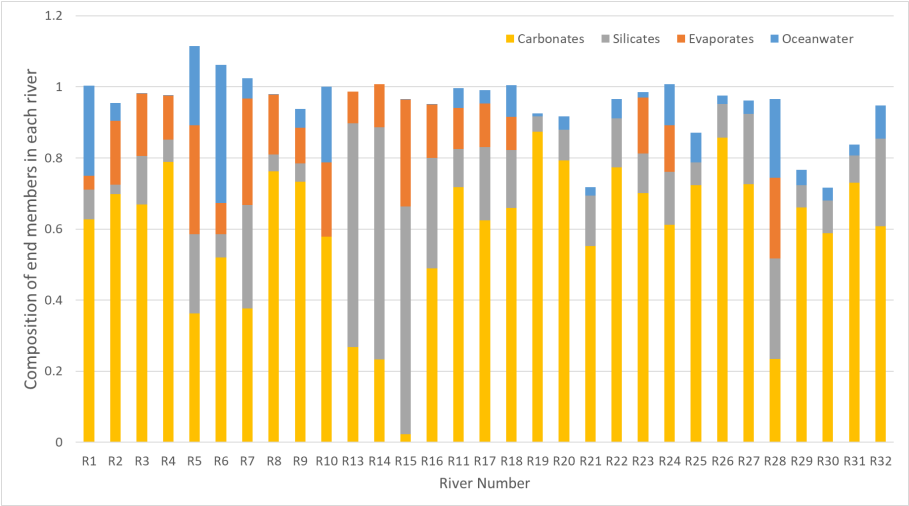

Figure 16: Contributions of each end members to total dissolved ions in the river water

With all the data put in the model, the end member composition narrowed into a smaller range (Fig.18 and Fig.19). The weathered carbonate is a mix of calcite ($CaCO_3$) and dolomite ($CaMg(CO_3)_2$), with more dolomite weathered than calcite. It is hard to tell the composition being weathered and contributing to river chemistry

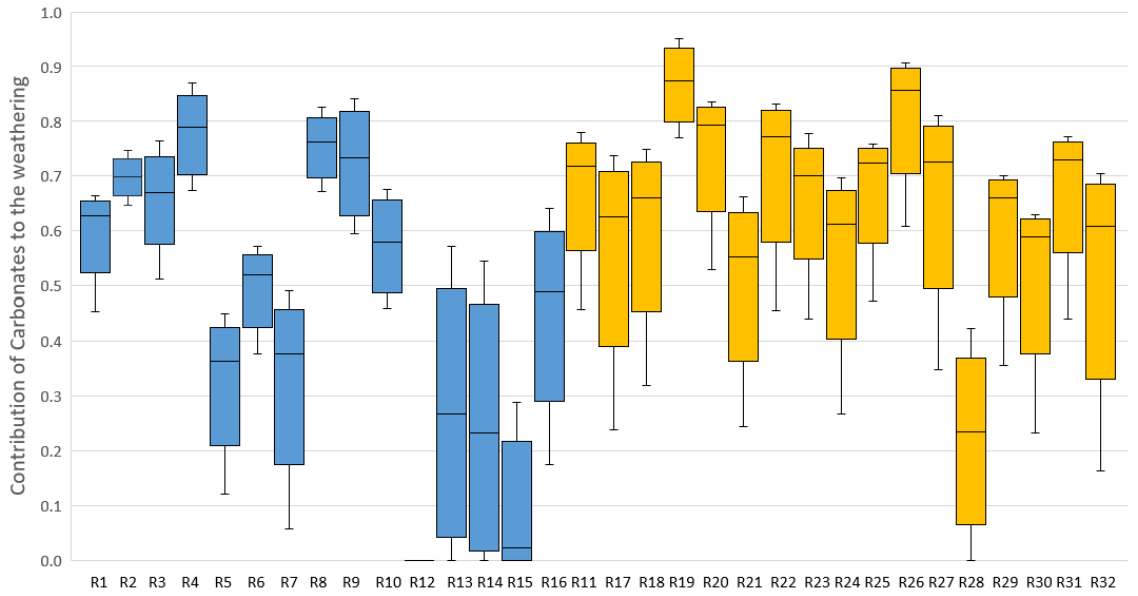
Contribution of Carbonates to the weathering
1.0
0.9
0.8
0.7
0.6
0.5
0.4
0.3
0.2
0.1
0.0
R1 R2 R3 R4 R5 R6 R7 R8 R9 R10 R12 R13 R14 R15 R16 R11 R17 R18 R19 R20 R21 R22 R23 R24 R25 R26 R27 R28 R29 R30 R31 R32

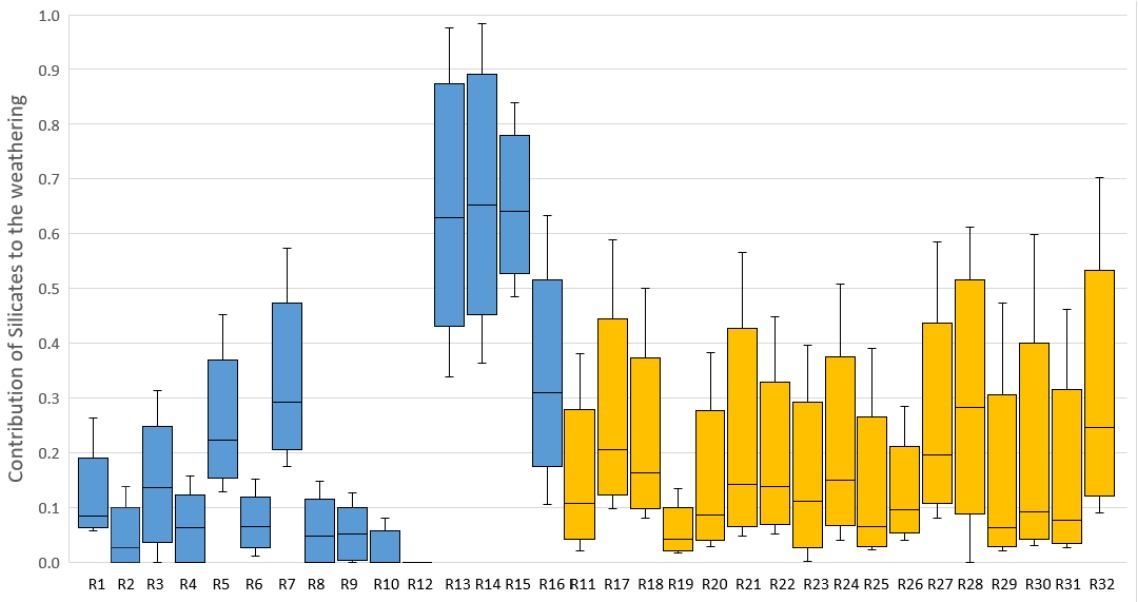
Contribution of Silicates to the weathering
1.0
0.9
0.8
0.7
0.6
0.5
0.4
0.3
0.2
0.1
0.0
R1 R2 R3 R4 R5 R6 R7 R8 R9 R10 R12 R13 R14 R15 R16 R11 R17 R18 R19 R20 R21 R22 R23 R24 R25 R26 R27 R28 R29 R30 R31 R32

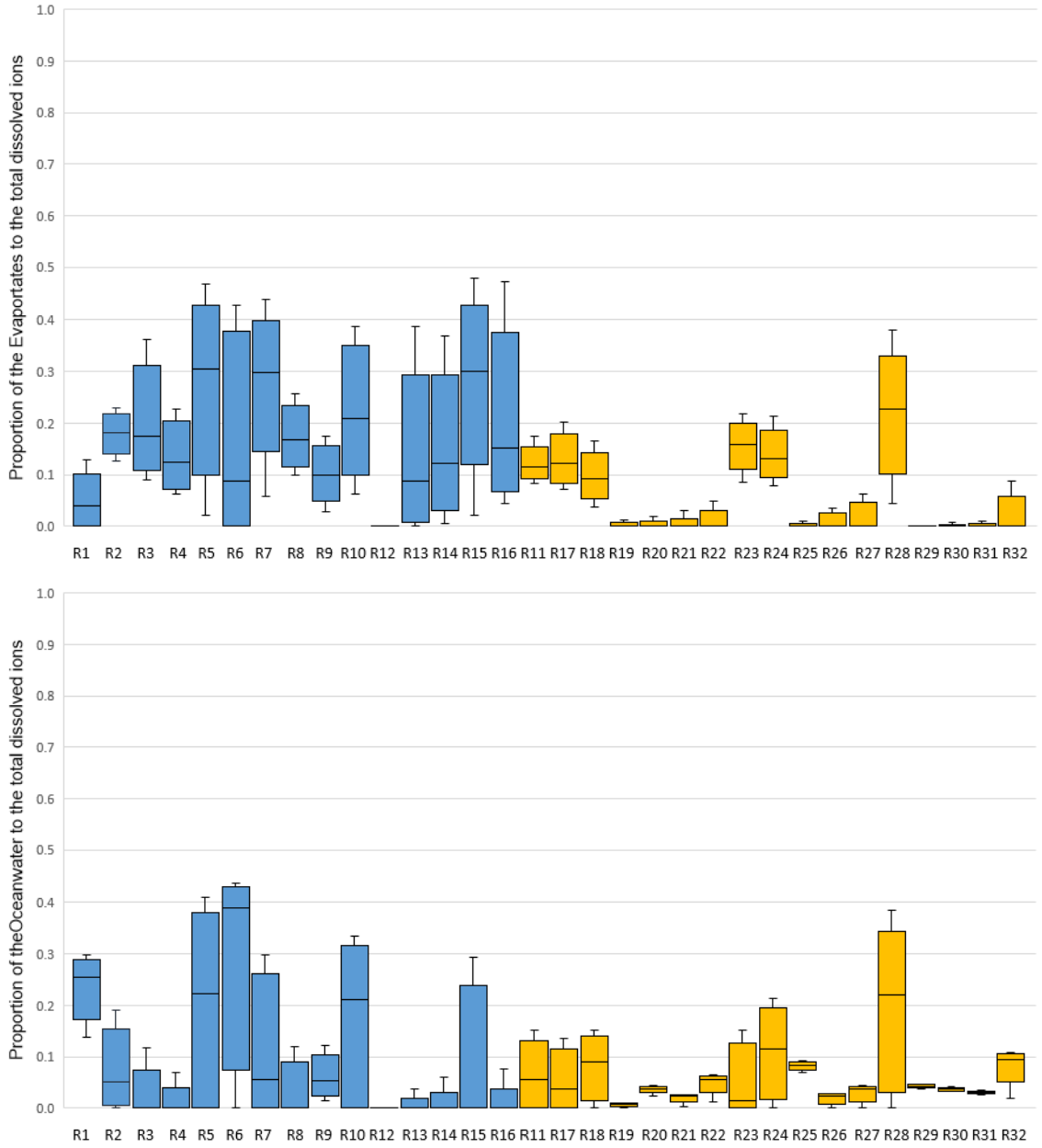

Figure 17: End members of the total ions in the river water

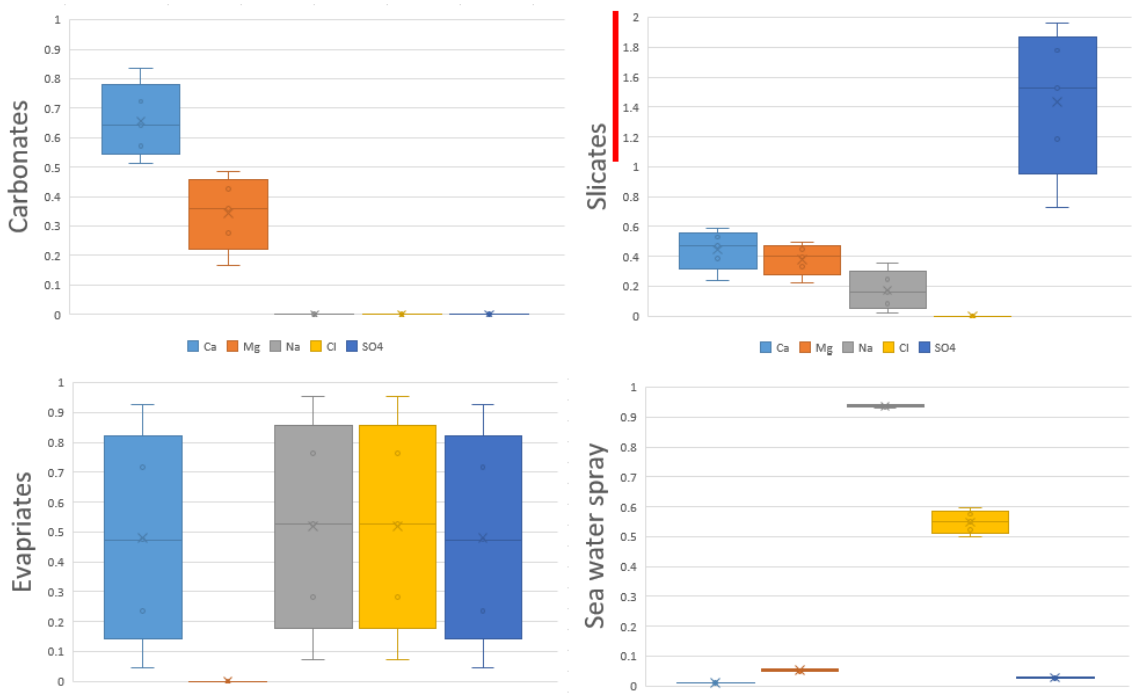

Figure 18: End members distribution with numbers of ratio (single cation over cation sum, box present 25-75%)

because of the uncertainty. The weathered silicates contains a mix of granite and shale. The sulfate is over 1 (not possible base on the chemical rules, pointed in Fig.18 in a red line), Here presents the fast erosion rate of pyrite compare to other materials. This aligned with real-world processes that pyrite is very easy to be weathered out (Nordstrom, 1982). As sulfur isotopes were also put into the model as a tracer, the model result calculated out that the silicates $\delta^{34}S$ value can be around -10 ‰, with a large rang between -28 to 8‰, and the interpreted evaporites S isotopes value of 11 to 33‰.

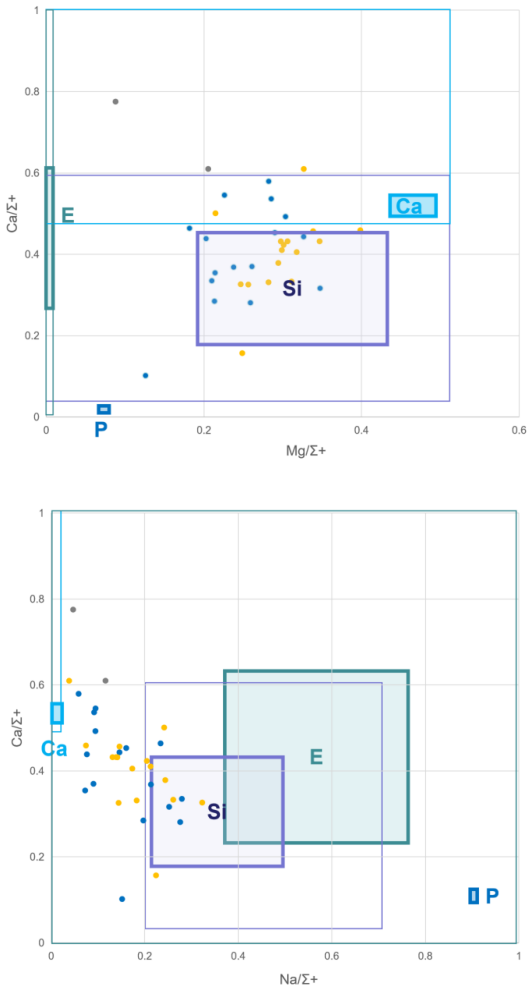

Figure 19: Input end-members and out put end-members by the model (using median values)
(Si=silicates; Ca=Carbonates; E=Evaporites; P=Precipitation form atmosphere). yellow presents Savanna tributary, green Present tributaries in rain forest group, gray present Congo and Kasai River. Same end-member is in same color, the output is deeper in color. a) presents the Mg/sum of the cations verses Ca/sum of the cations; b) presents the Na/sum of the cations verses Ca/sum of the cations.

6.1 Sulfur Source

Since carbonates primarily consist of calcite and dolomite, which generally do not contain sulfate ions, the source of sulfate is most likely from silicate or evaporite weathering. A detailed understanding of the isotopic composition of potential sulfate sources should be a prerequisite for evaluating the local sulfur cycles (Zhang et al., 2015). Natural sources of dissolved sulfate in river systems primarily originate from rock weathering, volcanic activities, organic matter, sulfide oxidation, and sea spray aerosols (Reiph et al., 2021; Zak et al., 2021). The $\delta^{34}S$ value is narrow in distribution, indicates that the dominate source of the Congo Basin is similar. Our result supports the review result from (Burke et al., 2018) that the major source of dissolved sulfur are from silicate weathering, with smaller contributions from sea water spray and evaporites.

Congo river and its tributaries is a typical river system that has low sulfate concentration, similar to Amazon and Niger (Burke et al., 2018). This poor concentration of dissolved sulfate is due to the lack of the intense weathering processes of pyrite or evaporites (Burke et al., 2018).

6.1.1 Weathering Fraction Composition relates dissolved Sulfate

The chemical weathering of sulfur-bearing minerals is considered as one of the most important factors contributes to the sulfur source, because the lithosphere is the largest sulfur reservoir in the Earth system and therefore supplies the majority of sulfur to river water (Jacobson et al., 2000). Oxidative weathering of sedimentary sulfide minerals (typically pyrite FeS_2) and dissolution of sedimentary sulfate minerals (gypsum $CaSO_4 \cdot 2\,H_2O$) are the main rock source of dissolved sulfate in river system (Relph et al., 2021).

The Matlab model utilizes river chemistry compositions along with sulfur isotopes to invert the original weathering end-member proportions. Based on Matlab, the model results presents the contributions from each sulfur-containing weathering parent (silicates, evaporites, and ocean sprays) to the total dissolved sulfate (Fig.20). Ideally, all contributions should sum to 100%, but the model presents some results that deviate from this ideal (less or more than 1), due to input data not being perfectly well matched by the model. Consequently, results in such cases are considered less reliable compared to results close to 1. The scenario that use ion concentrations and sulfur isotopes values, without alkalinity is the best fit result in model simulations,

but R13 - R16 and R28 still did not fit well with the model. These sample are characterized by high dissolved carbon (DOC) or Total suspended solids (TSS).

Focusing on the source of dissolved sulfate in river samples, the contribution proportions differ from those contributing to total ions (Fig.21). The box chart present 5%, 25%, 50%, 75%, and 95% simulated results that fit the model. Carbonates, defined as containing only carbonates and dolomite, do not contribute significantly to sulfate; thus, their contribution is not considered in this research. The sulfate sources predominantly come from either silicate (over 80% of the total dissolved sulfate) or evaporite weathering (less than 20%). Among all end members, silicate weathering emerges as the primary source of dissolved sulfate in all river waters. Evaporite weathering serves as the second largest source of soluble sulfate in river water, although it is not universally present in every river sample. Evaporites weathering contributes all rivers in forest area, but in the Savannah area, only R23, R24, and R28 are influenced by evaporites. the sulfate in other river samples primarily comes from silicate weathering (dominating) or ocean water spray (less than 10%). Both carbonate and silicate weathering exhibit large error bars, reflecting the high uncertainty of the results.

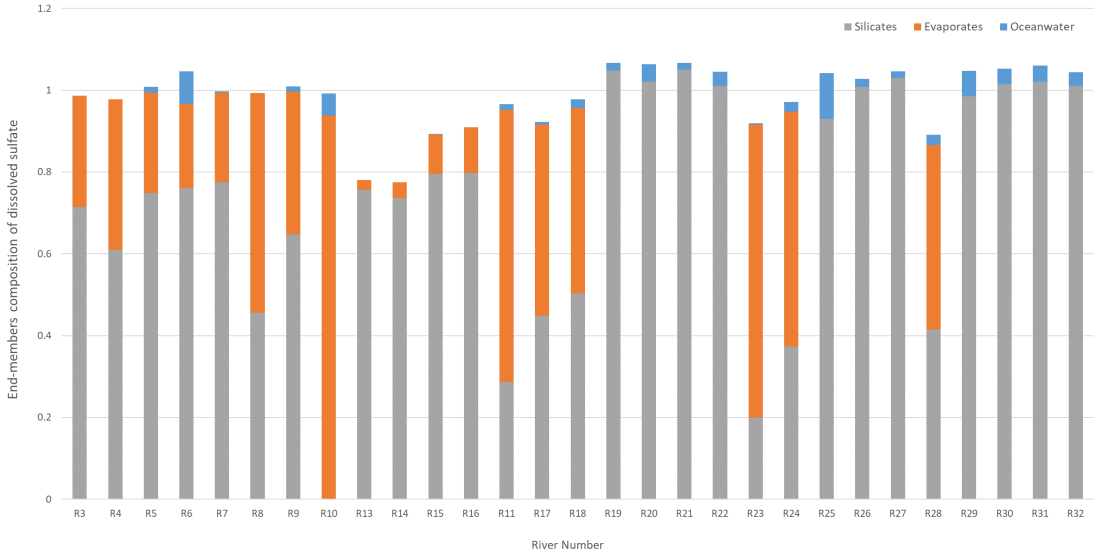

Figure 20: Contribution of sulfur sources to the dissolved sulfate.
Grey presents the silicates weathering, and the orange presents the evaporites; blue presents ocean water spray.

The world average riverine sulfate $\delta^{34}S$ is 4.8 ± 4.9 ‰(Burke et al., 2018), but the sampled river water ranges from 10-14‰, indicating a relatively heavy isotope

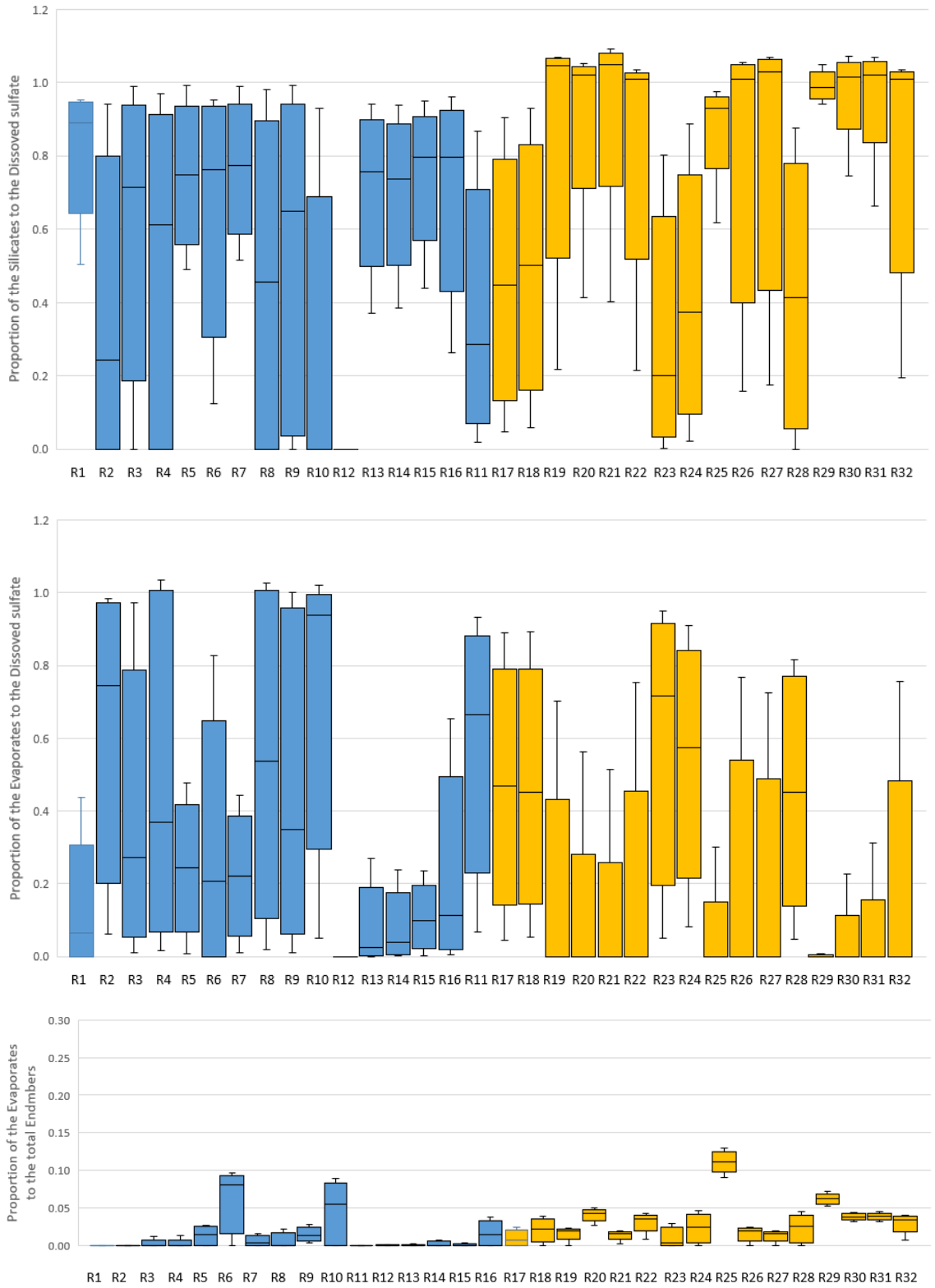

Figure 21: Silicates, evaporites and seawater spray contributions to the dissolved sulfate in river samples

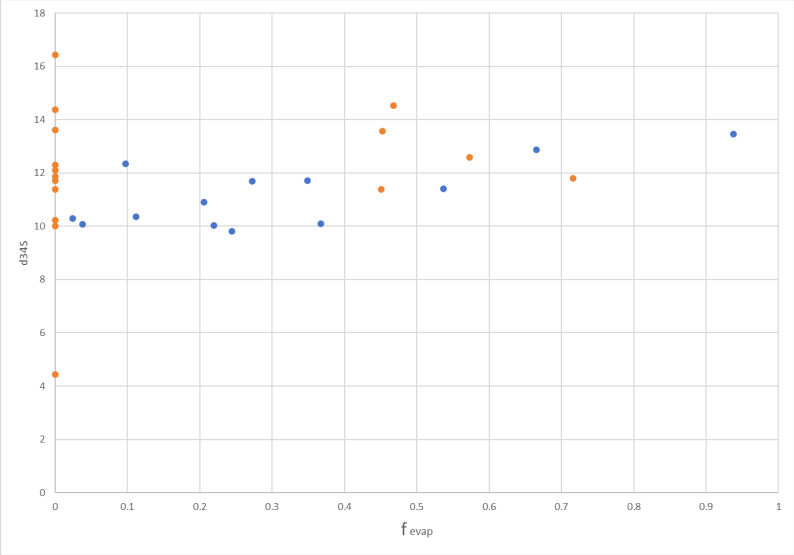

Figure 22: weak correlation between evaporate fraction and $\delta^{34}S$ (R=0.05), the mixing model can not explain all processes happening in Congo Basin

composition. If pyrite weathering is the main provider of the river's dissolved sulfate, the isotope composition is expected to be very light (ranging from negative to around zero). Therefore, there must be high $\delta^{34}S$ end-members to balance the light values generated by silicate weathering, resulting in the results observed in the Kasai River. In the model, evaporites and modern seawater are considered as high isotopic value members. However, the relationship between the fraction of the evaporites and the $\delta^{34}S$ value (Fig.22) does not show a strong correlation between each other, which indicates that endmembers are not unique in isotopes. They may partly overlap with each other so the model can not tell apart. Or the model does not perfectly suit real-world conditions. Several processes can cause the misfit of this model, which is detail explained in the Section 7.

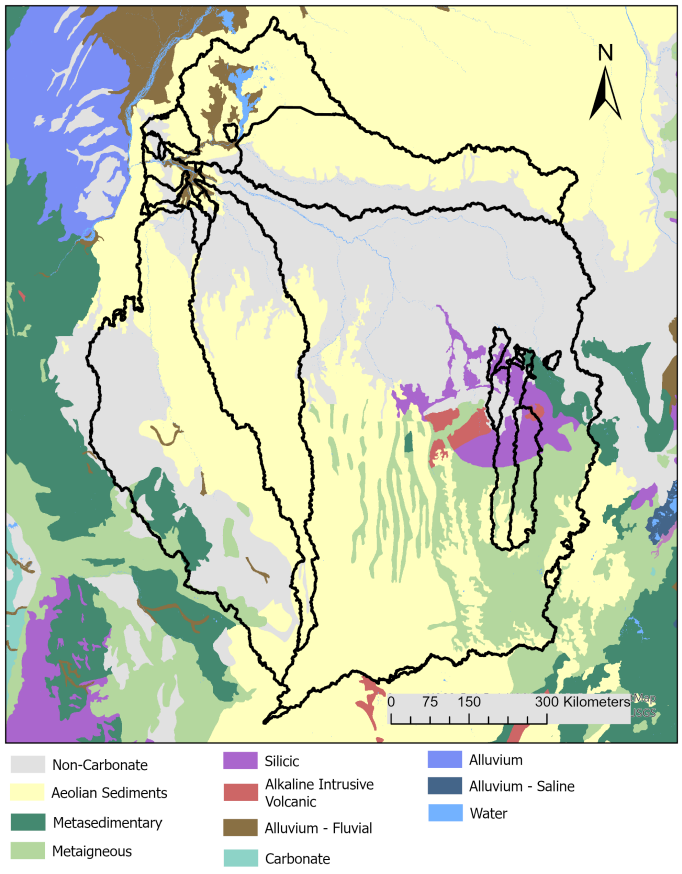

Figure 23: Geology map of the studying area.

6.1.2 Lithologic Formation relates isotopes in riverwater

Different catchment areas exhibit distinct compositions and proportions of surface lithology (Fig.23 and Fig. 24). Carbonate rocks are not the dominant rock type in geological maps, but river chemistry supports the notion that their easier and rapid weathering make carbonates important contributors to water chemistry. The same applies to evaporites. The rainforest area predominantly features sediments, whereas the savanna is characterized by contains igneous and metamorphic rock formations. Comparisons of lithological differences reveal the relationships between sulfur isotopes and lithology types, as illustrated in Fig. 25 . The surface lithology in the rainforest area is characterized by fan sediments or metasediments (Mushi et al., 2019), alluvium-fan deposits, and aeolian sediments. Notably, only R10 features alkaline intrusive volcanic rock in its surface lithology. In the Savanna area, the surface lithology comprises meta-igneous and intrusive rocks, suggesting that the

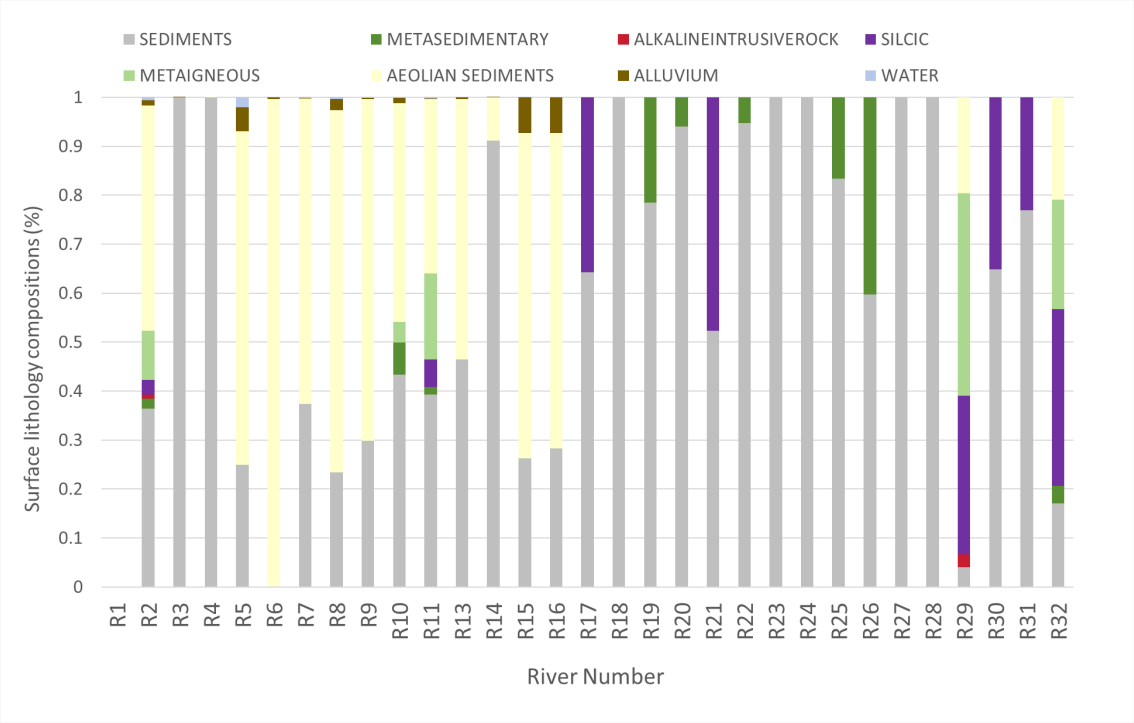

Figure 24: The composition of each geology formation in individual watershed area.

dissolved sulfate may be influenced by an igneous sulfur source.

By comparing different lithology formation, the sulfur isotopes character of different rock source presents. The generally distributed sediment formation (Fig.25, grey and yellow) has no correlation with $\delta^{34}S$, which is reasonable as these formation do not contain pyrite or evaporite formations. The metasediment has the sulfur source of high $\delta^{34}S$, higher than 16 ‰(Fig.25, deep green). In contrast, the metaignious, and alkineintrusives formation give a relative low $\delta^{34}S$ value lower than 10‰, which matched with the fact of general intrusive and igneous sulfur ranges of $\delta^{34}S$ from -10 to 10‰(Fig. 4, (Seal, 2006)(Relph et al., 2021)).

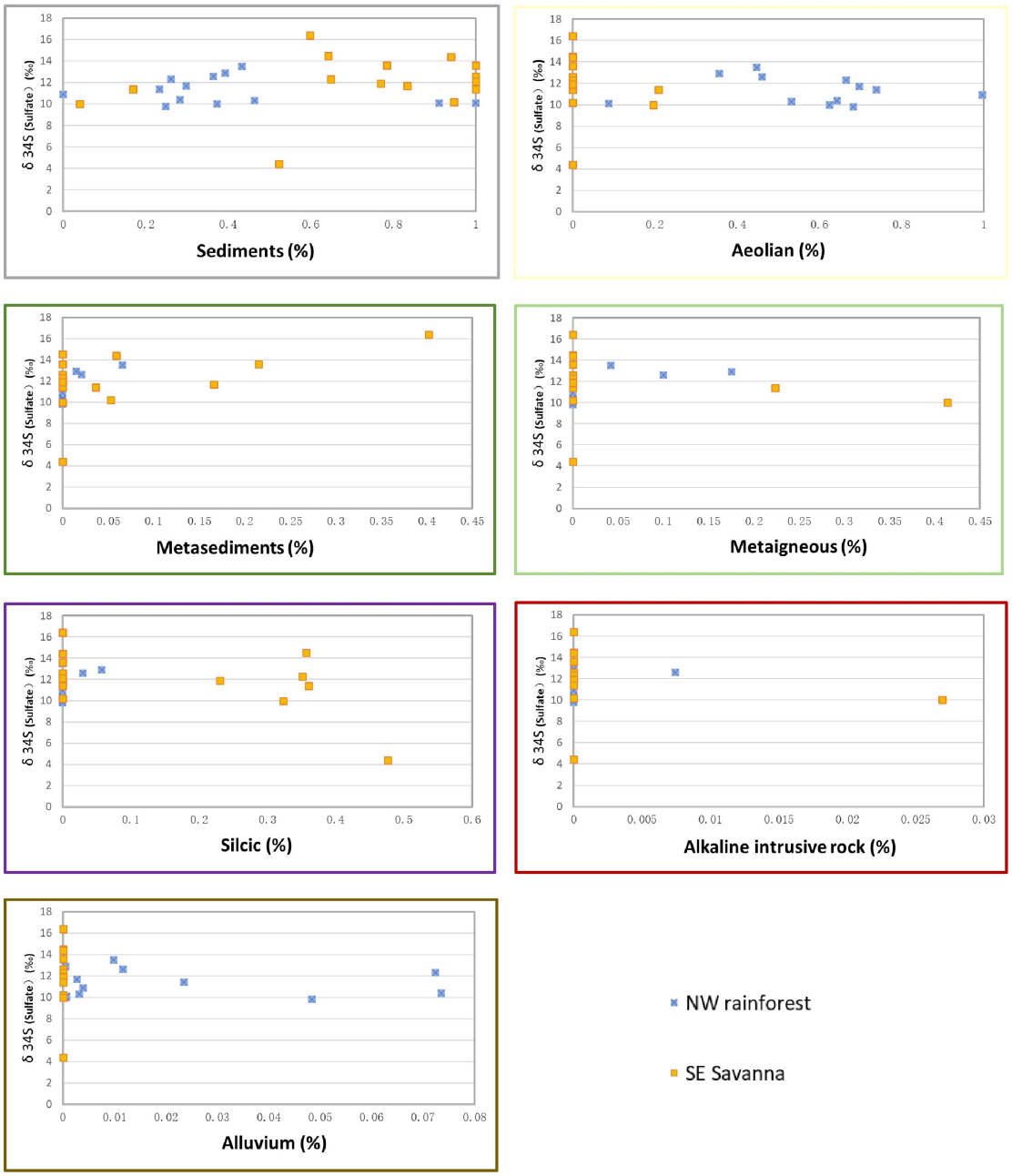

Figure 25: $\delta^{34}S$ and geology formations in Congo Basin.

6.1.3 Atmosphere sulfur source

Atmospheric deposits also play a significant role as an input source. Modeling results indicate that sea spray is the major atmospheric contributor of sulfate. In our study area, there are no active volcanoes nearby that significantly affect the riverine sulfur cycle; hence, this natural source is not considered.

Both natural pyrite and organic sulfur typically exhibit low $\delta^{34}S$ values, yet many samples in Kasai exceed 10 per mil. And model result point some watershed area do not contain evaporites, so simply weathering of sulfur-rich silicates or evaporites cannot explain all the measurement results. Additional processes besides rock weathering may be occurring in the study area (if not the case that end members isotopes values overlapped). Consequently, other high $\delta^{34}S$ and $\delta^{18}O$ sources must exist in this study area to counterbalance the pyrite values. Apart from evaporites, atmosphere precipitation sulfate is considered a significant source in the study area.

A plausible significant sulfur source is ocean spray. The modern ocean water sulfur isotopic composition is 21 $\delta^{34}S$ per mil, and this is considered a high $\delta^{34}S$ end member. This hypothesis is supported by MATLAB modeling results; the model was run several times under various scenarios to best match real-world processes. Results using modern seawater as the precipitation end member fit the majority of measurements well, presented in the results section (all above 0.8 of the sum of all end members). Continental effects studies support that the transformation of seawater spray does not efficiently change the isotopic composition; mountainous areas are more sensitive than flat basins (Winnick et al., 2014). Therefore, the sea spray isotopes remain the same as those of the modern ocean and are carried to the Congo Basin.

$\delta^{34}S$ values in precipitation can be influenced by the sources of sulfate in the atmosphere, including sea spray, volcanic emissions, or industrial pollution. Rainfall transports these sulfates to the Earth's surface, impacting the $\delta^{34}S$ values in surface waters and soils. Initially, precipitation samples were intended to be used as precipitation end members, but model fit proved suboptimal compared to using seawater composition. The fractional contributions from using actual precipitation data didn't sum up to 1 (all fraction percentages sum up to 1 is expected). These precipitation samples only represent one rainfall event or a small area of the basin and are insufficient to represent the entire study area.Significant differences exist

Samples	$\delta^{34}S$	$\delta^{18}O$	Ca	Mg	Na	K	Cl	SO_4^{2-}
P1	8.7	15.82	126.36	14.55	15.51	29.74	36.28	27.18
P2	7.3	18.68	17.31	5.83	6.59	3.89	4.91	4.67

Table 6: Chemical compaction of precipitation samples. Units in ‰and uM.

between both precipitation samples and ocean water composition. Precipitation samples 1 and 2, collected at the same location, vary from each other (Table 6); the differences between P1 and P2 underscore that precipitation samples are neither stable nor consistent, and cannot represent the general precipitation composition. Precipitation is influenced by several atmospheric mixing processes, including but not limited to local lake evaporation, intense windy weather, instantaneous temperature changes, or human activities such as biomass burning and air pollution. As a result, P1 and P2 is decided were decided to be invalid samples.

6.2 Sulfur and oxygen isotopes indicate sulfur sources

Based on the model results and both sulfur and oxygen isotopes, the sulfur sources and mechanics of the sulfur cycle in the Congo Basin were identified. Sulfur sources are from A) Low isotope ratio values source, pyrite; and B) high isotope ratio value sources, evaporites (or sea water deposits in some areas) (Fig.26). These sources mix in the river water. However, the fraction contributions of pyrite do not correlate to the sulfur isotope values, nor does the fraction of the ocean water, which casts doubt on the accuracy of the model result (Fig. 22 and Fig.27). Other processes affecting the sulfur cycle, besides those of the model end-members, also need to be considered.

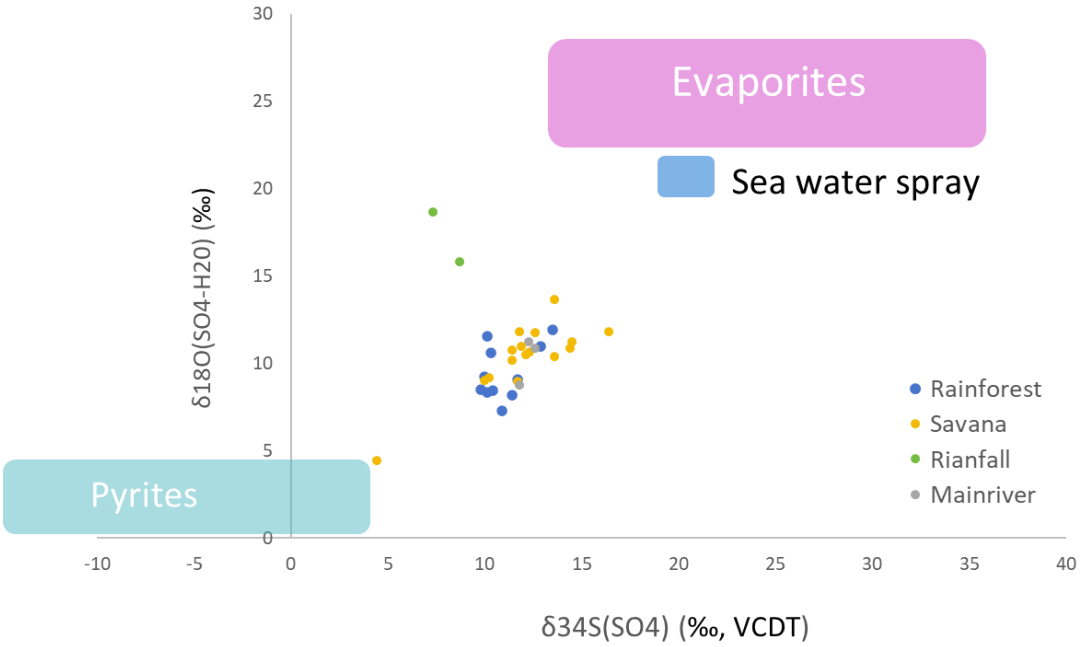

Figure 26: Combination of sulfur and oxygen isotopes, with inferred sources.

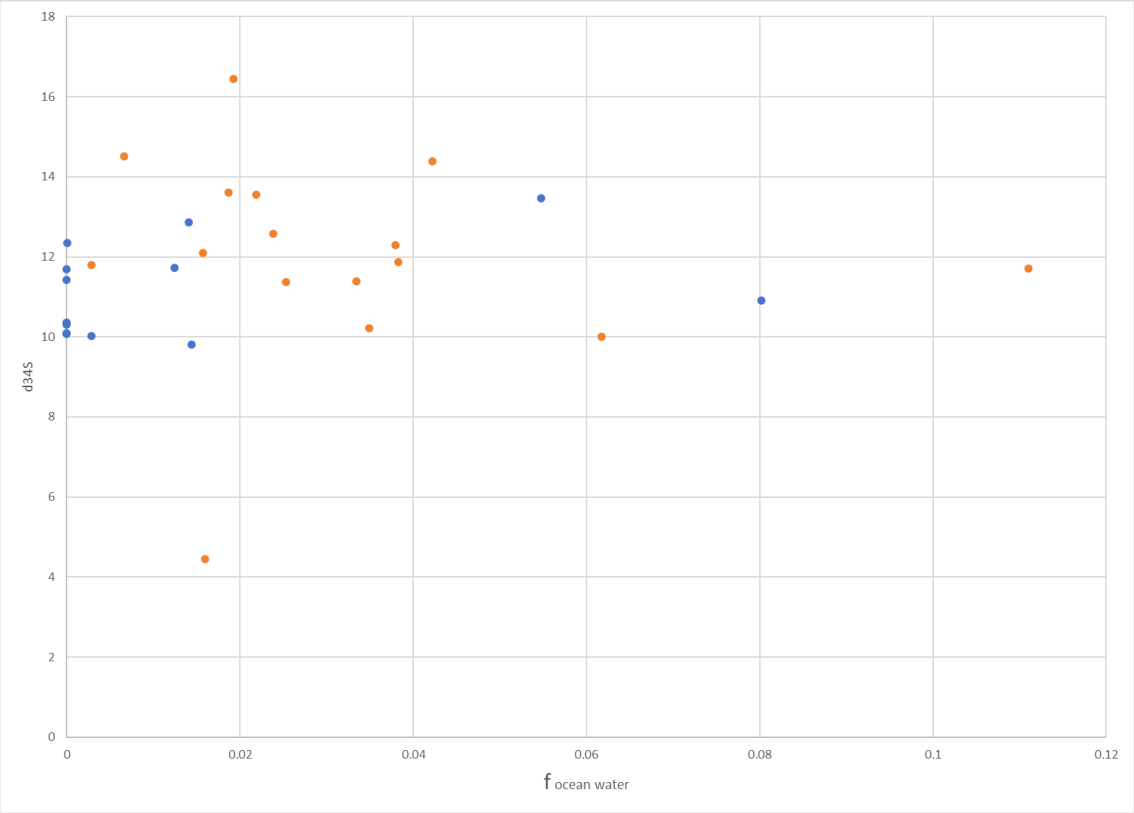

Figure 27: Fractional contribution of the ocean water relationship with the $\delta^{34}S$ isotopes values.

The fractional contribution of the different end members is not what is controlling the $\delta^{34}S$ composition of the sulfur in Congo Basin. Blue present rainforest group, yellow present Savanna.

6.3 Beyond the Model: The impact of other environmental factors

Besides the local geological formation and the atmosphere deposits, several other factors could be influencing the $\delta^{34}S$ values observed in these riverine samples, which is not able to be coded in the reverse model by formulas. Real world is complex, other important processes such as land use, soil cover, human activities also contributes sulfur to the environment, here the local geography information and isotopes data were analyzed statistically to evaluate their impact.

6.3.1 Land-cover

Sulfur cycling in terrestrial ecosystems is typically related to land cover, especially vegetation types and various economically driven land uses modified by human activities. Vegetation-related processes include the mineralization of roots, microbial oxidation and reduction processes, and both inorganic and organic sulfur transformations (Jacobson et al., 2000).

In the Kasai Basin, shrubs are the most widely distributed vegetation type, found in all river catchments. Land cover varies significantly between the rainforest and the Savanna areas (Fig.28 and Fig. 29). The rainforest is dominated by forests and shrubs, while the Savanna is characterized by shrubs and agricultural lands. Additionally, the Savanna area includes urban areas where human activities can influence the sulfur cycle.

Isotopic analysis of dissolved sulfate in the Kasai River reveals $\delta^{34}S$ values predominantly between +10‰ and +14.5‰ and $\delta^{18}O$ values concentrated between +8‰ and +12‰. The higher concentration of forest area results in more uniform sulfur isotopes around 10‰, in contrast, the denser grassland or shrub-covered area shows more decentralized distribution (Fig.30). Therefore, the sulfur source that dominates the rainforest area is around 10‰, and the source is likely homogeneous. The savanna area is expected to have more variable sulfur sources. Open savanna areas may more directly reflect isotopic signatures of underlying geological sources.

Rivers R13, R14, R15, and R16 are all rich in organic matter. Although there is no strong correlation line observed throughout the samples, high DOC content typically associates with lower $\delta^{34}S$ values (10‰). The Fimi River (R5) drains from

Lake Mai-Ndombe and its wetlands (Viennois et al., 2022), which explains its lowest sulfur and oxygen isotope values. Common plant sulfur-containing metabolites have negative $\delta^{34}S$ values (Tcherkez and Tea, 2013), and the decay of these materials may explain the lower sulfur isotope values. In areas densely covered by rainforest vegetation, the values are slightly lower, suggesting a possible explanation of stronger influence of organic matter decomposition and potential atmospheric deposition of biogenically derived sulfur. Conversely, savanna regions exhibit slightly higher $\delta^{34}S$ values, possibly due to more significant contributions from bedrock weathering and less influence from organic sulfur sources. Therefore, the source and cycling of sulfur in the Savanna area are more complex.

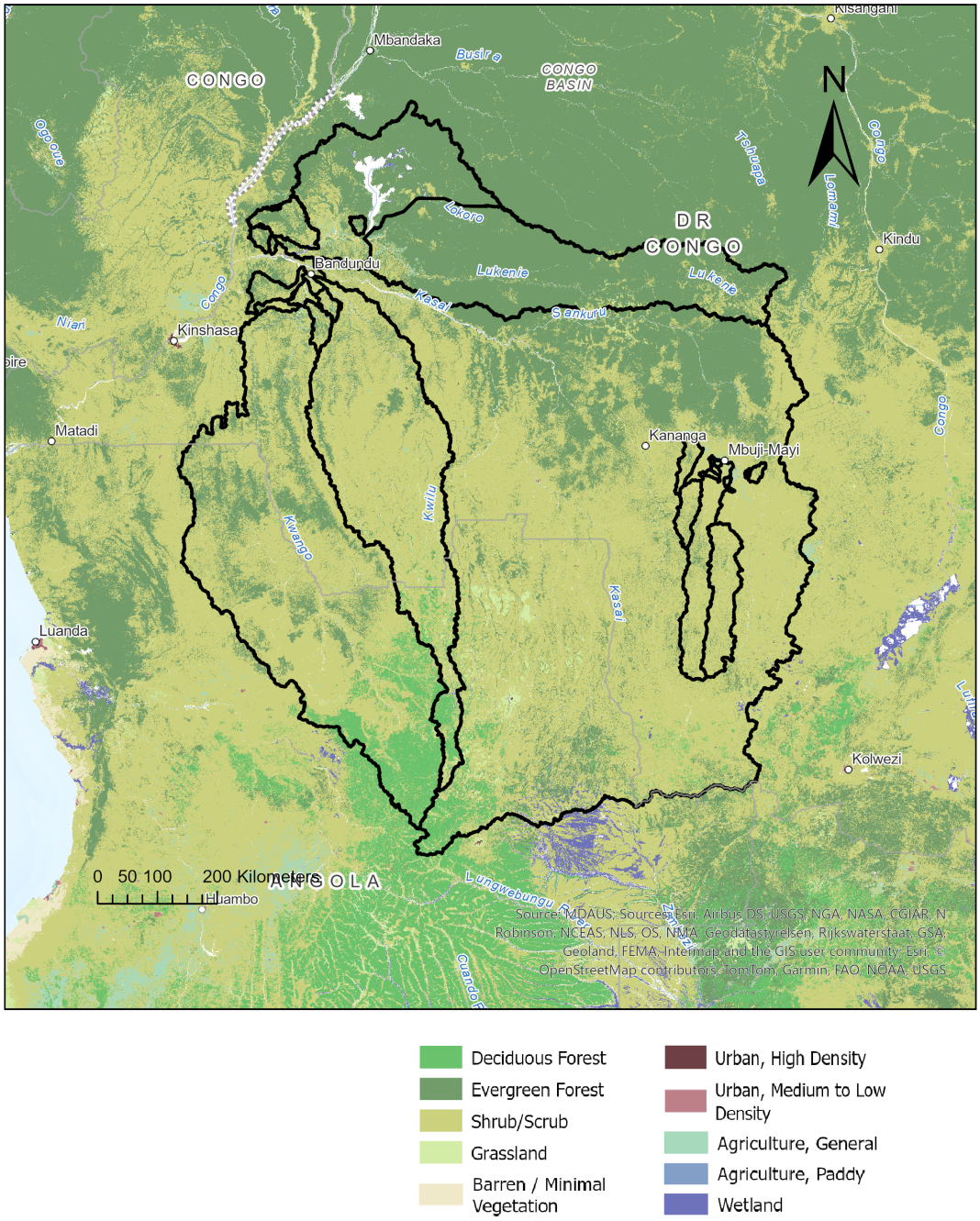

Figure 28: Land cover of the studying area

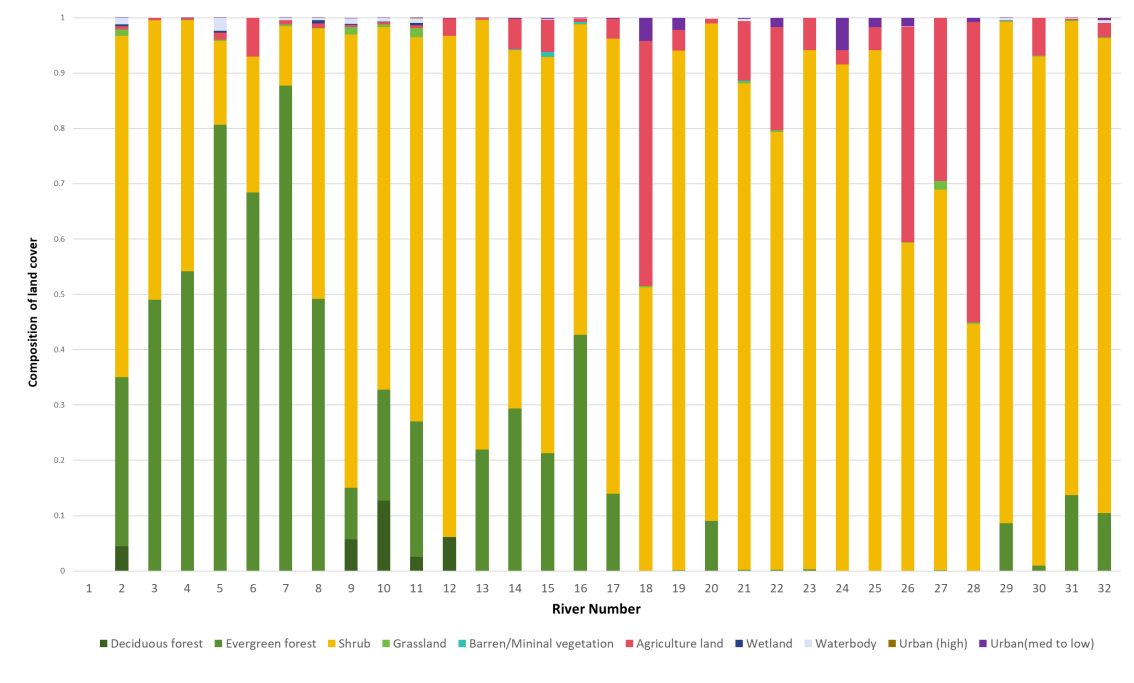

Figure 29: The distribution ration of different land covers

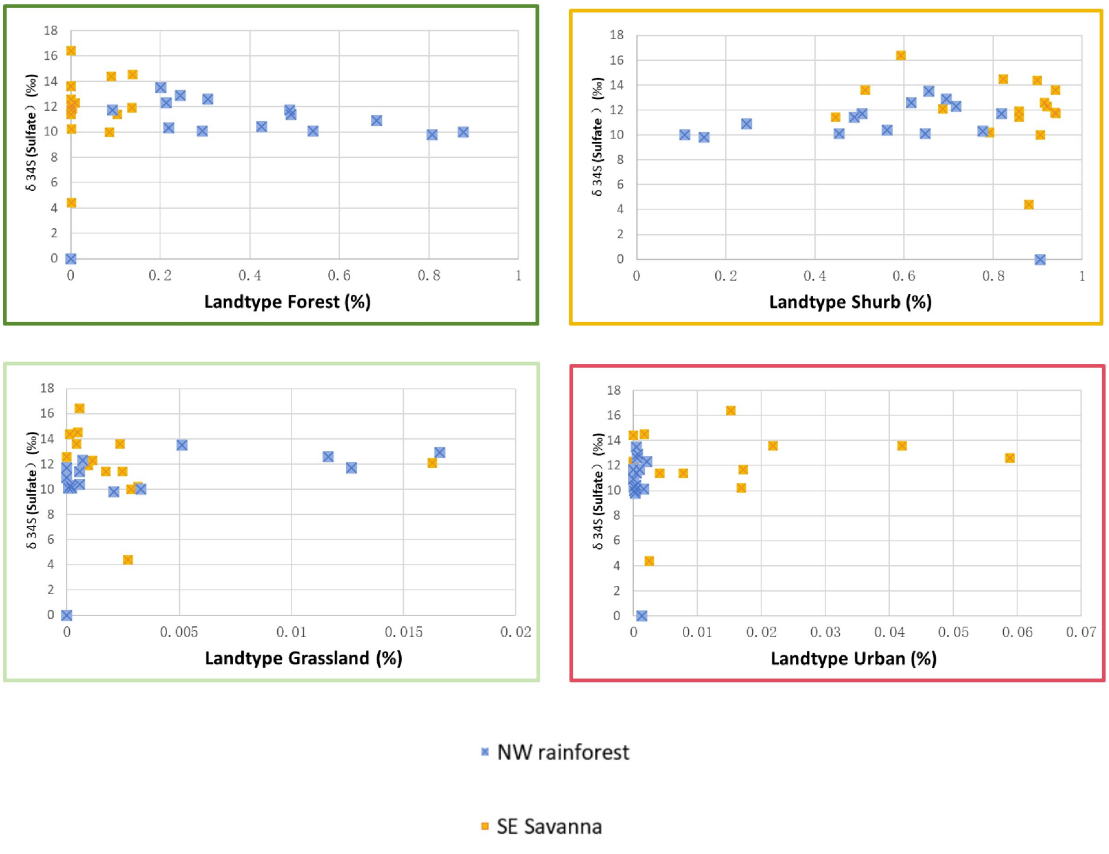

Figure 30: Relationships between vegetation cover and the sulfur isotopes value

6.3.2 Soil cover

Soil has the capacity to store, transform, and release sulfur compounds, which are vital for many ecological processes (Schoenau and Malhi, 2008). Thick weathering profiles reduces chemical weathering,and low relief tropical lowlands is typical been affected (Goudie and Viles, 2012). CChemical weathering is not favored where thick weathering profiles and insufficient primary minerals are present, because old surfaces covers have been highly leached and are unable to produce high chemical yields (Goudie and Viles, 2012).Weathering-limited and transport-limited conditions occur in lowland areas because the slight slopes limit the efficiency of transporting away the solid weathered products, leading to accumulated thick soil that protects the underlying fresh rock from contacting and fully reacting with water (Goudie and Viles, 2012). The high intensity of weathering in tropical climate generates mature soil profile in Congo Basin (Dinis et al., 2020), which is the reason why the Congo Basin is generally covered by thick layer of ferralsols (Fig.31). This reddish soil type present half of CO_2 flux consumed by silicate weathering when compare the similar runoff (Goudie and Viles, 2012).

Due to the tropical climate and flat topography, Congo Basin is covered by thick mature soil layer on the surface, mianly ferralsols and acrisols, with some gleysols near the Congo River in North area of the studying area. Soils in Congo Basin are general, but those of the equatorial areas (NW group) varies slightly from the drier Savanna (grassland) regions, Savanna area contains lixiols. As located in the warm, humid lowlands of the central basin, equatorial areas receive abundant precipitation and relatively fixed in situ with forest cover and low erosion rates. Rainforest area has more acrisols distribution and some river (R4,R7,R14,R15) contains gleysols, while R18,R19,R21, R23 and R24 have some lixisols covered area.

However, no correlation was found between S isotopes and the soil types in studied watersheds (Fig.32). This is may due to the fast weathering of the pyrite in the Earth system. Soil as a highly weathered material, contained less pyrite, also rapid weathering materials are all well decayed to unable contributes enormous dissolved ions into the water system.

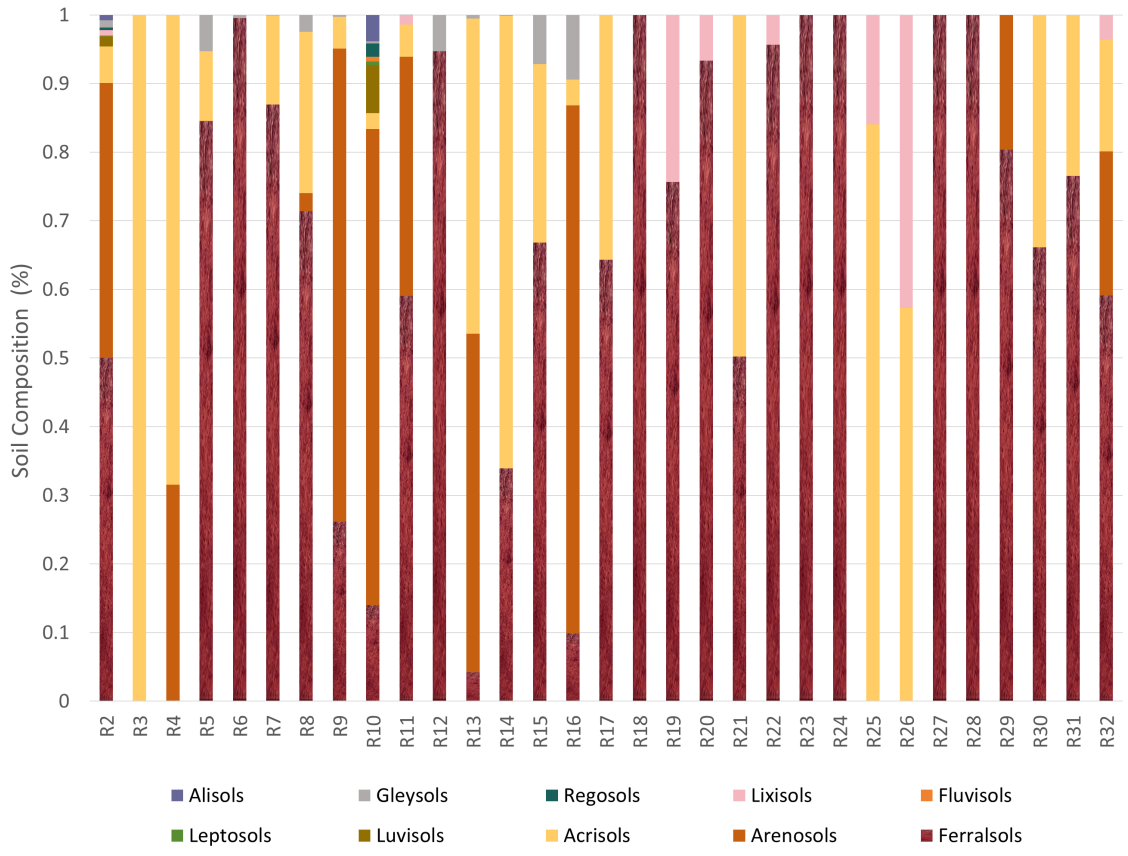

Figure 31: Composition of soil covering in each catchment area

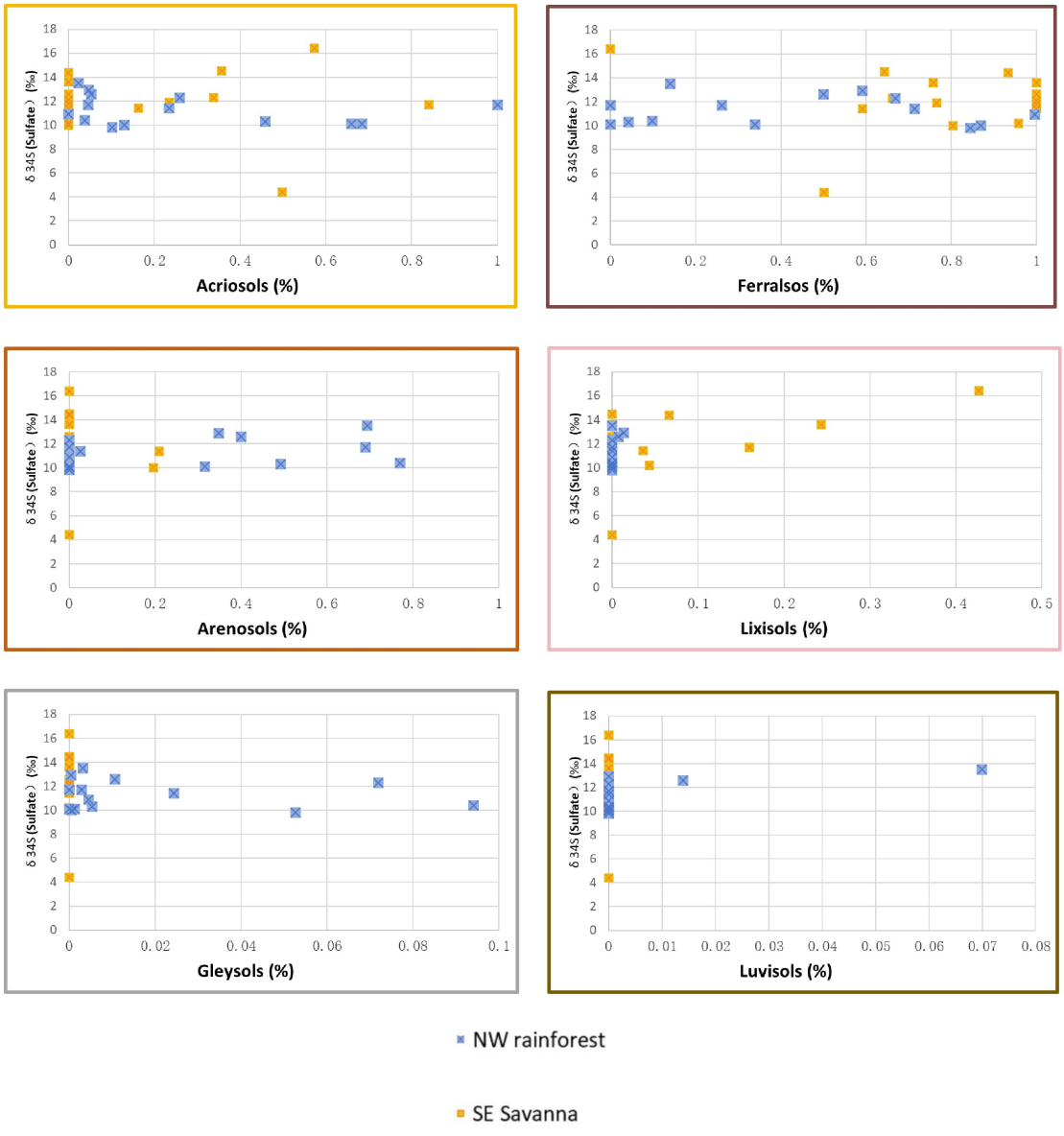

Figure 32: Sulfur isotopes and soil formations.

6.3.3 Anthropogenic Impacts

Human activities have significantly altered the continental sulfur cycle (Ver et al., 1999)(Charlson et al., 1992)(Zhang et al., 2024). The anthropogenic $SO_4\,2^-$source can be from atmospheric S deposition on land, acid mine drainage, fertilizer leaching from agricultural soils, wetland drainage, agricultural and industrial wastewater runoff, and sea level changes (Zak et al., 2021). The burning of fossil fuels, particularly coal, adds an unnatural quantity of hydrogen sulfide gas into the atmosphere, resulting in a higher concentration of sulfur dioxide that manifests as acid rain, with smoke and particulates (Germida et al., 2021). Human activities such as mining can also disturb natural erosion processes and generate acid mine drainage, which causes serious environmental problems. For the metal mine site, pollution drains high concentrations of dissolved sulfate and heavy metals into the local river system. The addition of sulfur from anthropogenic actions can be noticed by isotopes and ion concentration changes in time and space (Zhang et al., 2024), such as obvious changes downstream of a city or a rapid seasonal increase of atmospheric deposition from biomass and fossil fuel burning. However, based on the results, isotopes did not vary much in the study area (Fig.13). The impact of wildfires, biomass burning, city and industrial wastewater are therefore not significant or not clear. However, the large increase in ion concentration correlates to mining sites.

Mining actions have altered natural denudation rates(Depetris et al., 2014). Some sulfide minerals are economically important as metal ores, and therefore been extracted out from underground and polluted the hydro-system. In the Congo Basin, especially the Kasai Basin area, the affection of human activities is very limited. Mining activities are the only main factor that researched here. Mining can affect the S cycle by expose the rock and accelerates the oxidation and weathering processes, so affects the local water chemistry. Mining is a pillar industry in Congo. The study catchment area is dotted with open pit mines containing diamond, limestone, and metal mines (Fig.33). These large open-pit mines can affect the rate of soil erosion and increase the concentration of soluble ions. By comparing the area and type of the mining area, we found that the mining area gives the maximum and minimum $\delta^{34}S$ value, and the limestone mine also significantly increased the concentration of calcium and magnesium ions in the water body. Most mining site inside Congo is the diamond pit, instead of heavy metal mining. So the acid mining drainage that contains low pH sulfate rich pollution is not a serious problem and did not affects the sulfur cycle much.

R21 is the one that fits least well in the model, which is due to human activities largely accelerating the erosion processes and encouraging a significant amount of carbonates to efficiently enter the river. This is supported by the dissolved calcite concentration, which is extremely higher than that of the peer samples. The catchment of R21 is all covered by the diamond mining site (Fig. 34), but the affection is not as significantly as carbonates mining pits. compare to the undisturbed area in the studying area, the mining activities affection on sulfur cycle is relative light. The exposure of rock give a window to interpret the local lithology, R21, R22, R23 and R26 all located on the mine sits, R21-23 all shows low $\delta^{34}S$ values, relates to the silicates pyrites weathering (There is one Cu mining). This indicates the local pyrite $\delta^{34}S$ value is at least lower than 4.4 ‰. But the extremely high value of R26 tells another source that contains high isotopes values with the highest proportion of "metasedimentary", so the high isotopes values end-member can be higher than 16‰.

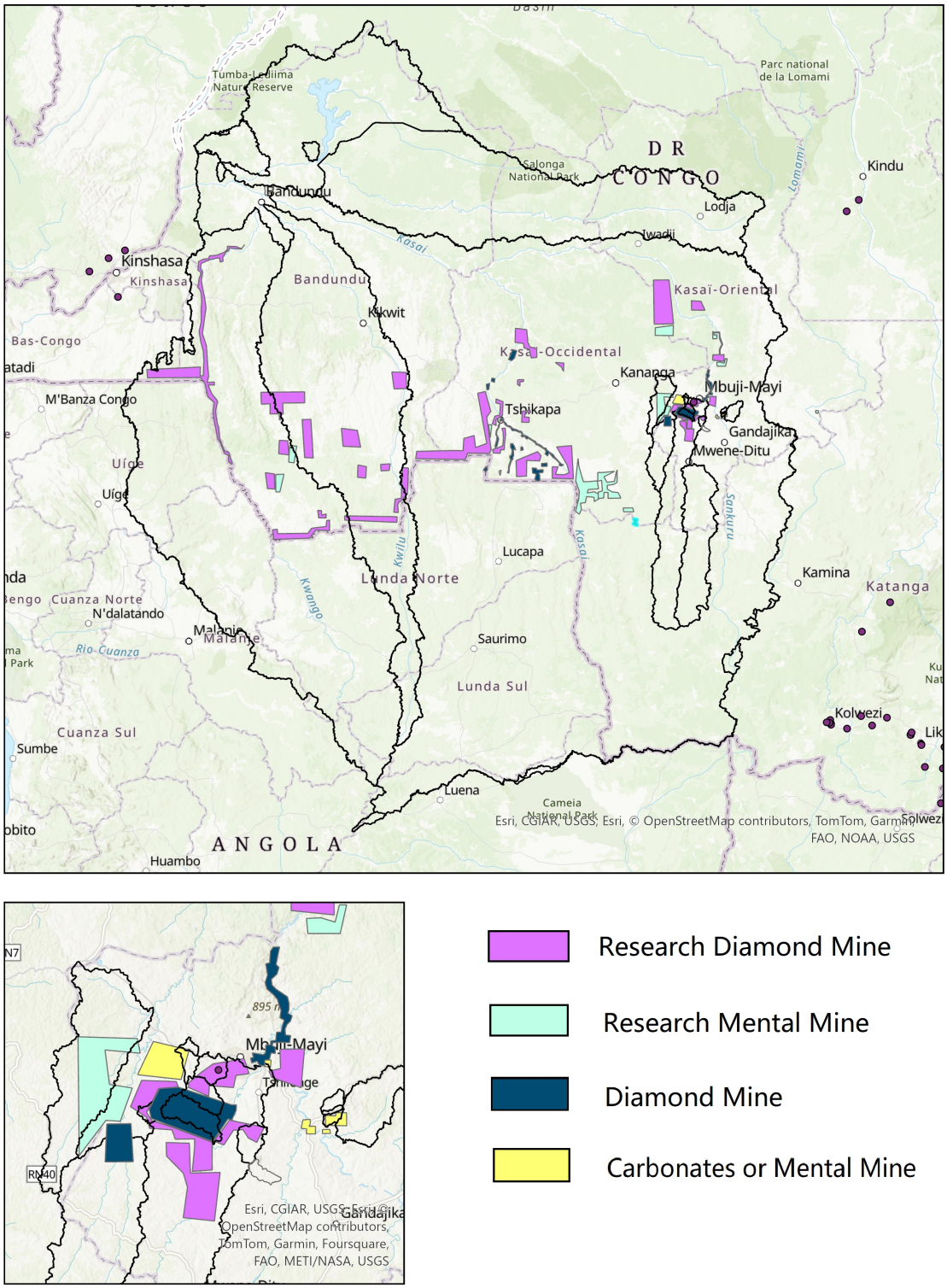

Figure 33: Mining sites locates in the studying area, mapped based on information from https://maps.congomines.org/

Figure 34: R21 Catchment area contains active mining sites.

6.3.4 Geomorphology

Rivers transport the products of continental denudation either in dissolved form (chemical erosion) or in solid form (physical erosion) (Gaillardet et al., 1995). Geomorphology significantly influences the weathering process and the hydrological cycle (Derakhshan-Babaei et al., 2020). Weathering processes continuously act on slopes, weakening underlying rocks and making weathered materials easier to be flushed out on the slope, exposing underlying materials (Derakhshan-Babaei et al., 2020). Steeper areas are presumed to have higher erosion rates, thereby enhancing lithological influence to the river chemistry. The southern part of the Congo Basin, with its deep topography, experiences higher erosion rates.

Based on the digital elevation model (DEM) of the studying area (Fig.35), the majority of tributaries watershed areas in the rainforest group (R3-R16) are situated around 400 meters above sea level on average, except for R9, R10, and R11, which are at double the average elevation of their peers due to their location in mountainous areas. Conversely, the Savanna area, with its differing average elevation, reaches about 700 meters on average. No relations was observed when correlates the isotopes data and average elevations (Fig.36).

The erosion parameter is quantified by the average slope degree (Fig.37). On average, the forest area is flatter than the Savanna area, but individual water catchment areas show significant variability, both rainforest and Savanna areas contain catchments with either low or high average slopes. The flattest areas, in the catchments of R12 and R15, average slopes are less than 1.5 degrees. Meanwhile, the steepest area, in R23, has an average slope of about 6 degrees. Strong correlation is not seen when relates both parameters, suggests the geomorphology do not play a key role in Congo Basin sulfur cycle. Although elevation and slope are significant, the geomorphology of our study site is not pronounced. In the Congo Basin, most rivers are flat and do not cut through any fresh rocks, and rivers flowing mostly through areas covered by thick, well-developed soil layers. The limited fresh material weathering means the direct relationship between river erosion and sulfur isotopes is not evident.

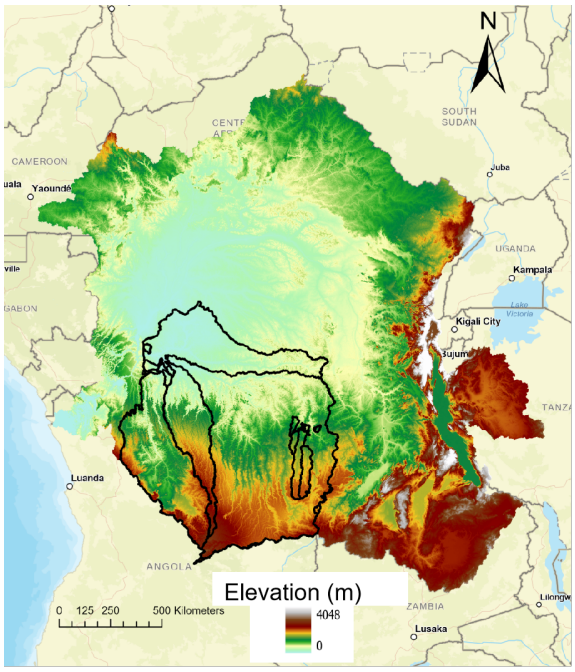

Figure 35: The elevation map of the studying area.

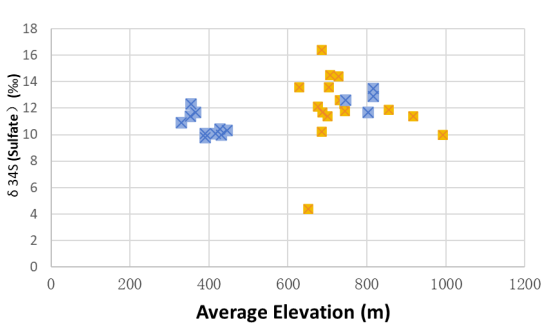

Figure 36: Average elevation and sulfur isotope data do not collects each other.

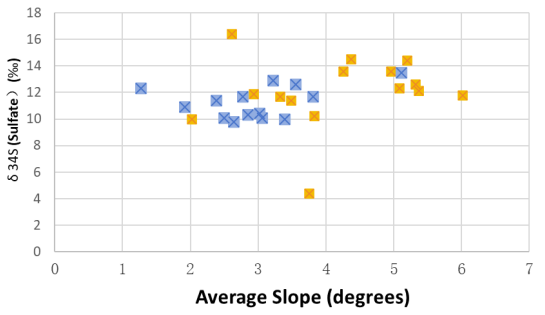

Figure 37: Watershed cover average slope and the S isotopes

6.4 The overprinting by bio-fractionation

Fraction of both evaporite and seawater spray end members did not show correlation with the isotopes values, which indicates water samples do not perfectly fit the mixing model. Therefore, isotopic results are affected by processes that deviate from simple mixing principles. It is evident that the sulfur cycle in the Congo Basin is more complex than simply reflecting a weighted mixture of lithologic sulfur sources. The evolution of heavier isotopes in $\delta^{34}S$ and $\delta^{18}O$ could be due to modifications by additional processes such as bacterial sulfate reduction in weakly developed soil or groundwater, followed by secondary sulfate precipitation (Turchyn et al., 2013). Thus, microbial activities that fractionate isotopic composition may be responsible for the observed shift towards heavier isotopes. These bioactivities consume light isotopes and leave heavier isotopes in the environment, thereby elevating both S and O isotopes (Böttcher et al., 2001).

Microbial sulfate reduction is a process where bacteria respire sulfate and produce sulfide as an end product (Antler et al., 2013). This process shifts the residual river $\delta^{34}S$ higher than the primary lithologic source of sulfur. If this process is active in the study area, inversion models become less accurate because this increase in $\delta^{34}S$ can mislead calculations and overestimate the contribution from high $\delta^{34}S$ end members such as evaporites and meteoric precipitation (Kemeny et al., 2021b).

The $\delta^{34}S$ can be significantly impacted by processes such as microbial sulfate reduction and/or sulfur assimilation and cycling. The rainforest, with its thick soil cover, provides the anoxic conditions preferred by sulfate-reducing bacteria (SRB). In contrast, the more open Savanna area may experience less bio-fractionation. In our isotopic results, biofractionation may exist, though its intensity is unclear. The presence of sulfate is a prerequisite for sulfate reduction. In freshwater environments (with sulfate concentrations ranging from 10 to 500 µM), freshwater sulfate reducers are advantageous because of their ability to utilize low sulfate concentrations (Canfield et al., 2005). Freshwater strains of sulfate reducers do not require high sulfate concentrations, as active metabolism of organic substrates occurs even at sulfate concentrations of less than 1 µM (Canfield et al., 2005). Therefore, sulfate reduction occurs in anoxic sulfate-containing sediment layers, supporting the likelihood of similar processes in the study area, even though concentrations are generally low (mostly less than 20 M in the Congo Basin).

Recent models have shown that MSR in the environment often achieve equilibrium S-isotope fractionation around 60-70‰(depending on temperature) (Wing and Halevy, 2014), and that any lower expressed fractionation factor is due to physical controls such as sedimentation and diffusion (Halevy et al., 2023). This processes may be limited in extremely high concentration (tens of millimolar) or low concentration (less than 0.1 mM) of dissolved sulfate in the environment (Wing and Halevy, 2014). Our river water samples contain dissolved sulfate concentration from 3 to 105 µM , indication the studying area is not a hard environment for sulfate-respiring bacteria and archaea. Therefore the overprinting of the biofractionation must exist in the studying area. Fractionation ratio of sulfur and oxygen in sulfate tends to lie between 1.4:1 and 4:1(Zhang et al., 2015), if the lowest $\delta^{34}S$ and $\delta^{18}O$ value point R21 is considered as the most close value to the pyrite source, with the fractionation ratio range from 1.4 to 1, all the sample is inside the area, which not able to generates any valuable conclusion. It is hard to identify if the microbio sulfur fractionation is operating or not, because the existence of evaporites disturb (evaporites has high isotopes values).

7 Limitations and Future Investigations

While this study provides valuable data and insights for both local and global biogeochemical cycles, it has several limitations and some aspects can be improved in the future, particularly the sampling, analysis, and modeling components.

7.1 Sampling Difficulties

Ideally, having local fresh pyrite crystals to determine the isotopic composition of this end member would be useful. However, this is a challenging task because the Congo Basin is covered by thick soil layers which makes drilling for fresh, unweathered pyrite rocks difficult. Moreover, based on the relatively low dissolved sulfate ion concentration, the sulfur minerals are not densely concentrated in the study area.

Obtaining representative precipitation samples is also crucial for precise research on atmospheric input composition. In reality, accurately capturing atmospheric input is challenging because samples can be significantly contaminated and affected by local environmental factors, such as nearby lake evaporation (Lake Mai-Ndombe), ash pollution, and human activities (Dominguez et al., 2008)(Han et al., 2017). Although precipitation samples were collected here, they varied significantly from each other and did not align with other samples in theoretical sulfur cycling. Triple-isotope may be a good way to distinguish nature and unnatural pollution (Dominguez et al., 2008).

7.2 Accuracy of the Model

The model results are expected to present a linear relationship between isotopes and evaporate fraction. However, the results are not perfect, which could be due to several reasons: 1) The model needs improvement and there may be other important end-members that have not been identified in the current model. 2) The input end-members are not accurate, or end-members are not distinctly distinguishable from each other in isotopic values. The end members overlap that confuse model calculation processes. 3) Other processes significantly alter the isotopic data, such as microbio-fractionation activities.

Since the end-member compositions are currently unknown, how isotopes are modified during the weathering and transport processes remains unclear. Together

with the close isotopic data between modern ocean and evaporites, it is even more challenging to generate accurate results. Unlike other river systems such as the Mekong River (Relph et al., 2021) or the Yellow River (Zhang et al., 2020), evaporites are too rare to be represented on Congo geological maps. The weak sulfur intensity in the Congo Basin amplifies the influence of each factor on isotopic results.

7.3 Distinguishing between Bio-fractionation and High $\delta^{34}S$ End-members

Isotopes are used as tracers in modeling, but isotopic tracers can be significantly affected by biological activities, thereby rendering the results inaccurate. As mentioned, it is difficult to determine if microbial activities dominate the isotopic composition in the Kasai Basin. With current results, the high isotopic values in river water could be either from active microbial activities or evaporate dissolution. This research suggests that these processes may be active in the anaerobic environment in deep soil or rocks. To confirm whether these processes exist and to assess their intensity, further research is needed, such as microbial analysis and triple oxygen isotopic analysis (Hemingway et al., 2020).

7.4 Future Outlook

As mentioned above, challenges need to be solved through more samples and further isotopes analyses. Rock core samples and soil samples is necessary. Pyrite weathering process is the dominated mechanism of the local sulfur cycle, further understanding in this aspect is encouraged. The weathering rate is controlled by ground water table and porewater chemistry (Kanzaki et al., 2020), so these related environmental data are also needed. Sulfur and oxygen isotopes already give much information about the local sulfur cycles, other isotopes analyses such as triple oxygen isotopic analysis is necessary.

Although geological formations are relatively stable on the human timescale, with climate change and increasing human activities, the natural environment will be largely affect, which includes but not limited to land cover change (transition from rainforest to grassland or cropland can cause soil erosion loss and increase the erosion rates), wetland shrinks influence the microbe's activities (Pester et al., 2012), biomass burning and higher risk of wild fire under climate change, higher fossil fuel pollution and mining impacts. Current research in the Kasai Basin has not shown

significant pollution or extreme contributions by human activities, yet the human impact on the sulfur cycle is increasing and is becoming the largest contributor (Zak et al., 2021). Thus, the human impact on the Congo Basin's sulfur cycle is expected to increase in the near future (Zak et al., 2021). Therefore, continuous monitoring and studying of large river systems both spatially and temporally is necessary, especially in delicate natural environments such as the Congo Basin.

8 Conclusion

The $\delta^{34}S$ isotope ratios in river sulfate can be modulated by various geochemical processes, this study concern the source of sulfate, weathering process, and human activities affects. The combination of isotope analysis, water chemistry results and model results indicates the how sulfur cycles within the Congo Basin. The sulfur cycle in the Congo Basin is primarily driven by a combination of pyrite weathering, evaporite dissolution, and atmospheric inputs, particularly ocean spray. Primary source of sulfur in the , is local rock weathering, which fundamentally sets the tone of the sulfur cycle. The isotopic composition of sulfur ($\delta^{34}S$) in the river waters predominantly ranges between 10-14‰, reflecting a relatively narrow range of isotopic variation. Combined with the $\delta^{18}O$, high δ values suggest substantial contributions from evaporite and atmospheric sources, while lower values are associated with silicate weathering. Weathering processes are predominantly due to carbonates, with some contribution from silicates weathering or evaporites dissolution. Although evaporites are not a common geological formation in the study area, they are an important source of dissolved sulfate in some tributaries. Different sulfur source contributes slightly different in each tributaries.

Once sulfur is released from the rocks, it is modified by various agents including bacteria, plants, and human activities. Biological activities can fractionate isotopes into heavier values, therefore significantly shifting isotopic data. But it is not confirmed , in Congo Basin, weather the evaporites or bio-fractionation alter the isotopes into heavier direction, more data is required. The current findings indicate that human activities, such as mining, are beginning to impact the sulfur cycle in the Kasai Basin. However, significant pollution or extreme contributions have not yet been observed. With ongoing climate change and increasing anthropogenic activities, it is expected that these impacts will become more pronounced, necessitating continued monitoring and research. Compared to other river systems that show clear variations between each sampling site, the data from the Congo is relatively stable and does not reveal much about each part of the sulfur cycling process through isotopic analysis. This may be due to the very low concentration of dissolved sulfate in the system and the heavily weathering environment that efficiently consumes pyrite.

Biogeochemaical cycles in earth system is complex, each individual fators has intricate interconnections with its related factors, which produced the interdependent outcomes. Other parameters such as climate, topography, ecosystem, and soil cover

may also influence the sulfur cycle and isotopic values, but these influences are not clearly and confidently discernible within the data obtained from our research. It is challenging to find locations that are perfect contrasts, and even though we regard Earth as a natural laboratory, we are still unable to control every parameter of natural processes. More data in related fields would clarify the truth.

The study faced several challenges, particularly in obtaining fresh pyrite samples and representative precipitation samples, which are critical for precise end-member characterization. The variability in precipitation samples and the difficulty of drilling through thick soil layers to access fresh rock samples add complexity to the analysis. Additionally, the model used to determine sulfur sources has limitations due to overlapping isotopic values of end-members and potential bio-fractionation processes that were not fully accounted for. The application of MATLAB-based model has helped refine the understanding of sulfur sources and weathering processes. Despite this, the model's accuracy is challenged by the overlapping isotopic values of end-members and unaccounted processes. Future model improvements should focus on better characterizing end-members, expanding sampling efforts, and incorporating additional isotopic tracers. The thick layer of soil covering most areas of the basin makes sampling of rock-type pyrite difficult. For future related research, collecting solid pyrite samples and analyzing water samples using the triple oxygen isotope method would help clarify local end-member isotopic data and determine if microbial activities are a controlling factor in the Congo Basin.

References

Alsdorf, D., Beighley, E., Laraque, A., Lee, H., Tshimanga, R., O'Loughlin, F., et al. (2016). Opportunities for hydrologic research in the congo basin. *Reviews of Geophysics*, 54(2):378–409.

Antler, G., Turchyn, A. V., Rennie, V., Herut, B., and Sivan, O. (2013). Coupled sulfur and oxygen isotope insight into bacterial sulfate reduction in the natural environment. *Geochimica et Cosmochimica Acta*, 118:98–117.

Bao, H., Cao, X., and Hayles, J. A. (2016). Triple oxygen isotopes: fundamental relationships and applications. *Annual Review of Earth and Planetary Sciences*, 44:463–492.

Barthel, M., Bauters, M., Baumgartner, S., et al. (2022). Low N2O and variable CH4 fluxes from tropical forest soils of the congo basin. *Nat Commun*, 13:330.

Bauters, M. (2018). *Biogeochemical cycles of contrasting tropical forests of the Congo basin*. PhD thesis, Ghent University, Belgium.

Bayon, G., Schefuß, E., Dupont, L., Borges, A. V., Dennielou, B., Lambert, T., et al. (2019). The roles of climate and human land-use in the late holocene rainforest crisis of central africa. *Earth and Planetary Science Letters*, 505:30–41.

Bernasconi, S. M., Meier, I., Wohlwend, S., Brack, P., Hochuli, P. A., Bläsi, H., et al. (2017). An evaporite-based high-resolution sulfur isotope record of late permian and triassic seawater sulfate. *Geochimica et Cosmochimica Acta*, 204:331–349.

Böttcher, M. E., Thamdrup, B. O., and Vennemann, T. W. (2001). Oxygen and sulfur isotope fractionation during anaerobic bacterial disproportionation of elemental sulfur. *Geochimica et Cosmochimica Acta*, 65(10):1601–1609.

Brand, W. A., Coplen, T. B., Aerts-Bijma, A. T., Böhlke, J. K., Gehre, M., Geilmann, H., et al. (2009). Comprehensive inter-laboratory calibration of reference materials for δ^{18}o versus vsmow using various on-line high-temperature conversion techniques. *Rapid Communications in Mass Spectrometry: An International Journal Devoted to the Rapid Dissemination of Up-to-the-Minute Research in Mass Spectrometry*, 23(7):999–1019.

Burke, A., Present, T. M., Paris, G., Rae, E. C., Sandilands, B. H., Gaillardet, J., et al. (2018). Sulfur isotopes in rivers: Insights into global weathering budgets,

pyrite oxidation, and the modern sulfur cycle. *Earth and Planetary Science Letters*, 496:168–177.

Byrne, P., Wood, P. J., and Reid, I. (2012). The impairment of river systems by metal mine contamination: a review including remediation options. *Critical Reviews in Environmental Science and Technology*, 42(19):2017–2077.

Calmels, D., Gaillardet, J., Brenot, A., and France-Lanord, C. (2007). Sustained sulfide oxidation by physical erosion processes in the mackenzie river basin: Climatic perspectives. *Geology*, 35:1003–1006.

Canfield, D. E., Kristensen, E., and Thamdrup, B. (2005). The sulfur cycle. In *Advances in Marine Biology*, volume 48, pages 313–381. Academic Press.

Canfield, D. E. and Raiswell, R. (1999). The evolution of the sulfur cycle. *American Journal of Science*, 299(7-9):697–723.

Charlson, R. J., Anderson, T. L., and McDuff, R. E. (1992). The sulfur cycle. In *International Geophysics*, volume 50, pages 285–300. Academic Press.

Charlson, R. J., Anderson, T. L., and McDuff, R. E. (2000). The sulfur cycle. *Earth system science: from biogeochemical cycles to global change*, pages 343–359.

Chen, Q., Bao, H., and Shen, X. (2008). Radiolytic synthesis of baso4 microspheres. *Radiation Physics and Chemistry*, 77(8):974–977.

Colbourn, G., Ridgwell, A., and Lenton, T. M. (2015). The time scale of the silicate weathering negative feedback on atmospheric co2. *Global Biogeochemical Cycles*, 29(5):583–596.

Creese, A., Washington, R., and Jones, R. (2019). Climate change in the congo basin: processes related to wetting in the december–february dry season. *Climate Dynamics*, 53:3583–3602.

Deng, K., Yang, S., and Guo, Y. (2022). A global temperature control of silicate weathering intensity. *Nature Communications*, 13(1):1781.

Depetris, P. J., Pasquini, A. I., and Lecomte, K. (2014). Chemical weathering processes on the earth's surface. In *Weathering and the Riverine Denudation of Continents*, SpringerBriefs in Earth System Sciences. Springer, Dordrecht.

Derakhshan-Babaei, F., Nosrati, K., Tikhomirov, D., Christl, M., Sadough, H., and Egli, M. (2020). Relating the spatial variability of chemical weathering and erosion to geological and topographical zones. *Geomorphology*, 363:107235.

Dinis, P. A., Garzanti, E., Hahn, A., Vermeesch, P., and Cabral-Pinto, M. (2020). Weathering indices as climate proxies. a step forward based on congo and sw african river muds. *Earth-Science Reviews*, 201:103039.

Dominguez, G., Jackson, T., Brothers, L., Barnett, B., Nguyen, B., and Thiemens, M. H. (2008). Discovery and measurement of an isotopically distinct source of sulfate in earth's atmosphere. *Proceedings of the National Academy of Sciences*, 105(35):12769–12773.

Fan, B.-L., Zhao, Z.-Q., Tao, F.-X., Liu, B.-J., Tao, Z.-H., Gao, S., and Zhang, L.-H. (2014). Characteristics of carbonate, evaporite and silicate weathering in huanghe river basin: A comparison among the upstream, midstream and downstream. *Journal of Asian Earth Sciences*, 96:17–26.

Farquhar, J. and Wing, B. A. (2003). Multiple sulfur isotopes and the evolution of the atmosphere. *Earth and Planetary Science Letters*, 213:1–13.

Farquhar, J., Wu, N., Canfield, D. E., and Oduro, H. (2010). Connections between sulfur cycle evolution, sulfur isotopes, sediments, and base metal sulfide deposits. *Economic Geology*, 105(3):509–533.

Gaillardet, J., Dupré, B., and Allègre, C. J. (1995). A global geochemical mass budget applied to the congo basin rivers: erosion rates and continental crust composition. *Geochimica et Cosmochimica Acta*, 59(17):3469–3485.

Galimov, E., editor (2012). *The Biological Fractionation of Isotopes*. Elsevier.

Gao, Y., Ma, M., Yang, T., Chen, W., and Yang, T. (2018). Global atmospheric sulfur deposition and associated impaction on nitrogen cycling in ecosystems. *Journal of Cleaner Production*, 195:1–9.

Geological Atlas of Africa (2008). Tectonostratigraphic synopsis. In *Geological Atlas of Africa*. Springer, Berlin, Heidelberg.

Germida, J. J., Wainwright, M., and Gupta, V. V. (2021). Biochemistry of sulfur cycling in soil. In *Soil biochemistry*, pages 1–53. CRC Press.

Goldich, S. S. (1938). A study in rock-weathering. *The Journal of Geology*, 46(1):17–58.

Goudie, A. S. and Viles, H. A. (2012). Weathering and the global carbon cycle: Geomorphological perspectives. *Earth-Science Reviews*, 113(1-2):59–71.

Grossman, E. L. and Joachimski, M. M. (2020). Oxygen isotope stratigraphy. In *Geologic Time Scale 2020*, pages 279–307. Elsevier.

Halevy, I., Fike, D. A., Pasquier, V., Bryant, R. N., Wenk, C. B., Turchyn, A. V., and Claypool, G. E. (2023). Sedimentary parameters control the sulfur isotope composition of marine pyrite. *Science*, 382(6673):946–951.

Han, X., Guo, Q., Strauss, H., Liu, C.-Q., Hu, J., Guo, Z., and Kong, J. (2017). Multiple sulfur isotope constraints on sources and formation processes of sulfate in beijing pm2.5 aerosol. *Environmental science & technology*, 51(14):7794–7803.

Harrison, I., Brummett, R. E., and Stiassny, M. L. (2016). The congo river basin.

Hemingway, J. D., Olson, H., Turchyn, A. V., Tipper, E. T., Bickle, M. J., and Johnston, D. T. (2020). Triple oxygen isotope insight into terrestrial pyrite oxidation. *Proceedings of the National Academy of Sciences*, 117(14):7650–7657.

Hermes, A. L., Dawson, T. E., and Hinckley, E. L. S. (2022). Sulfur isotopes reveal agricultural changes to the modern sulfur cycle. *Environmental Research Letters*, 17(5):054032.

Huang, X., Song, Y., Zhao, C., Li, M., Zhu, T., Zhang, Q., and Zhang, X. (2014). Pathways of sulfate enhancement by natural and anthropogenic mineral aerosols in china. *Journal of Geophysical Research: Atmospheres*, 119(24):14–165.

Ivanov, M. V. and Freney, J. R., editors (1983). *The Global Biogeochemical Sulphur Cycle*, volume 19. Wiley, Chichester.

Jacobson, M., Charlson, R. J., Rodhe, H., and Orians, G. H. (2000). *Earth System Science: from biogeochemical cycles to global changes*. Academic Press.

Jørgensen, B. B. (2021). Sulfur biogeochemical cycle of marine sediments. *Geochemical Perspectives*, 10(2):145–146.

Jørgensen, B. B., Findlay, A. J., and Pellerin, A. (2019). The biogeochemical sulfur cycle of marine sediments. *Frontiers in Microbiology*, 10:436320.

Kanzaki, Y., Brantley, S. L., and Kump, L. R. (2020). A numerical examination of the effect of sulfide dissolution on silicate weathering. *Earth and Planetary Science Letters*, 539:116239.

Kemeny, P. C., Lopez, G. I., Dalleska, N. F., Torres, M., Burke, A., Bhatt, M. P., et al. (2021a). Sulfate sulfur isotopes and major ion chemistry reveal that pyrite oxidation counteracts CO_2 drawdown from silicate weathering in the langtang-trisuli-narayani river system, nepal himalaya. *Geochimica et Cosmochimica Acta*, 294:43–69.

Kemeny, P. C., Torres, M. A., Lamb, M. P., Webb, S. M., Dalleska, N., Cole, T., et al. (2021b). Organic sulfur fluxes and geomorphic control of sulfur isotope ratios in rivers. *Earth and Planetary Science Letters*, 562:116838.

Lee, C. L. and Brimblecombe, P. (2016). Anthropogenic contributions to global carbonyl sulfide, carbon disulfide and organosulfides fluxes. *Earth-Science Reviews*, 160:1–18.

Li, C. and Ji, H. (2016). Chemical weathering and the role of sulfuric and nitric acids in carbonate weathering: Isotopes (^{13}c, ^{15}n, ^{34}s, and ^{18}o) and chemical constraints. *Journal of Geophysical Research: Biogeosciences*, 121(5):1288–1305.

Li, Q., Gao, Y., and Yang, A. (2020). Sulfur homeostasis in plants. *International Journal of Molecular Sciences*, 21(23):8926.

Milesi, J.-P. et al. (2006). An overview of the geology and major ore deposits of central africa: Explanatory note for the 1: 4,000,000 map "geology and major ore deposits of central africa". *Journal of African Earth Sciences*, 44(4-5):571–595.

Miller, S. N., Semmens, D. J., Goodrich, D. C., Hernandez, M., Miller, R. C., Kepner, W. G., and Guertin, D. P. (2007). The automated geospatial watershed assessment tool. *Environmental Modelling & Software*, 22(3):365–377.

Mushi, C. A., Ndomba, P. M., Trigg, M. A., Tshimanga, R. M., and Mtalo, F. (2019). Assessment of basin-scale soil erosion within the congo river basin: A review. *Catena*, 178:64–76.

Nordstrom, K. (1982). Aqueous pyrite oxidation and the consequent formation of secondary iron minerals. *Acid Sulfate Weathering*, 10:37–56.

Pacheco, F. A., Landim, P. M., and Szocs, T. (2013). Anthropogenic impacts on mineral weathering: a statistical perspective. *Applied Geochemistry*, 36:34–48.

Pei, Q., Saikawa, E., Kaspari, S., Widory, D., Zhao, C., Wu, G., et al. (2021). Sulfur aerosols in the arctic, antarctic, and tibetan plateau: Current knowledge and future perspectives. *Earth-Science Reviews*, 220:103753.

Pester, M., Knorr, K.-H., Friedrich, M. W., Wagner, M., and Loy, A. (2012). Sulfate-reducing microorganisms in wetlands–fameless actors in carbon cycling and climate change. *Frontiers in microbiology*, 3:19769.

Price, F. T. and Shieh, Y.-N. (1979). Fractionation of sulfur isotopes during laboratory synthesis of pyrite at low temperatures. *Chemical Geology*, 27(3):245–253.

Relph, K. E., Stevenson, E. I., Turchyn, A. V., Antler, G., Bickle, M. J., Baronas, J. J., et al. (2021). Partitioning riverine sulfate sources using oxygen and sulfur isotopes: Implications for carbon budgets of large rivers. *Earth and Planetary Science Letters*, 567:116957.

Roberts, E., Jelsma, H., and Hegna, T. (2015). Mesozoic sedimentary cover sequences of the congo basin in the kasai region, democratic republic of congo. In de Wit, M., Guillocheau, F., and de Wit, M., editors, *Geology and Resource Potential of the Congo Basin*. Springer, Berlin, Heidelberg.

Ross, M. R., Nippgen, F., Hassett, B. A., McGlynn, B. L., and Bernhardt, E. S. (2018). Pyrite oxidation drives exceptionally high weathering rates and geologic co2 release in mountaintop-mined landscapes. *Global Biogeochemical Cycles*, 32(8):1182–1194.

Schippers, A. and Jørgensen, B. B. (2002). Biogeochemistry of pyrite and iron sulfide oxidation in marine sediments. *Geochimica et Cosmochimica Acta*, 66(1):85–92.

Schoenau, J. J. and Malhi, S. S. (2008). Sulfur forms and cycling processes in soil and their relationship to sulfur fertility. *Sulfur: A missing link between soils, crops, and nutrition*, 50:1–10.

Schoonen, M. (2018). Sulfur cycle. In White, W., editor, *Encyclopedia of Geochemistry*. Springer, Cham.

Seal, R. R. (2006). Sulfur isotope geochemistry of sulfide minerals. *Reviews in mineralogy and geochemistry*, 61(1):633–677.

Sonwa, D. J., Oumarou Farikou, M., Martial, G., and Félix, L.-F. (2020). Living under a fluctuating climate and a drying congo basin. *Sustainability*, 12(7):2936.

Tcherkez, G. and Tea, I. (2013). 32s/34s isotope fractionation in plant sulphur metabolism. *Journal of Experimental Botany*, 64(7):1693–1709.

Tipper, E. T., Gaillardet, J., Galy, A., Louvat, P., Bickle, M. J., and Capmas, F. (2010). Calcium isotope ratios in the world's largest rivers: a constraint on the maximum imbalance of oceanic calcium fluxes. *Global Biogeochemical Cycles*, 24(3).

Torres, M. A., West, A. J., Clark, K. E., Paris, G., Bouchez, J., Ponton, C., et al. (2016). The acid and alkalinity budgets of weathering in the andes–amazon system: Insights into the erosional control of global biogeochemical cycles. *Earth and Planetary Science Letters*, 450:381–391.

Torres, M. S., Morales, A. R., Peralta, A. S., and Kroneck, P. M. (2020). Sulfur, the versatile non-metal. In Sosa, M. and Kroneck, P., editors, *Transition Metals and Sulfur–A Strong Relationship for Life*, pages 19–50. De Gruyter.

Tourian, M. J. et al. (2023). Current availability and distribution of congo basin's freshwater resources. *Communications Earth & Environment*, 4(1):174.

Tshimanga, R. M., N'kaya, G. D. M., and Alsdorf, D. (2022). *Congo Basin Hydrology, Climate, and Biogeochemistry: A Foundation for the Future*, volume 269. John Wiley & Sons.

Turchyn, A. V. et al. (2013). Isotope evidence for secondary sulfide precipitation along the marsyandi river, nepal, himalayas. *Earth and Planetary Science Letters*, 374:36–46.

Turner, B. F., White, A. F., and Brantley, S. L. (2010). Effects of temperature on silicate weathering: Solute fluxes and chemical weathering in a temperate rain forest watershed, jamieson creek, british columbia. *Chemical Geology*, 269(1-2):62–78.

Ver, L. M. B., Mackenzie, F. T., and Lerman, A. (1999). Biogeochemical responses of the carbon cycle to natural and human perturbations; past, present, and future. *American Journal of Science*, 299(7-9):762–801.

Verhegghen, A., Mayaux, P., De Wasseige, C., and Defourny, P. (2012). Mapping congo basin vegetation types from 300 m and 1 km multi-sensor time series for carbon stocks and forest areas estimation. *Biogeosciences*, 9(12):5061–5079.

Viennois, G., Bétard, F., Freycon, V., Barbier, N., and Couteron, P. (2022). Automated landform classification and mapping using a combined textural-morphometric approach: the congo basin and surroundings. *Remote Sensing of Environment*, 269:112818.

Vile, M. A., Bridgham, S. D., Wieder, R. K., and Novák, M. (2003). Atmospheric sulfur deposition alters pathways of gaseous carbon production in peatlands. *Global Biogeochemical Cycles*, 17(2).

Weyhenmeyer, G. A., Hartmann, J., Hessen, D. O., Kopáček, J., Hejzlar, J., Jacquet, S., ..., and Zechmeister, T. (2019). Widespread diminishing anthropogenic effects on calcium in freshwaters. *Scientific Reports*, 9(1):10450.

Wing, B. A. and Halevy, I. (2014). Intracellular metabolite levels shape sulfur isotope fractionation during microbial sulfate respiration. *Proceedings of the National Academy of Sciences of the United States of America*, 111:18116–18125.

Winnick, M. J., Chamberlain, C. P., Caves, J. K., and Welker, J. M. (2014). Quantifying the isotopic 'continental effect'. *Earth and Planetary Science Letters*, 406:123–133.

Young, E. D., Galy, A., and Nagahara, H. (2002). Kinetic and equilibrium mass-dependent isotope fractionation laws in nature and their geochemical and cosmochemical significance. *Geochimica et Cosmochimica Acta*, 66(6):1095–1104.

Yu, X., Hu, R., Tao, M., Qian, L., Wang, F., Wang, S., and He, Z. (2023). Microbially driven sulfur cycling in the river–wetland–ocean continuum. *Ocean-Land-Atmosphere Research*, 2023:0027.

Zak, D., Hupfer, M., Cabezas, A., Jurasinski, G., Audet, J., Kleeberg, A., et al. (2021). Sulphate in freshwater ecosystems: A review of sources, biogeochemical cycles, ecotoxicological effects and bioremediation. *Earth-Science Reviews*, 212:103446.

Zhang, D., Li, X.-D., Zhao, Z.-Q., and Liu, C.-Q. (2015). Using dual isotopic data to track the sources and behaviors of dissolved sulfate in the western north china plain. *Applied Geochemistry*, 52:43–56.

Zhang, D., Xue, T., Xiao, J., Chai, N., and Gong, S. G. (2024). Significant influence of water diversion and anthropogenic input on riverine sulfate based on sulfur and oxygen isotopes. *Journal of Hazardous Materials*, 461:132622.

Zhang, D., Zhao, Z. Q., Peng, Y., Fan, B., Zhang, L., Li, J., and Chen, A. (2020). Sulfur cycling in the yellow river and the sulfate flux to the ocean. *Chemical Geology*, 534:119451.

A Appendix: Ions Concentrations of river water samples

River Numbers	Na_uM	K_uM	Mg_uM	Ca_uM	SO4_uM	Cl_uM
R1	120.47	40.11	82.98	75.61	27.92	76.23
R2	44.65	26.84	40.36	63.09	14.75	36.82
R3	12.84	14.85	20.62	33.47	17.74	17.78
R4	11.89	16.19	28.64	58.82	14.69	19.09
R5	19.35	12.16	7.27	11.6	12.43	23.22
R6	16.06	10.73	7.54	8.18	3.18	22.05
R7	21.42	18.15	11.94	18.51	22.87	28.23
R8	16.39	15.43	25.49	47.91	12.49	24.4
R9	11.71	16.53	13.97	33.71	6.47	8.62
R10	76.46	39.32	29.71	75.88	15.57	99.2
R11	51.93	30	58.08	78.86	18.44	28.83
R12	65.9	269.64	27.36	22.14	31.56	156.29
R13	16.34	80.83	24.12	39.93	88.17	80.53
R14	20.61	63.59	29.77	42.22	105.54	64.66
R15	26.4	40.87	14.3	19.08	55.76	48.44
R16	14.83	54.92	19.71	42.65	42.43	61.66
R17	52.88	31.56	48.45	61.84	21.81	21.78
R18	20.2	38.42	17.97	22.83	5.82	8.82
R19	125.65	82.65	535.87	1000.39	21.31	15.11
R20	103.28	41.5	119.74	161.54	8.5	12.8
R21	362.51	64.4	161.09	376.01	29.45	17.55
R22	60.96	36.14	76.11	94.83	8.91	11.62
R23	44.75	44.64	52.24	73.73	22.44	27.6
R24	67.08	74.92	51.75	60.81	19.64	36.69
R25	135.99	50.2	95.66	131.36	6.23	23.6
R26	66.54	61.1	178.45	205.66	14.42	11.06
R27	48.14	43.93	50.62	73.47	9.93	6.12
R28	18.44	30.47	10.23	6.46	6.34	13.52
R29	86.1	31.29	51.33	54.94	2.92	6.42
R30	102.97	33.19	39.33	52.04	3.94	5.44
R31	105.62	36.75	77.75	109.28	5.49	7.58
R32	44.13	15.02	26.63	34.26	6.51	8.13
P1	15.51	29.74	14.55	128.36	27.18	36.28
P2	6.59	3.89	5.83	17.31	4.67	4.91

B Appendix: Isotopes Data of river water samples

heightRiver numbers	$\delta^{34}S_{SO_{42}^-mean}$	$\delta^{34}S_{SO_{42}^-std}$
R1	11.8	0.2
R2	12.6	0.1
R3	11.7	0.5
R4	10.1	0
R5	9.8	0
R6	10.9	0.1
R7	10	0.1
R8	11.4	0.1
R9	11.7	0
R10	13.5	0
R11	12.9	0
R13	10.3	0.1
R14	10.1	0.1
R15	12.3	0.1
R16	10.4	0.1
R17	14.5	0.1
R18	13.6	0
R19	13.6	0.1
R20	14.4	0
R21	4.4	0.2
R22	10.2	0.2
R23	11.8	0.1
R24	12.6	0.1
R25	11.7	0
R26	16.4	0
R27	12.1	0.2
R28	11.4	0.1
R29	10	0.2
R30	12.3	0.1
R31	11.9	0
R32	11.4	0
P1	8.7	0
P2	7.3	0

River numbers	$\delta^{18}O_{H_2O mean}$	$\delta^{18}O_{H_2O std}$	$\delta^{18}O_{SO_4{}^{2-} mean}$	$\delta^{18}O_{SO_4{}^{2-} std}$	$\Delta d^{18}O$
R1	-2.37	0.41	6.4	0.5	8.77
R2	-3.28	0.03	7.6	0.5	10.88
R3	-3.43	0.08			
R4	-3.51	0.03	4.8	0.3	8.31
R5	-1.58	0.1	6.9	0.4	8.48
R6	-2.49	0.1	4.8	0.4	7.29
R7	-2.62	0.11	6.6	0.3	9.22
R8	-2.79	0.07	5.4	0.6	8.19
R9	-3.58	0.05	5.5	0.3	9.08
R10	-3.6	0.09	8.3	0.5	11.9
R11	-3.18	0.08	7.8	0.9	10.98
R12					
R13	-3.42	0.03	7.2	0.5	10.62
R14	-3.06	0.12	8.5	0.5	11.56
R15	-3.51	0.09	7.7	0.3	11.21
R16	-2.95	0.07	5.5	0.4	8.45
R17	-3.24	0.02	8	0.4	11.24
R18	-3.11	0.06	7.3	0.2	10.41
R19	-3.26	0.06	10.4	0.4	13.66
R20	-1.95	0.13	8.9	0.8	10.85
R21	-2.84	0.06	1.6	0.8	4.44
R22	-3.1	0.05	6.1	0.3	9.2
R23	-3.4	0.06	8.4	0.1	11.8
R24	-3.47	0.09	8.3	0.5	11.77
R25	-3.39	0.03	5.6	0.2	8.99
R26	-3.33	0.03	8.5	0.4	11.83
R27	-3.29	0.03	7.2	0.5	10.49
R28	-3.26	0.05	7.5	0.3	10.76
R29	-3.73	0.05	5.3	0.1	9.03
R30	-3.35	0.13	7.3	0.7	10.65
R31	-4.06	0.44	6.9	0.1	10.96
R32	-3.57	0.02	6.6	0.1	10.17
P1	-1.32	0.04	14.5	0.5	15.82
P2	-3.98	0.23	14.7	1	18.68

C Appendix: Other Hydro-chemical Data of river water samples

River Numbers	pH	Alk_uEq/L	DOC_mg/L	DOC_mg/L	TSS_mg/L
R1	6.9	314.7	7.8	7.8	17.3
R2	6.8	188.7	4	4	19
R3	6.2	69.8	2.7	2.7	13.5
R4	6.5	138.5	2	2	9.3
R5	4.2	-63.1	20.9	20.9	8.9
R6	4.3	-72.1	24.4	24.4	5.5
R7	5.4	16	3.4	3.4	11.1
R8	6	101.9	4.2	4.2	5.88
R9	6.5	70.8	1.7	1.7	13.4
R10	7.2	192.7	1.5	1.5	29.8
R11	7.3	306.1	1.8	1.8	27.2
R12	5.9	172.5	19.2	19.2	38
R13	4.9	5.9	10.9	10.9	14
R14	4.6	-2.8	13.7	13.7	8.3
R15	4	-56.1	28.2	28.2	2.1
R16	6	50.3	6	6	19.9
R17	7.3	149.2	4.3	4.3	52.9
R18	6.5	92.8	1.1	1.1	80.7
R19	8	2923.6	2.7	2.7	20.2
R20	7.7	617.6	5	5	34.67
R21	8.3	1293.8	3.5	3.5	1700.89
R22	7.8	341.9	2	2	326.67
R23	7.2	255.4	1.3	1.3	11.64
R24	7.3	269	1.7	1.7	26.67
R25	7.6	567.1	3.4	3.4	170.79
R26	7.7	819.7	2.6	2.6	4332.49
R27	7.2	279.8	1.6	1.6	22.84
R28	5.9	50	0.9	0.9	1150.61
R29	7.2	264.6	5.6	5.6	20.5
R30	7.3	286	1.7	1.7	18.35
R31	6.6	453	4.9	4.9	62.5
R32	7.8	114.4	5.7	5.7	25.48
P1	6.1	271.8			
P2	5.5	7.6			

D Appendix: Elevation and Average Slope Data of the studying area

River numbers	Elevation_m	Average slope_degrees
R2	745.479	3.55471
R3	365.695	2.77452
R4	390.552	3.06195
R5	390.833	2.64573
R6	330.423	1.92248
R7	431.516	3.39585
R8	353.336	2.38118
R9	802.556	3.80723
R10	816.425	5.11944
R11	815.672	3.22237
R13	445.695	2.85089
R14	416.961	2.49587
R15	353.899	1.26879
R16	427.295	3.02634
R17	706.849	4.37574
R18	703.508	4.26346
R19	629.227	4.96291
R20	727.737	5.20448
R21	651.259	3.75085
R22	686.015	3.83334
R23	744.994	6.01882
R24	731.435	5.32008
R25	687.802	3.32355
R26	685.583	2.61409
R27	675.813	5.37686
R28	701.051	3.48377
R29	992.89	2.02503
R30	742.672	5.08488
R31	855.082	2.93677
R32	916.732	2.37296

Personal Declaration:

I hereby declare that the submitted thesis result from my own, independent work. All external sources are explicitly acknowledged in the thesis.

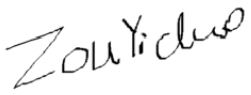

Zou Yiduo
Zurich 4.28.2024